Hao Li

Towards a Better Understanding of Protein-Polysaccharide Electrostatic Interactions and Their Application in Designing Delivery Systems

Thesis submitted in fulfillment of the requirements for the degree of

Doctor (PhD) in Bioscience Engineering: Food Sciences and Nutrition

GHENT UNIVERSITY

FACULTY OF BIOSCIENCE ENGINEERING

Promotors: Prof. dr. ir. Paul Van der Meeren
Particle and Interfacial Technology research group
Department of Green Chemistry and Technology
Ghent University
Dr. ir. Ali Sedaghat Doost
Particle and Interfacial Technology research group
Department of Green Chemistry and Technology
Ghent University

Dean: Prof. dr. Els Van Damme

Rector: Prof. dr. ir. Rik Van de Walle

For citation:

Li, H. (2023). Towards a Better Understanding of Protein-Polysaccharide Electrostatic Interactions and Their Application in Designing Delivery Systems, PhD thesis, Ghent University

Cover design

Schematic representation: pH-responsive whey protein-pectin interactions at the oil-water interface and a whey protein/pectin bilayer-coated oil droplet visualized by Cryo-SEM; The influence of pH variations on the hydrophobic compound bound to the inner cavity of β-lactoglobulin in the presence of pectin.

ISBN: 9789463576468

Acknowledgements

While it has been nearly four years since I enrolled as a doctoral student, it feels like just a few months. When I look back, this period left me with a very memorable and enjoyable experience. First, I would like to express my gratitude to Prof. Paul van der Meeren for accepting me as a doctoral student. I'm lucky to have worked with him. Without Paul's consistent help and guidance during the four years, I cannot imagine how I would have completed my PhD. He has always patiently listened to me and provided professional feedback. I often had strange research ideas, but Paul always helped to analyze them and encouraged me to think. With his mentoring, now I have grown to be a researcher who can do scientific research independently and is able to guide other young students. Besides, Paul has always been a nice and friendly person in life. I still clearly remember that he invited our group members to have lunch and enjoy the afternoon time in his house. I would also like to thank my co-promotor, Dr. Ali Sedaghat Doost. He has always been a friendly and reliable person, and I can always ask him for help during my PhD.

I would like to thank Quenten Denon, a great lab technician in the PaInT group. Quenten has always been willing to share his experience and knowledge with me. In addition, I would like to thank Katja Van Nieuland, an excellent lab technician in the ISOFYS group. You make everything in the lab work well and I can conduct my experiments smoothly thanks to your efforts. I would like to thank Saskia Van der Looven, who helps me deal with complicated administrative issues. Many thanks to Jianfeng, Chunxia, Chak, Ferre, Arne, Yulin, Di, A'yun, Xue, Lingshan, Rishav and many PaInT colleagues for making a comfortable working environment and for giving me help during my PhD. Especially, thanks to Lorenz for helping me start QCM-D work in the initial months of my PhD.

The successful accomplishment of my PhD also relies on great help from other research groups. I would like to thank Prof. Andre Skirtach (Nano-Biotechnology Laboratory) and Prof. Koen Dewettinck (Food Structure and Function Research Group) for allowing me to use their lab equipment. Especially, many thanks to Benny Lewille for helping me prepare the samples.

I would like to thank the jury members, Prof. Peter Bossier, Prof. John Van Camp, Prof. Filip Van Bockstaele, Prof. Christophe Blecker, Prof. Tara Grauwet, and Prof. Julia Keppler. Thank you for your guidance and suggestions for improving this dissertation.

Last, I would like to thank my family for your endless support. My warmest thanks give to Teng, my girlfriend, one of the most important persons in my life, you make my life special and colorful.

Table of Contents

Abbreviations

AFM	Atomic force microscopy
β-Lg	β-lactoglobulin
Cryo-SEM	Cryo-scanning electron microscopy
DE	Degree of esterification
DMSO	Dimethyl sulfoxide
FI	Maximum fluorescence intensity
HMP	High-methoxy pectin
IEP	Isoelectric point
LMP	Low-methoxy pectin
LMWS	Low molecular weight surfactant
MCE	Mixed cellulose ester
MCT	Medium-chain triglycerides
NMR	Nuclear Magnetic Resonance
O/W	Oil-in-water
PSD	Particle size distribution
PBS	Sodium phosphate buffer solution
QCM-D	Quartz crystal microbalance with dissipation monitoring
RPM	Revolutions Per Minute
RGE	Rabbit gastric extracts
SGF	Simulated gastric fluid
SAMs	Self-assembled monolayers
3D	Three-dimensional
WPI	Whey protein isolate

Symbols

A	Surface area
$D_{4,3}$	Volume moment mean diameter
$D_{3,2}$	Surface area moment mean diameter
ΔD	Dissipation shift
E_d'	Interfacial (dilatational) elastic modulus
E_d''	Interfacial (dilatational) viscous modulus
Δf/n	Normalized frequency shift
K_d	Dissociation constant (K_d)
log K_{ow}	Octanol-water partition coefficient
λ_{max}	Maximum emission wavelength
γ	Interfacial tension

Summary

Protein-polysaccharide electrostatic interactions have received increasing research interest during the last two decades due to their potential importance in food processing and novel food formulations. One of the most attractive food applications is the construction of colloidal delivery vehicles for hydrophobic ingredients, which are designed to encapsulate, protect, and control the release of these ingredients. However, this requires a better understanding and more intelligent manipulation of the protein-polysaccharide interactions under complex environmental conditions. Proteins and many polysaccharides are charged biopolymers. The heterogeneous distribution of surface charges on proteins (simultaneous existence of both positive and negative charges) may facilitate their interaction with charged polysaccharides across a wide pH range, including both below and above their isoelectric point. This dissertation aims to provide deeper insights into protein-polysaccharide electrostatic interactions at the oil-water interface or in bulk, and their responsive behaviors upon exposure to changing environmental conditions (e.g. pH, salt, and gastrointestinal fluids). The potential application of protein-polysaccharide complexation in two types of delivery systems for hydrophobic ingredients (i.e. oil-in-water emulsion, and intermolecular soluble complexes) is examined. In this dissertation, whey protein isolate (WPI enriched with β-lactoglobulin) and pectin (both low- and high-methoxy pectin) were selected as characteristic models of globular proteins and anionic polysaccharides since the combination is an ideal model for studying protein-polysaccharide interactions in soft matter systems because of their well-studied molecular characteristics.

Emulsions are interface-dominated materials whose properties are largely determined by their interfacial components. The WPI-pectin complexes can form an adsorption layer at the oil-water interface, which may be used to customize the properties of O/W emulsions. However, direct insights into the interfacial protein-polysaccharide (dis)assembly behaviors under changing environmental conditions have been very limited due to the lack of appropriate methodologies that can directly access the complex interfacial phenomena. Hereby, our study employed state-of-the-art techniques to understand the real-time and in-situ interfacial interactions between

WPI and pectin under changing environmental conditions (e.g. pH, salt, and gastrointestinal fluids).

Individual β-lactoglobulin (β-Lg) molecules can also be used as a carrier for small hydrophobic compounds, which is mainly ascribed to the ligand-binding properties of the protein. However, most studies in this field only focused on the interactions between β-Lg and various hydrophobic compounds at neutral pH, despite the fact that the acidic pH conditions are more relevant to food systems (e.g. in beverages) and after ingestion (e.g. in gastric fluids). Besides, β-Lg molecules tend to aggregate and precipitate in some acidic beverage applications (pH 4-6) due to the proximity of the protein's IEP. To address these issues, pectin can be mixed with β-Lg to form intermolecular soluble complexes that exhibit good colloidal stability in the pH range. However, it remains unclear to what extent the pH variations and the complexation with anionic pectin affect the ligand-binding properties of the protein.

In Chapter 1, the basis of food proteins and polysaccharides, as well as the current understanding of their non-covalent and covalent interactions were demonstrated. Besides, the mechanisms of emulsion stabilization and destabilization were discussed. Moreover, the interfacial properties of proteins at fluid interfaces, the ligand-binding properties of β-Lg, and the structure of pectin were reviewed. Afterwards, the outline and objectives of this dissertation were provided.

In Chapter 2, a real-time quartz crystal microbalance with dissipation monitoring (QCM-D) technique was applied to investigate the effect of pH on the sequential adsorption of whey proteins and low-methoxy pectin (LMP) on a hydrophobic surface (i.e. alkyl-terminated gold sensor) mimicking the oil-water interface. The pH-responsive conformational changes of the pre-adsorbed WPI layer at the hydrophobic surface and their reversibility were evaluated. Subsequently, LMP was introduced to the WPI layer for investigating their interfacial complexation as a function of pH (both below and above the isoelectric point of WPI). Finally, the disassembly behavior of the mixed biopolymer layer was explored. Results from the study indicated that QCM-D was well suited to investigate the effects of (changing) environmental conditions on the characteristics of the adsorbed layer. WPI adsorbed onto the surface and formed a viscoelastic layer at neutral pH, which can be described as a heterogeneous and highly

hydrated layer. When the pH of the continuous phase approached the IEP of WPI, the adsorbed protein layer became more densely packed and less hydrated due to structural rearrangements of the protein molecules. Furthermore, those changes were found to be reversible. The adsorption of LMP onto the pre-formed WPI layer was observed over a wide pH range from pH 3.0 to 6.5, i.e. both below and above the IEP of WPI. Besides, the LMP adsorption was more favorable upon lowering the pH level. Above pH 6.5, no interfacial complexation was observed. When the resulting WPI-LMP bilayer was exposed to neutral pH, the adsorbed pectin exhibited a pH-responsive desorption due to charge inversion. These results suggested the reversibility of the interfacial WPI-LMP complexation and implied that the driving forces of these processes were mainly electrostatic interactions.

In Chapter 3, the sequential adsorption of WPI and LMP at the medium chain triglyceride-water interface as a function of pH was further investigated with a modified drop shape tensiometer allowing external phase exchange. The complex interfacial phenomena (e.g. pH-induced interfacial (dis)assembly) were elucidated using dynamic interfacial tension and interfacial dilatational rheology. The initial WPI adsorption rapidly reduced the oil-water interfacial tension, but the successive pH variations and LMP addition hardly influenced the interfacial tension. Regarding the observations obtained from interfacial dilatational rheology, the WPI layer exhibited solid-like properties, regardless of the pH level. A maximum interfacial dilatational elasticity was reached when the pH was close to the IEP of WPI, corresponding to the minimum hydration degree determined by QCM-D above. LMP adsorption onto the protein layer increased the interfacial viscoelasticity, and this effect was more pronounced when the pH was below the IEP of WPI. Moreover, the adsorbed LMP at acidic pH conditions exhibited pH-responsive desorption upon exposure to neutral pH, as evidenced by the restored interfacial viscoelasticity, in line with the QCM-D results. Furthermore, in comparison with the individual WPI layer, the thicker and more rigid WPI/LMP bilayer better inhibited droplet flocculation and coalescence in O/W emulsions.

The previous two chapters clearly demonstrated the pH-responsive behavior of the adsorbed pectin. Considering the indigestibility nature of pectin in the human gastric phase, it was hypothesized that WPI/pectin bilayer emulsions/microcapsules might be

ideal delivery systems to the small intestine. To test this hypothesis, in Chapter 4, a novel multiscale approach (from interface to bulk) was applied to investigate the gastric digestion stability of WPI/pectin bilayers at the oil-water interface. The in vitro gastric digestion followed the harmonized INFOGEST static digestion protocol, and gastric enzymes (pepsin and gastric lipase) were obtained from rabbit gastric extracts. Two types of pectin (LMP and HMP) were used in this work. The complicated interfacial phenomena (e.g. interfacial complexation, proteolysis, and lipolysis) during in vitro gastric digestion were evaluated using QCM-D, ζ-potential, dynamic interfacial tension, and interfacial dilatational rheology. Besides, the evolution of the particle size and microstructure of bulk emulsions during the gastric phase of in vitro digestion was investigated by static light scattering and light microscopy. Compared with WPI-stabilized emulsions, the presence of an additional pectin layer could prevent or at least largely delay gastric destabilization (giving rise to coalescence or/and oiling off). Especially, the esterification degree of the pectin used was found to largely affect the emulsion behavior during gastric digestion.

In Chapter 5, the research focus was on the effect of pH variations (3.0-7.0) and pectin complexation on the ability of β-Lg molecules to bind small hydrophobic compounds. Three solvatochromic fluorescent probes (i.e. Nile red, retinol, and curcumin) were selected as representative models of hydrophobic compounds bound to the inner cavity or/and the outer surface of β-Lg. The most favorable pH for β-Lg binding with Nile red or retinol was observed at pH 7.0 because of the open conformation (i.e. accessible inner cavity) of β-Lg. At pH 3.0-4.5, the interactions between the two probes and β-Lg were less favorable and the dyes could only be bound to the outer surface of β-Lg. For the pre-formed β-Lg-Nile red or β-Lg-retinol complexes at pH 7.0, acidification caused the release of the hydrophobic probes from the inner cavity of β-Lg (e.g. burst release from pH 7.0 to 5.5). Even though the anionic pectin can interact with β-Lg to form intermolecular complexes below pH 6.5, the release behavior cannot be prevented. In contrast, the binding of curcumin to β-Lg was less affected by pH variations, suggesting that curcumin was mainly bound to the outer surface of β-Lg. Besides, adding anionic pectin (either LMP or HMP) barely affected the curcumin binding. Not limited to the three hydrophobic probes used, the obtained results can provide valuable insights into the binding of other hydrophobic compounds to β-Lg as well.

In Chapter 6, the main conclusions drawn from this dissertation were summarized. Some applications and implications of the current findings were discussed. Lastly, future perspectives in this field were provided.

Samenvatting

Eiwit-polysacharide elektrostatische interacties hebben de afgelopen twee decennia steeds meer onderzoeksinteresse gekregen vanwege hun potentiële belang bij voedselverwerking en nieuwe voedselformuleringen. Een van de meest aantrekkelijke voedseltoepassingen is de constructie van colloïdale transportmiddelen voor hydrofobe ingrediënten, die ontworpen zijn om de afgifte van deze ingrediënten in te kapselen, te beschermen en te beheersen. Dit vereist echter een beter begrip en een intelligentere manipulatie van de eiwit-polysacharide-interacties onder complexe omgevingsomstandigheden. Eiwitten en veel polysachariden zijn geladen biopolymeren. De heterogene verdeling van oppervlakteladingen op eiwitten (gelijktijdige aanwezigheid van zowel positieve als negatieve ladingen) kan hun interactie met geladen polysachariden over een breed pH-bereik vergemakkelijken, zowel onder als boven hun iso-elektrisch punt. Dit proefschrift beoogt diepere inzichten te verschaffen in de elektrostatische interacties tussen eiwitten en polysachariden op het olie-water-grensvlak of in bulk, en hun responsieve gedrag bij blootstelling aan veranderende omgevingsomstandigheden (bijv. pH, zout en gastro-intestinale vloeistoffen). De mogelijke toepassing van eiwit-polysacharide-complexering in twee soorten afgiftesystemen voor hydrofobe ingrediënten (d.w.z. olie-in-water-emulsie en intermoleculair oplosbare complexen) wordt onderzocht. In dit proefschrift werden wei-eiwitisolaat (WPI verrijkt met β-lactoglobuline) en pectine (zowel low- als high-methoxy pectine) geselecteerd als karakteristieke modellen van globulaire eiwitten en anionische polysachariden, aangezien de combinatie een ideaal model is voor het bestuderen van eiwit-polysacharide interacties in systemen met zachte materie vanwege hun goed bestudeerde moleculaire kenmerken.

Emulsies zijn door het grensvlak gedomineerde materialen waarvan de eigenschappen grotendeels worden bepaald door hun grensvlakcomponenten. De WPI-pectinecomplexen kunnen een adsorptielaag vormen op het olie-water-grensvlak, die kan worden gebruikt om de eigenschappen van O/W-emulsies aan te passen. Desondanks zijn directe inzichten in het grensvlak eiwit-polysacharide (de)assemblagegedrag onder veranderende omgevingsomstandigheden zeer beperkt vanwege het gebrek aan geschikte methodologieën die rechtstreeks toegang hebben tot

de complexe grensvlakfenomenen. Hierbij gebruikte onze studie state-of-the-art technieken om de real-time en in-situ grensvlakinteracties tussen WPI en pectine onder veranderende omgevingsomstandigheden (bijv. pH, zout en gastro-intestinale vloeistoffen) te begrijpen.

β-Lg-moleculen kunnen ook worden gebruikt als drager voor kleine hydrofobe verbindingen, wat voornamelijk wordt toegeschreven aan de ligandbindende eigenschappen van het eiwit. De meeste onderzoeken op dit gebied waren echter alleen gericht op de interacties tussen β-Lg en verschillende hydrofobe verbindingen bij een neutrale pH, ondanks het feit dat de zure pH-omstandigheden relevanter zijn voor voedselsystemen (bijv. in dranken) en na inname (bijv. in de maag). Vloeistoffen). Bovendien hebben β-Lg-moleculen de neiging om te aggregeren en neer te slaan in sommige toepassingen van zure dranken (pH 4-6) vanwege de nabijheid van het eiwit IEP. Om deze problemen aan te pakken, kan pectine worden gemengd met β-Lg om intermoleculair oplosbare complexen te vormen met verbeterde colloïdale stabiliteit in dit pH-bereik. Het blijft echter onduidelijk in welke mate de pH-variaties en de complexvorming met anionisch pectine de ligandbindende eigenschappen van het eiwit beïnvloeden.

In Hoofdstuk 1 werden de basis van voedingseiwitten en polysachariden, evenals het huidige begrip van hun niet-covalente en covalente interacties, gedemonstreerd. De mechanismen van emulsiestabilisatie en -destabilisatie werden besproken. Bovendien werden de grensvlakeigenschappen van eiwitten op vloeistofgrensvlakken, de ligandbindende eigenschappen van β-Lg en de structuur van pectine beoordeeld. Daarna werden de hoofdlijnen en doelstellingen van dit proefschrift verstrekt.

In Hoofdstuk 2 werd een real-time kwartskristal microbalans met dissipatie monitoring (QCM-D) techniek toegepast om het effect van de pH op de sequentiële adsorptie na te gaan van wei-eiwitten en low-methoxy pectine (LMP) op een hydrofoob oppervlak dat de olie-water interfase nabootst. De pH-gevoelige conformatieveranderingen van de vooraf geadsorbeerde WPI-laag aan het hydrofobe oppervlak en hun reversibiliteit werden geëvalueerd. Vervolgens werd LMP geïntroduceerd in de WPI-laag om hun grensvlakcomplexatie te onderzoeken als functie van de pH (zowel onder als boven het iso-elektrische punt van WPI). Ten slotte

werd het demontagegedrag van de gemengde biopolymeerlaag onderzocht. Uit de resultaten van het onderzoek bleek dat QCM-D zeer geschikt was om de effecten van (veranderende) omgevingsomstandigheden op de eigenschappen van de geadsorbeerde laag te onderzoeken. WPI adsorbeerde op het oppervlak en vormde een visco-elastische laag bij neutrale pH, die kan worden beschreven als een heterogene en sterk gehydrateerde laag. Toen de pH van de continue fase de IEP van WPI naderde, werd de geadsorbeerde eiwitlaag dichter opeengepakt en minder gehydrateerd als gevolg van structurele herschikkingen van de eiwitmoleculen. Bovendien bleken die veranderingen omkeerbaar te zijn. De adsorptie van LMP op de voorgevormde WPI-laag werd waargenomen over een breed pH-bereik van pH 3,0 tot 6,5, d.w.z. zowel onder als boven de IEP van WPI. Bovendien was de LMP-adsorptie gunstiger bij verlaging van de pH-waarde. Boven pH 6,5 werd geen grensvlakcomplexatie vastgesteld. Wanneer de resulterende WPI-LMP-dubbellaag werd blootgesteld aan neutrale pH, vertoonde het geadsorbeerde pectine een pH-gevoelige desorptie als gevolg van ladingsinversie. Deze resultaten suggereerden de reversibiliteit van de grensvlak WPI-LMP-complexatie en impliceerden dat de drijvende krachten van deze processen voornamelijk elektrostatische interacties waren.

In Hoofdstuk 3 werd de sequentiële adsorptie van WPI en LMP aan het middenketen triglyceride-water grensvlak als functie van de pH verder onderzocht met een gemodificeerde druppeltensiometer die externe fase-uitwisseling mogelijk maakt. De complexe fenomenen op het grensvlak (bijv. pH-geïnduceerde (de)montage van het grensvlak) werden opgehelderd met behulp van dynamische grensvlakspanning en grensvlakdilatatiereologie. De initiële WPI-adsorptie verminderde snel de olie-watergrensvlakspanning, maar de opeenvolgende pH-variaties en LMP-toevoeging hadden nauwelijks invloed op de grensvlakspanning. Met betrekking tot de waarnemingen verkregen uit grensvlakdilatatiereologie, vertoonde de WPI-laag vaste eigenschappen, ongeacht de pH-waarden. Een maximale grensvlakdilatatie-elasticiteit werd bereikt wanneer de pH dicht bij de IEP van WPI lag, wat overeenkomt met de minimale hydratatiegraad bepaald door QCM-D hierboven. LMP-adsorptie op de eiwitlaag verhoogde de visco-elasticiteit van het grensvlak, en dit effect was meer uitgesproken wanneer de pH lager was dan de IEP van WPI. Bovendien vertoonde het geadsorbeerde LMP bij zure pH-omstandigheden pH-gevoelige desorptie bij

blootstelling aan neutrale pH, zoals blijkt uit de herstelde grensvlakvisco-elasticiteit, in overeenstemming met de QCM-D-resultaten. Bovendien kan, in vergelijking met de individuele WPI-laag, de dikkere en stijvere WPI/LMP-dubbellaag de uitvlokking van druppels en de samensmelting van de O/W-emulsie beter remmen.

De voorgaande twee hoofdstukken hebben het pH-gevoelige gedrag van het geadsorbeerde pectine duidelijk aangetoond. Gezien de onverteerbare aard van pectine in de menselijke maagfase, werd verondersteld dat WPI/pectine dubbellaagsemulsies/microcapsules ideale toedieningssystemen voor de dunne darm zouden kunnen zijn. Om deze hypothese te testen, werd in Hoofdstuk 4 een nieuwe multischaalbenadering (van interfase tot bulk) toegepast om de maagverteringstabiliteit van WPI/pectine dubbellagen op het olie-water grensvlak te onderzoeken. De maagdigestie in vitro volgde het geharmoniseerde INFOGEST-protocol voor statische digestie en maagenzymen (pepsine en maaglipase) werden verkregen uit maagextracten van konijnen. In dit werk werden twee typen pectine (LMP en HMP) gebruikt. De gecompliceerde grensvlakverschijnselen (bijv. grensvlakcomplexatie, proteolyse en lipolyse) tijdens in vitro maagdigestie werden geëvalueerd met behulp van QCM-D, ζ-potentieel, dynamische grensvlakspanning en grensvlakdilatatiereologie. Bovendien werd de evolutie van de deeltjesgrootte en microstructuur van bulkemulsies tijdens de maagfase van in vitro vertering onderzocht door middel van statische lichtverstrooiing en lichtmicroscopie. Vergeleken met WPI-gestabiliseerde emulsies kan de aanwezigheid van een extra pectinelaag maagdestabilisatie (die aanleiding geeft tot coalescentie en/of olieafzetting) voorkomen of in ieder geval grotendeels vertragen. Vooral de veresteringsgraad van de gebruikte pectine bleek het gedrag van de emulsie tijdens de maagvertering grotendeels te beïnvloeden.

In hoofdstuk 5 lag de onderzoeksfocus op het effect van pH-variaties (3,0-7,0) en pectinecomplexvorming op het vermogen van β-Lg-moleculen om kleine hydrofobe verbindingen te binden. Drie solvatochrome fluorescerende probes (d.w.z. Nijlrood, retinol en curcumine) werden geselecteerd als representatieve modellen van hydrofobe verbindingen gebonden aan de binnenholte en/of het buitenoppervlak van β-Lg. De gunstigste pH voor β-Lg-binding met Nijlrood of retinol werd waargenomen bij pH 7,0 vanwege de open conformatie (d.w.z. toegankelijke binnenholte) van β-Lg. Bij pH 3,0-

4,5 waren de interacties tussen de twee sondes en β-Lg minder gunstig en konden de kleurstoffen alleen worden gebonden aan het buitenoppervlak van β-Lg. Voor de voorgevormde β-Lg-Nijl rode of β-Lg-retinolcomplexen bij pH 7,0 veroorzaakte de verzuring het vrijkomen van de hydrofobe sondes uit de binnenholte van β-Lg (bijv. burst-vrijgave van pH 7,0 tot 5,5). Hoewel de anionische pectine kan interageren met β-Lg om intermoleculaire complexen te vormen onder pH 6,5, kan het afgiftegedrag niet worden voorkomen. Daarentegen werd de binding van curcumine aan β-Lg minder beïnvloed door pH-variaties, wat suggereert dat curcumine voornamelijk gebonden is aan het buitenoppervlak van β-Lg. Bovendien had het toevoegen van anionische pectine (ofwel LMP ofwel HMP) nauwelijks invloed op de binding van curcumine. Niet beperkt tot de drie bestudeerde hydrofobe probes, kunnen de verkregen resultaten ook waardevolle inzichten verschaffen in de binding van andere hydrofobe verbindingen aan β-Lg.

In hoofdstuk 6 zijn de belangrijkste conclusies uit dit proefschrift samengevat. Enkele toepassingen en implicaties van de huidige bevindingen werden besproken. Tot slot werden toekomstperspectieven op dit gebied gegeven.

Chapter 1 General Introduction

1.1 Introduction

Protein-polysaccharide interactions have received great interest during the last two decades due to their potential importance in food engineering and novel food formulations (Dickinson, 2008; Wijaya et al., 2017). Proteins exhibit several structural and functional characteristics, such as surface activity, ligand-binding, gelation, self-assembly, environmental response and electrical properties (Livney, 2010). Polysaccharides are widely used in food products for a variety of purposes, e.g. stabilizer, thickener, gelling agent and sometimes emulsifier (Stephen et al., 2016). In protein-polysaccharide mixtures, either non-covalent complexes or covalent conjugates may be formed under certain environmental conditions (e.g. pH, temperature). A combination of protein and polysaccharide may not only combine the attributes of the biopolymers constituting them, but also present new structural and functional properties not possessed by their parent biopolymers. As an example, anionic pectin can be added to acid milk drinks to reduce the aggregation and precipitation of casein micelles at their isoelectric point (IEP) (Tuinier et al., 2002). Maillard conjugates of whey protein and pectin are prepared by a dry-heating method under controlled humidity, whereas these products can effectively stabilize oil-in-water (O/W) emulsions against heat-induced droplet flocculation (Setiowati et al., 2017). Besides, the emulsifying performance of the protein is not compromised upon conjugation. In both cases, the molecular chains of pectin function as electrostatic and steric stabilizers to prevent the particles/droplets from aggregation.

A colloid system is a type of mixture in which one substance consisting of microscopically dispersed particles is suspended throughout another substance. Common food colloids include dispersions, emulsions, foams, and gels. As shown in Figure 1.1, various structures over multiple length scales in a colloid system, such as complexes/coacervates, covalent conjugates, aggregates, and macro-/micro-gels, can be fabricated from food proteins and polysaccharides using bottom-up or/and top-down methods (Pan & Zhong, 2016; Wijaya et al., 2017). Additionally, the amphiphilicity of biopolymers may enable these molecules or particles to act as interfacial stabilizers at fluid-fluid interfaces (e.g. oil-water and air-water) to construct metastable emulsions and foams (Dickinson, 2011, 2015).

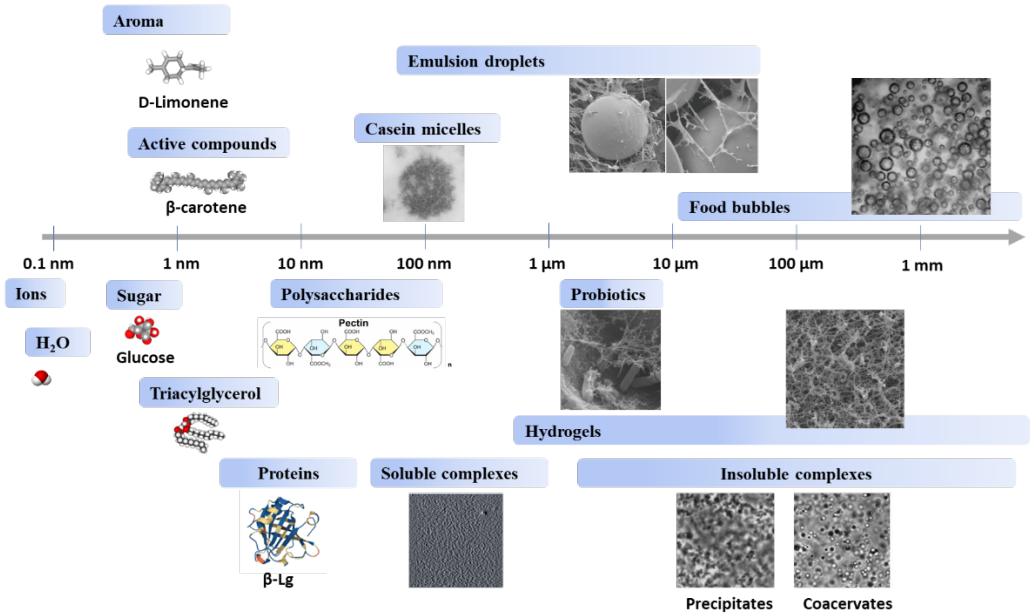

Figure 1.1: Length scales of common components in protein-polysaccharide based delivery systems. The soluble/insoluble complexes were obtained by protein-polysaccharide non-covalent complexation. The microscopy images were reprinted with permission from McMahon & McManus (1998), Wijaya et al. (2017a), Mao et al. (2019), Wijaya et al. (2017b), Girard et al. (2004)*,* Jones et al. (2010)*,* Mekhloufi et al. (2005)*, and Narchi et al. (2009). The 3D structure of β-Lg (1BEB) follows from RCSB PDB.*

One emerging application of these food colloids is to act as nano-/micro delivery vehicles, which are designed to encapsulate, protect, and control the release of functional ingredients. A lot of functional ingredients may benefit from using a delivery system. They include micronutrients, nutraceuticals, pigments, lipids, antimicrobials, antioxidants, probiotics, and flavours, which are usually isolated and purified from natural sources. The formulation of these functional ingredients into food systems is usually limited by their chemical instability, limited solubility, undesirable flavour/taste, poor handling characteristics, unwanted release profile, poor viability (e.g. for probiotics) and low bioavailability (Garti & McClements, 2012). In this context, food proteins attracted considerable attention since the structural and physicochemical attributes of food protein that can greatly facilitate the functionality of delivery systems, as discussed above. Moreover, the combination of polysaccharides

(e.g. indigestible and charged polysaccharide) with proteins may further modify and extend the functional performance of proteins.

In addition to the fabrication of colloidal structures, a delivery system also requires more intelligent manipulation of protein-polysaccharide interactions either at the O/W interface or in bulk so that the encapsulated ingredients can be delivered on demand. Moreover, the response behavior and fate of these biopolymer-based structures upon exposure to changing environmental conditions (e.g. food processing, gastrointestinal digestion) must be understood.

1.2 Food proteins and polysaccharides

1.2.1 Food proteins

Proteins are macromolecules that comprise one or more long chains of amino acid residues. There are four distinct levels of protein structure to describe a protein. The primary structure of a protein refers to the sequence of amino acids bound together through peptide bonds in the polypeptide chain. The secondary structure refers to highly regular local sub-structures on the polypeptide chain, including two main types, i.e. α-helices and β-strands. They are mainly defined by patterns of hydrogen bonds between the main-chain peptide groups. The tertiary structure refers to the 3D structure created by a single polypeptide chain, which may include one or several domains. Here, the secondary structures are folded into a compact globular structure driven by specific interactions, such as hydrophobic interactions, salt bridges, hydrogen bonds and disulfide bonds. The quaternary structure is the 3D structure consisting of the aggregation of two or more individual polypeptide chains (subunits) that operate as a single functional unit (multimers). The formation of quaternary structure is driven by non-covalent interactions and disulfide bonds as in tertiary structure. As such, proteins from different biological origins exhibit varying characteristics, including amino acid composition, conformation, electrical properties, molecular weight, surface activity and hydrophobicity.

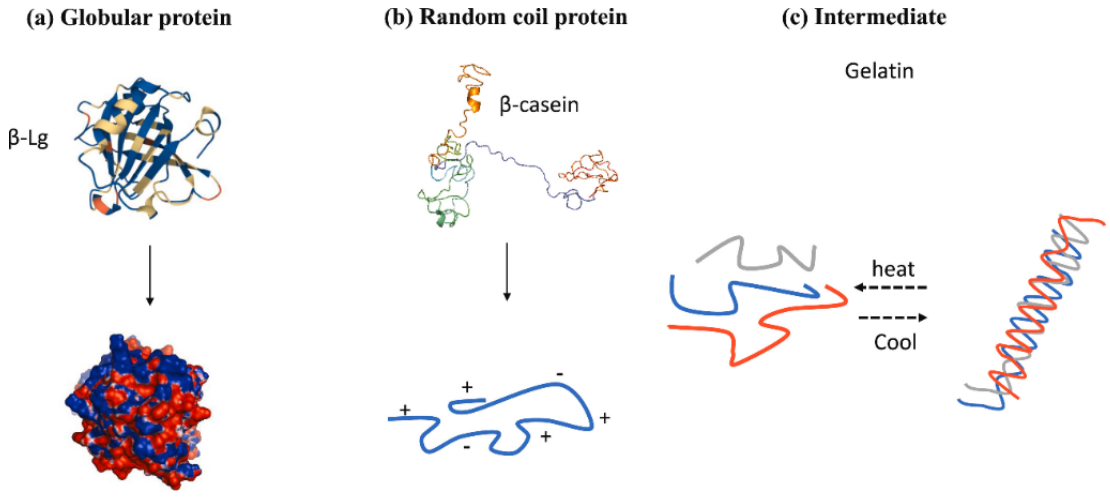

Figure 1.2: Schematic representation of the physical description of food proteins. (a) a folded globular protein (β-lactoglobulin: 1BEB from RCSB PDB), charge distribution of the β-lactoglobulin molecule at neutral pH visualized by PyMOL (red and blue indicate negatively charged and positively charged spots, respectively); (b) a predicted structure of β-casein, which can be seen as an ampholytic polyelectrolyte, containing both positive and negative charges; (c) the intermediate case of gelatin, showing a reversible temperature-dependent molecular conformation.

Native proteins tend to adopt three-dimensional (3D) conformations in which the total free energy is minimized (Figure 1.2), which are generally divided into globular (folded) proteins and random-coil (unfolded) proteins (Mezzenga & Fischer, 2013). For the globular proteins, the more hydrophilic groups are exposed to water, whereas the more hydrophobic segments are confined within the interior. For instance, whey protein fractions (e.g. β-lactoglobulin (β-Lg) and α-lactalbumin), lysozyme, ovalbumin and soy globulins are naturally present in the globular conformation. Generally, the 3D structure of a globular protein can be readily altered upon heat treatment (e.g. above the denaturation temperature) at various pH and ionic strength conditions. For instance, β-Lg molecules unfold and subsequently self-assemble into various aggregates upon heating, such as rod-like fibrils at pH 2.0 (also with acid hydrolysis), spherical microgels at pH 5.8, or worm-like fractals at pH 7.0 (Jung et al., 2008).

In contrast, the random coil proteins present an unstructured or unfolded state (Figure 1.2b). Common examples are the main fractions of casein micelles, such as β-casein, and α-casein. Furthermore, some proteins behave differently from these two types,

such as gelatin. The structure of gelatin can be reversibly controlled by temperature variations (Figure 1.2c).

Proteins are charged biopolymers because of the ionization of basic side groups (e.g. -NH_2 to -NH_3^+) and acidic side groups (e.g. -COOH to -COO^-) in amino acid residues as a function of pH. The charge distribution along a poly-peptide chain is usually heterogeneous. For instance, globular β-Lg exhibits a net negative charge at pH 7.0 but still contains many positively charged groups on its surface (Figure 1.2a). This is also the case for random-coil proteins exhibiting a chain-like structure. The is also the case for flexible protein exhibiting a chain-like structure. The iso-electric point (IEP) of a protein can be determined by isoelectric focusing or estimated from the zeta potential of the protein as a function of pH, corresponding to a balance between the amount of positive and negative charges.

1.2.2 Food polysaccharides

Polysaccharides are the most abundant carbohydrates found in food. They are long-chain polymeric carbohydrates composted of monosaccharides units connected by glycosidic linkages. Polysaccharides are often extracted from plants (e.g. cellulose, starch, pectin), algae (sodium alginate, carrageenan), shellfish (chitin), bacteria (xanthan gum) or fungi (beta-glucan) (Cui, 2005). Their molecular properties (such as charge density, molecular weight, conformation, gelation characteristics, and viscosity) are largely determined by the nature of their monosaccharide units. Besides, some natural extracts (e.g. gum Arabic, soluble soybean polysaccharides and sugar beet pectin) are essentially protein-polysaccharide conjugates and exhibit surface activities (Nakauma et al., 2008).

Polysaccharides can be classified into three types according to the charged group(s) on their monomer unit: anionic type, cationic type and neutral type. Common anionic groups include carboxyl groups (e.g. -COO^- in pectin and alginate) and sulphate groups (e.g. -SO_4^- in carrageenan). These polysaccharides have less negative charge at lower pH due to the protonation effect. Chitosan has a few amino groups (-NH_2), which exhibit a soluble, protonated cationic form (-NH_3^+) in acidic to neutral solutions. Besides, there are some neutral and uncharged polysaccharides with reducing ends

(e.g. dextran), which can be used to fabricate Maillard conjugates with proteins (Wooster & Augustin, 2006).

1.3 Protein-polysaccharide interactions

1.3.1 Non-covalent interactions

Four specific types of phase phenomena may be observed in mixed protein-polysaccharide solutions, including soluble complexes (I), insoluble complexes/ coacervates (II), co-solubility (III) and segregation (IV) (Figure 1.3). The phase behavior of a mixed protein-polysaccharide solution may be driven by electrostatic interactions, hydrogen bonds, and hydrophobic interactions (Doublier et al., 2000; Girard et al., 2002), which can be influenced by a wide range of factors, including pH, ionic strength, temperature, nature of the biopolymers, and mass ratios. An early study indicated that the complexation between β-lg and pectin was mainly driven by electrostatic interaction as the pH was lower than the protein IEP (Girard et al., 2002). Another work indicated that the formation of gelatin-pectin complexes when the pH was higher than the IEP of gelatin was ascribed to the formation of hydrogen bonds and local electrostatic interactions (Antonov et al., 1996). Additionally, hydrophobic interactions were demonstrated to be related to the interactions between β-lg and synthetic (amphiphilic) polyelectrolytes with different hydrophilicity (Gao & Dubin, 1999).

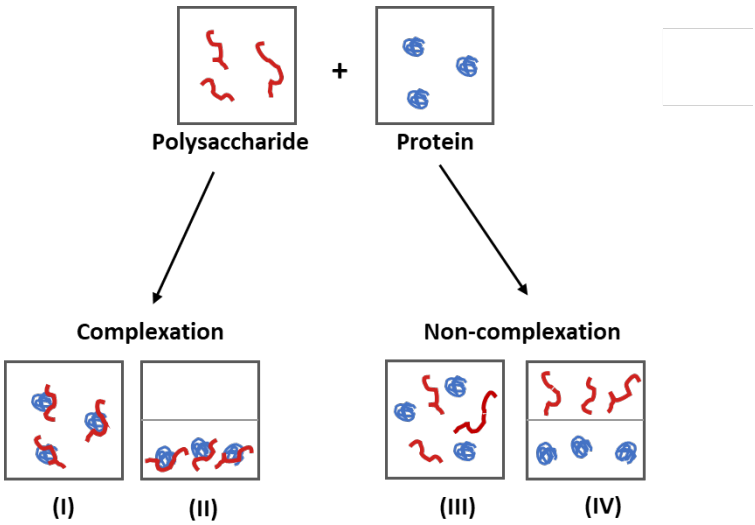

Figure 1.3: Schematic representation of protein-polysaccharide non-covalent interactions in solution: soluble complexes (I), insoluble complexes/coacervates (II), co-solubility (III) and segregation (IV).

1.3.1.1 Complexation

Complexation happens at favorable conditions for associative interactions, i.e. net attractive interactions existing between proteins and polysaccharides. Soluble complexes can be formed when the net charge is far from neutral due to the repulsive interactions between residual charges of the biopolymers. Besides, the formation of soluble complexes is also facilitated when the polysaccharide contains a certain amount of neutral sugar side chains (e.g. soluble soybean polysaccharide) (Li et al., 2019). The particle size of these soluble complexes (In Figure 1.3 I) is generally in the submicron range, and they exhibit a relatively low settling velocity (as discussed later).

In contrast, when the charge of the resulting complexes is close to neutral, large and insoluble complexes (e.g. several micrometers) can be typically observed, leading to a two-phase system within hours or days. One precipitated phase has both biopolymers in a complex matrix and another upper phase contains mainly the solvent water or is depleted in both biopolymers (Figure 1.3 II). Apart from the precipitation phenomena, it should be noted that the associative complexation between proteins and polysaccharides may also lead to a liquid-liquid phase separation phenomenon and produce coacervate droplets, e.g. the complexation between gelatin and gum Arabic. These coacervate droplets are capable of wetting the O/W interface and have been used to design microcapsules (Ducel et al., 2005; Rousi et al., 2019).

The so-called soluble or insoluble complexes can be described by Stokes' law (Equation 1.1) and the settling velocity (v) of these complexes can be estimated. Accordingly, v is proportional to the square of the particle hydrodynamic radius and to the ratio of density difference relative to dynamic viscosity. Note that this model only applies to rigid particles at infinite dilution. In concentrated systems, the phase volume of the particles cannot be neglected (Wagoner et al., 2016).

$$v = \frac{2}{9}\frac{(\rho_p - \rho_f)}{\eta} g r^2 \qquad (1.1)$$

Where v is the velocity of sedimentation in m/s, ρ_p is the density of the particles (i.e. complexes) in kg/m^3, ρ_f is the density of the continuous fluid in kg/m^3, g is the gravity field strength in m/s^2, r is the hydrodynamic radius in m, and η is the dynamic viscosity of the continuous phase in kg/m·s.

1.3.1.2 Non-complexation (co-solubility and segregation)

Co-solubility and segregation are observed under unfavorable conditions for associative interactions whereby both biopolymers carry the same charge sign or are uncharged. In diluted solutions, biopolymers can be co-soluble (Figure 1.3 III) due to the absence of intermolecular attraction. At high concentrations, the enthalpy of mixing exceeds the entropy difference and there is a relatively high positive free energy of mixing. Consequently, the biopolymers prefer to be surrounded by identical molecules, leading to phase separation into two distinct immiscible phases, whereby one phase is rich in protein (and poor in polysaccharide) and the other phase is rich in polysaccharide (and poor in protein), as shown in Figure 1.3 IV. Water-in-water emulsions can be prepared based on this phenomenon (Nicolai & Murray, 2017).

1.3.2 Covalent interaction

Proteins and polysaccharides can be linked by covalent bonds to form intermolecular complexes, referred to as covalent conjugates. A common method to fabricate protein-polysaccharide covalent conjugates is through the Maillard reaction, which involves a series of complicated chemical reactions. Among them, the early-stage condensation reaction between the carbonyl group at the reducing end of polysaccharides and the amino group of a protein is of great interest to food researchers in this field (de Oliveira et al., 2016). This reaction is also called protein glycation, which does not require additional chemicals as it occurs naturally under controlled conditions of temperature, incubation time, pH, and moisture. Besides, some enzymes can induce the conjugation of protein and polysaccharide. For instance, laccase has been used to cross-link proteins and certain types of polysaccharides containing ferulic ester groups (e.g. sugar beet pectin) (Li et al., 2021). Due to the presence of a minor protein moiety in gum Arabic, transglutaminase has been adopted to prepare casein-gum Arabic conjugates (Flanagan & Singh, 2006). Recently, it has been reported that casein-propylene glycol

alginate conjugates can be prepared in alkaline conditions through a transacylation reaction (Li & Zhong, 2021).

1.4 Food emulsion basis

Emulsions are dispersions of liquid droplets in an immiscible phase, e.g. oil-in-water (O/W) emulsions and water-in-oil (W/O) emulsions, which are widely present in foods, pharmaceuticals, and personal care products. There are more complex systems, such as water-in-oil-in-water (W/O/W) and oil-in-water-in-oil (O/W/O) multiple emulsions. All food emulsions are thermodynamically unstable systems that will eventually destabilize with time. The thermodynamic instability of emulsions can be understood by comparing the Gibbs free energy of an oil/water mixed system before and after emulsification (Equation 1.2).

$$\Delta G = \gamma \Delta A - T\Delta S_c \approx \gamma \Delta A \qquad (1.2)$$

Where ΔG is the change in Gibbs free energy, γ is the oil-water interfacial tension, ΔA is the change in contact area between the oil and water phases, T is the absolute temperature, and ΔS_c is the change in configurational entropy.

In this equation, the $\gamma \Delta A$ contribution is always positive upon emulsification, whereas $-T\Delta S_c$ is negative but it is usually several orders of magnitudes smaller than $\gamma \Delta A$. Therefore, the emulsion formation is usually thermodynamically unfavorable. It should be noted that there are some exceptions where the interfacial tension is very small, and the overall system is thermodynamically favorable. In this case, a spontaneous emulsification process occurs, and the produced emulsion is called a microemulsion. The positive ΔG also indicates that the formation of emulsions requires energy input. Additionally, the presence of surface-active ingredients (also called emulsifiers) can reduce the interfacial tension, making it easier to prepare emulsion droplets in a smaller size.

Some low molecular weight surfactants (LMWS) have been widely used as emulsifiers, e.g. tween 80, or sodium stearoyl lactylate. They are very effective to reduce the O/W interfacial tension and stabilize O/W emulsions due to a special molecular structure consisting of a hydrophobic tail and a hydrophilic head. Likewise, food biopolymers (e.g. proteins, polysaccharides, and glycated proteins) with amphiphilic characteristics

also exhibit surface activity, though these biopolymers are generally less effective than LMWS to reduce the O/W interfacial tension. Food emulsions tend to destabilize during storage and processing. An overview of possible destabilization mechanisms in O/W emulsions is illustrated in Figure 1.4.

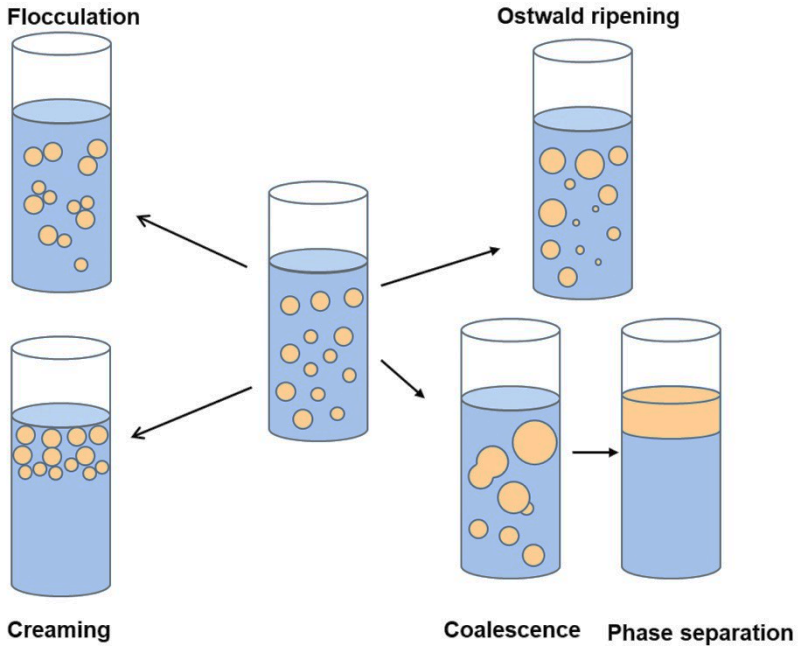

Figure 1.4: An overview of common emulsion destabilization mechanisms in an O/W emulsion. Note: the blue color indicates the continuous water phase, whereas the yellow color indicates the oil phase (with a lower density than the continuous phase).

1.5 Fundamentals of whey proteins

1.5.1 Whey proteins and the major fraction (β-Lactoglobulin)

Whey is a by-product during the manufacture of cheese or casein. It contains around 20% of the total bovine milk protein (Deeth & Bansal, 2018). In Table 1.1, the major whey proteins comprise β-lactoglobulin (β-Lg), α-lactalbumin (α-La), and bovine serum albumin (BSA). There are also some minor fractions, e.g. immunoglobulins, and lactoferrin. Whey protein isolate is a type of high-purity (usually 90%) protein powder. Nowadays, it is usually produced from pasteurized whey through ion-exchange technology, followed by isolation and spray-drying.

β-Lg has a molecular weight of 18.4 kDa, corresponding to a polypeptide chain of 162 residues. Its secondary structure comprises nine β-strands and one three-turn α-helix;

eight of the β-strands fold up into a flattened β-barrel (i.e. a cavity). At neutral pH, β-Lg exists in a dimeric form, as shown in Figure 1.5. One β-Lg monomer contains two disulfide bonds that are important to retain its folded globular structure and one free thiol group.

Table 1.1: Major protein fractions in bovine milk whey and their properties.

Protein	Percent (%)	Molecular weight (kDa)	Isoelectric point	Number of disulfide bond	Number of free thiol group
β-Lg	50-55	18.4	5.2	2	1
α-La	20-25	14.2	4.2	4	0
BSA	1-6	66.4	4.5-4.8	17	1

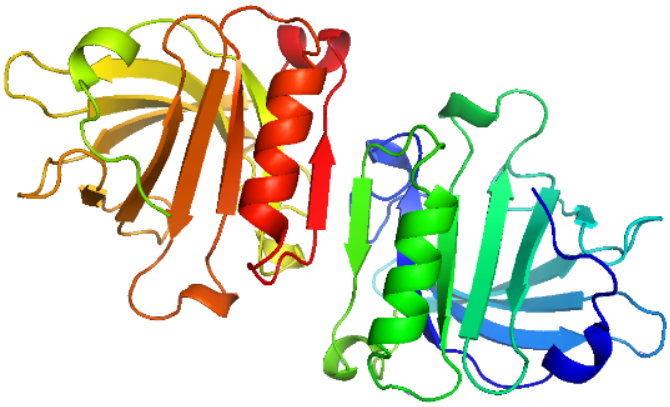

Figure 1.5: Molecular structure of a β-Lg dimer (molecular weight 36.8 kDa) The protein structure (IBEB) is obtained from RCSB PDB and visualized by PyMOL.

Besides, this overall globular conformation allows β-Lg to bind a wide range of hydrophobic ligands within its central cavity. This type of protein is classified as a lipocalin (Flower, 1996). Some variants of β-Lg are also found, mainly β-Lg A and β-Lg B. These two variants are structurally very similar and only vary in two amino acid residues (Deeth & Bansal, 2018). β-Lg has a remarkable stability at low pH even at pH 2.0. However, it denatures at alkaline pH. At the intermediate pH, β-Lg exhibits a dimer-monomer equilibrium depending on the pH (Brown, 1993; Stender et al., 2019). Generally, at pH 1.8-4.0, the monomer form is dominant with increasing dissociation

as the pH is lowered. In the pH 4.0-5.2 region, larger oligomeric structures are reversibly formed due to the proximity of the IEP. At pH 5.2-7.5, β-Lg mainly exists in the dimeric form.

1.5.2 β-Lg at fluid-fluid interfaces

Since proteins are amphiphilic molecules, they are able to adsorb onto fluid-fluid interfaces, e.g. oil-water and air-water interfaces. For instance, β-Lg exhibits good interfacial activities and is effective to reduce the interfacial tension of the interfaces, stabilizing emulsions and foams. Upon adsorption at the interfaces, globular β-Lg undergoes conformational changes (e.g. unfolding), where some (previously hidden) hydrophobic amino acids become oriented towards the hydrophobic phase (oil or air) and hydrophilic amino acids toward the more hydrophilic phase (water). These conformational changes are also called surface denaturation. Moreover, these adsorbed protein molecules at interfaces form a membrane-like (viscoelastic) film around oil droplets due to intermolecular non-covalent and even covalent interactions (e.g. through disulfide bonds) (Dickinson & Matsumura, 1991). The interfacial rheology (e.g. interfacial shear viscosity) can be used to describe the lateral interactions between the adsorbed β-Lg molecules.

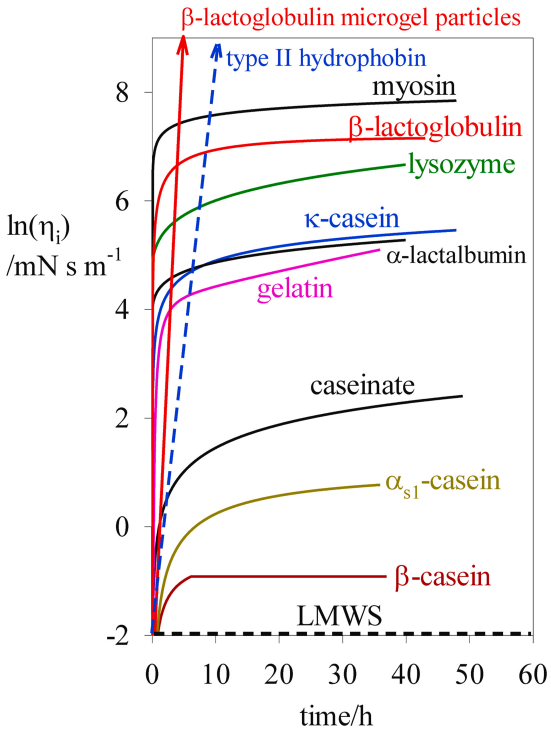

Figure 1.6: Evolution of the interfacial shear viscosity for adsorbed films of various food proteins as a function of adsorption time at the n-tetradecane–water interface (bulk protein concentration = 10^{-3} wt%, pH = 7, 20-25 °C). The dashed horizontal line represents typical values for LMWS and surface-active lipids, i.e., below 0.1 mN s m^{-1}. Image taken from Murray et al. (2021)

In Figure 1.6, it can be observed that globular proteins (β-Lg, lysozyme) have a much higher interfacial viscosity than flexible proteins (e.g. casein fractions). Moreover, the interfacial shear viscosities of proteins are much higher than those of LMWS. The rheological properties (i.e. both dilatational and shear rheology) of an interfacial layer have been suggested to be relevant to the stability of emulsions/foams (Murray, 2011). Since different interfacial components exhibit considerably varying rheological response, the interfacial rheology may be a valuable tool to study the dynamic changes within the adsorbed layers at the oil-water interface under changing environmental conditions. Recently, interfacial (both shear and dilatational) rheology and dynamic surface tension have been demonstrated to be useful tools for probing in vitro gastrointestinal digestion of protein-based interfacial films at the O/W interface (Maldonado-Valderrama, 2019; Scheuble et al., 2016).

1.5.3 Ligand binding of β-Lg

β-Lg belongs to the lipocalin family of proteins, which can accommodate hydrophobic ligands within their central cavity. Two additional binding sites for ligands may exist on its outer surface as well. β-Lg can bind ligands of various natures, including fatty acids, vitamins, polyphenols, carotenoids, flavor compounds, metal ions, and pharmaceuticals (Livney, 2010; Shafaei et al., 2017). This list is far from exhaustive. The binding affinity of β-Lg with a hydrophobic compound may be influenced by pH, ionic strength, and temperature. Factors that determine the nature of the protein (e.g. molecular conformation) may influence the binding equilibrium.

Many bioactive compounds are hydrophobic and chemically instable. Upon binding with β-Lg, the aqueous dispersibility and chemical stability of these hydrophobic molecules are generally improved. For instance, the existence of β-Lg obviously suppresses the crystallization of hydrophobic naringenin in water, as well the precipitation of norbixin (Møller et al., 2020; Shpigelman et al., 2014). The

photostability of folic acid can be improved upon complexation with β-Lg (Liang & Subirade, 2012). These benefits upon complexation may further enhance the bioavailability of a bioactive compound after ingestion. β-Lg is a stable protein at pH 2.0 even in the presence of pepsin due to its compact structure. Therefore, β-Lg may function as a carrier of small hydrophobic ligands which are thus protected during transit in the stomach. In the small intestine, β-Lg is broken down into smaller peptides by trypsin. Accordingly, the ligand binding properties of proteins may aid the design of food-grade delivery systems.

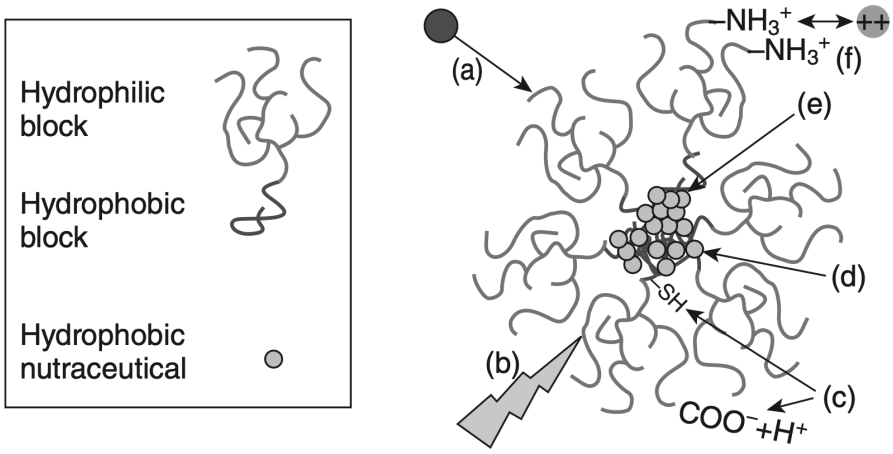

Figure 1.7: The protection mechanisms of hydrophobic compounds by amphiphilic biopolymers and their relevant assemblies. Image taken from Livney (2012)

Livney (2012) proposed some mechanisms for the encapsulation/protection of hydrophobic bioactives by food biopolymers and their relevant assemblies (Figure 1.7), in which the biopolymeric amphiphiles were highlighted. Moreover, the block-wise distribution of hydrophobic and hydrophilic monomers enhances the amphiphilic behaviour. The possible mechanisms include (a) steric shielding from reactants and enzymes; (b) blocking (absorbing or scattering) radiation, e.g. UV; (c) chemical protection, e.g. pH buffering, antioxidant capacity, and free radical quenching by the polymer and its functional groups; (d) immobilization by binding, and sometimes by core vitrification; (e) controlled crystallization of entrapped nutraceuticals; (f) repulsion of oxidizing ions of the same charge-sign.

1.6 Fundamentals of pectin

Pectins are a complex group of structural heteropolysaccharides. They are present in the primary cell walls and middle lamella of many plants, where they are frequently associated with other cell wall components, such as cellulose, hemicellulose, and lignin (Stephen et al., 2016). The physicochemical properties of a pectin may depend on its bio-origin, extraction method, and processing. Commercially available pectins are commonly obtained from apples, citrus, and sugar beet. In the food industry, the degree of esterification of pectin has been one of the most important specifications since it plays an important role in the functional properties of the pectin (e.g. gelation properties, electrical properties).

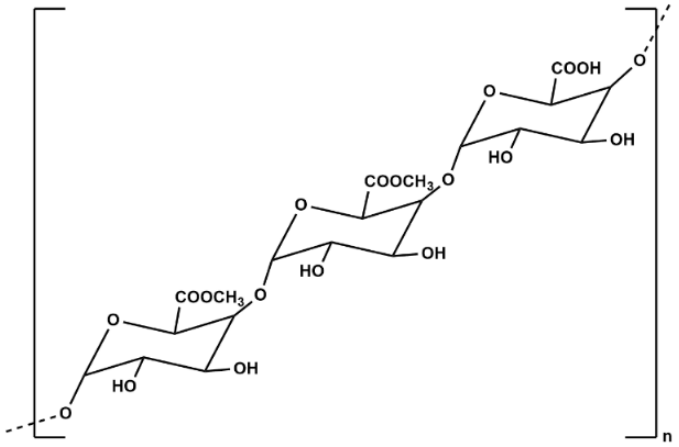

Figure 1.8: Typical repeating and partially methyl-esterified galacturonic acid units in a pectin molecule

The main structure of pectin molecule is a biopolymeric chain of α-1,4-linked galacturonic acid units (Figure 1.8). In natural products, the carboxyl groups along the chain are mainly esterified with methoxy groups. As such, a de-esterification step (e.g. acid, alkali or enzyme treatments) is generally carried out at the industrial level to produce low-methoxy pectin. When the degree of esterification of pectin is higher than 50%, it is called high-methoxy pectin (HMP). In contrast, the DE of low-methoxy pectin (LMP) is less than 50%. Accordingly, LMP has a higher charge density than HMP. There is a considerable amount of carboxyl groups in LMP, which can be crosslinked by divalent cations e.g. calcium ions, and the resulting complex structure can be described by the so-called egg-box model (Stephen et al., 2016). In contrast, the methoxylated carboxyl groups are non-charged and thus cannot bind calcium ions. It

should be noted that the distribution of the methyl esters along the pectin chain may be random or blocky, probably influencing the physicochemical properties of pectin and its interactions with other biopolymers (Biswas et al., 2022; Xu et al., 2018). Pectin is generally considered a hydrocolloid and not effectively surface active. However, some types of pectin ingredients (e.g. citrus HMP, sugar beet pectin) are demonstrated to be surface-active, which are able to adsorb onto the O/W interface and stabilize emulsions (Nakauma et al., 2008; Schmidt et al., 2017).

1.7 Human gastrointestinal digestion: in vivo and in vitro simulation

To design effective delivery systems for controlling the digestion and release of hydrophobic ingredients, it is necessary to understand how a delivery system behaves as it passes through the human gastrointestinal tract. Human digestion can be divided into four successive units: mouth, stomach, small intestine, and large intestine. As shown in Figure 1.9, the focus of the following discussion will be on digestion in the human upper gastrointestinal tract, since the digestion process in the large intestine is primarily determined by gut microbiota.

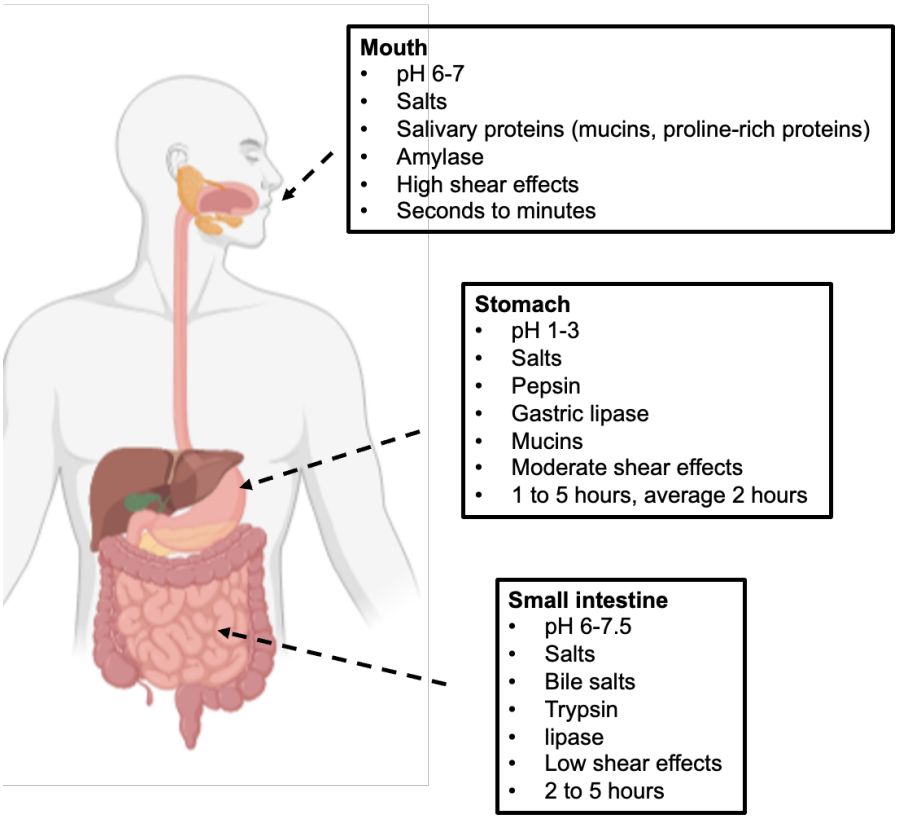

Figure 1.9: Schematic representation of the possible changes in human upper gastrointestinal tract.

The time for foods spent in the mouth ranges from a few seconds to a few minutes depending on the food characteristics (e.g. texture). Saliva in the mouth is a complex fluid that a food system first encounters upon oral consumption. Saliva has a pH between 6 and 7 and contains 99% water and 1% proteins (e.g. mucin, amylase, proline-rich proteins) and low molecular weight salts. Subsequently, the gastric fluids are highly acidic (pH 1-3) and contain two digestive enzymes (pepsin and gastric lipase), salts and mucins. The residence time of a food bolus in the stomach varies from 1 to 5 hours with an average of 2 hours depending on the physiochemical properties of the food. The small intestinal fluids have a pH between 6.0 to 7.5 and contain a mixture of lipolytic (lipase), proteolytic (trypsin, chymotrypsin) and amylolytic enzymes (pancreatic amylase), biosurfactants (bile salts), and salts. The transit time varies from 2 to 5 hours depending on the food type. There are some food components that are not digested or only partially digested in the upper gastrointestinal tract because they are resistant to digestive enzymes. These components will enter the large intestine (colon) and be subjected to microbes. Complicated enzymatic reactions and fermentation may occur in this stage. The residence time can be 12 to 24 hours. Apart from the above physicochemical factors, there are some shear forces or/and peristalsis during various stages of digestion, which may facilitate the mixing of various components, as well as potentially breaking down various structures (e.g. lipid droplets).

Since in vivo trials can be difficult to undertake, expensive, or not justifiable on ethical grounds, in vitro models have been widely used for decades to mimic the digestion of food, which can be divided into static and dynamic methods, aiming to mimic the digestion in the upper gastrointestinal tract. However, even though in vitro dynamic models can better mimic the dynamics of the human digestion process, they are still relatively expensive and complex to set up and maintain for food researchers. Some standardized static models have been shown to be very useful in predicting outcomes of in vivo digestion. The most renowned one among them is the INFOGEST static protocol for food digestion (Brodkorb, et al., 2019), which was adopted in chapter 4 of this dissertation. Because of the relatively short transit time in the mouth for liquid samples, the oral stage was omitted in this work.

1.8 Essential methods

1.8.1 Quartz crystal microbalance with dissipation monitoring

Quartz crystal microbalance with dissipation monitoring (QCM-D) is a surface-sensitive and real-time technique for detecting mass variations on a sensor surface. The detection resolution can be at the nanogram scale. Moreover, the monitoring of dissipation also provides insight into the viscoelastic properties of adsorbed materials on the sensor surface. The basic principle of QCM-D is related to the piezoelectric characteristics of quartz crystals. The word "piezoelectricity" means pressure and the electricity that is generated by the pressure, or vice versa. A typical QCM-D sensor is comprised of a circular piece of quartz sandwiched between two metal electrodes. Therefore, applying an alternating voltage to quartz leads to an oscillatory motion of the crystal lattice (Dixon, 2008). If the frequency of the applied voltage harmonizes the resonant frequency (or its multiples called overtones) of the crystal, the resonance is excited (Reviakine et al., 2011).

The resonance frequency is related to the thickness (mass) of the quartz crystal. If the resonance frequency changes, it is possible to detect thickness (mass) changes (Dixon, 2008). Besides, QCM-D gives information about dissipation. By switching off the applied alternating voltage, the decay time of the crystal's oscillation reflects the viscoelastic properties of the adsorbed materials. Generally, the faster the energy dissipates (or decays) within an adsorption layer, the higher the dissipation value is, which is described as more liquid-like characteristics.

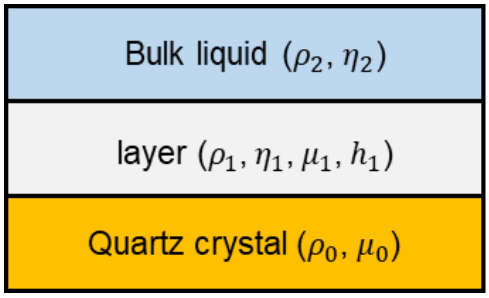

Figure 1.10: Model geometry of a QCM-D sensor during measurement.

If the adsorbed materials form a homogeneous, thin, and rigid layer, there is a linear relationship between the resonance frequency change ($\Delta f/n$) and the adsorbed mass

per unit surface area (Δm), which can be described by the Sauerbrey equation (Equation 1.3). The dissipation (D) is defined by Equation 1.4. A rigid adsorption layer only provides frequency changes, and the dissipation change (ΔD) is close to 0 (i. e. less than 1×10^{-6}).

$$\Delta m = -C * (\Delta f/n) = \rho_1 * h_1 \qquad (1.3)$$

$$D = \frac{E_{dissipated}}{2\pi\, E_{stored}} \qquad (1.4)$$

Where n (= 1, 3, 5....) is the overtone number, and C (=17.7 ng cm^{-2} Hz^{-1} for the AT-cut crystal used) is constant. ρ_1 and h_1 are the density and thickness of the adsorbed layer, as illustrated in Figure 1.10.

When a viscoelastic layer is formed (e.g. $\Delta D > 1 \times 10^{-6}$), the adsorbed mass becomes underestimated by the Sauerbrey equation. The relationship between the QCM-D response and the properties of the viscoelastic layer can be explained by the Kelvin-Voigt model (equations 1.5 and 1.6). More details can be found in Voinova et al. (1999).

$$\Delta f \approx -\frac{1}{2\pi\rho_0 h_0}\left\{\frac{\eta_2}{\delta_2} + h_1\rho_1\omega - 2h_1\left(\frac{\eta_2}{\delta_2}\right)^2 \frac{\eta_1\omega^2}{\mu_1^2 + \omega^2\eta_1^2}\right\} \qquad (1.5)$$

$$\Delta D \approx \frac{1}{\pi f \rho_0 h_0}\left\{\frac{\eta_2}{\delta_2} + 2h_1\left(\frac{\eta_2}{\delta_2}\right)^2 \frac{\eta_1\omega}{\mu_1^2 + \omega^2\eta_1^2}\right\} \qquad (1.6)$$

Where ρ_0 and h_0 are the density and thickness of the quartz crystal piece. ρ_1, η_1, μ_1 and h_1 are the density, shear viscosity, shear elasticity, and thickness of the adsorbed layer. ρ_2 and η_2 are the density and viscosity of the bulk liquid. δ_2 is the viscous penetration depth of the shear wave. ω is the angular frequency of the oscillation.

Note that the shear moduli of the adsorption layer obtained by QCM-D are determined in a high frequency region (e.g. around 10^7 Hz).

1.8.2 Drop shape tensiometry

Drop shape tensiometry is a technique used to measure the interfacial tension using axisymmetric drop shape analysis. The shape of a drop/bubble is determined by the surface tension and external forces (e.g. gravity). The surface tension tends to minimize the surface area and to get the drop in a spherical shape, whereas gravitation/

buoyancy elongates the drop from this spherical shape and typically results in a pear-like shape. The balance can be described by the Young-Laplace equation (1.7) of capillarity. If no external forces other than gravity occur, the pressure difference is a linear function of the elevation (equation 1.8).

$$\Delta P = \gamma \left(\frac{1}{R_1} + \frac{1}{R_2} \right) \qquad (1.7)$$

$$\Delta P = \Delta P_0 + (\Delta \rho) g z \qquad (1.8)$$

Where ΔP is the pressure difference across the interface, R_1 and R_2 are the two principal radii of curvature, and γ is the fluid-fluid interfacial tension. ΔP_0 is the pressure difference at a reference plane and z is the vertical coordinate of the drop measured from the reference plane. g is gravity acceleration. $\Delta \rho$ is the density difference between the two fluids.

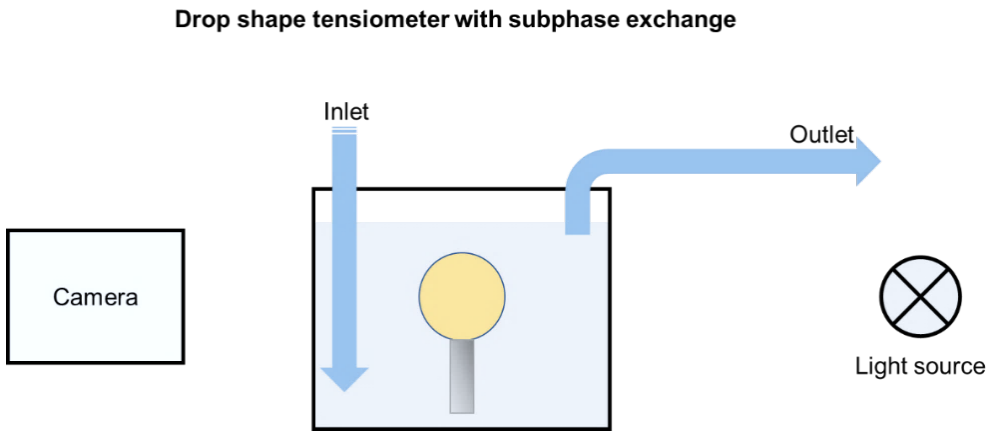

Figure 1.11: Schematic representation of a drop shape tensiometer with subphase exchange

As illustrated in Figure 1.11, a rising oil drop or air bubble is formed at the tip of a capillary tube (i.e. U-shaped needle), surrounded by an aqueous phase, when the continuous aqueous phase has the higher density. A camera is used to capture images of the drop/bubble in real time. The instrument software uses algorithms to analyze the drop's contour and to fit it with models based on the Young-Laplace equation, whereby the interfacial tension γ can be obtained. Besides, a syringe dosing unit can control variations in volume or surface area of the drop at various frequencies and amplitudes (i.e. strain), for instance in a sinusoidal way, resulting in changes in interfacial pressure (i.e. stress). Accordingly, the dilatational rheological properties of

adsorbed layers can be determined. This will be described in chapter 3. Moreover, in this work, the drop shape tensiometry was equipped with a flow-through setup driven by a peristaltic pump in order to enable subphase exchange.

1.9 Objectives and outline of the research

Protein-polysaccharide electrostatic interactions have many applications for the design of novel food formulations. One of the most attractive applications is the construction of colloidal delivery vehicles for hydrophobic ingredients, which are designed to encapsulate, protect, and control the release of these ingredients. However, this requires a better understanding and more intelligent manipulation of protein-polysaccharide interactions under complex environmental conditions. In this context, this dissertation aims to provide deeper insights into protein-polysaccharide electrostatic interactions at the oil-water interface or in bulk, and their responsive behaviors upon exposure to changing environmental conditions (e.g. pH, salt, and gastrointestinal fluids). Specially, the potential application of protein-polysaccharide complexation in two types of delivery systems (i.e. O/W emulsions and intermolecular complexes) was examined. Whey protein isolate (WPI enriched with β-lactoglobulin) and pectin (both low- and high-methoxy pectin) were selected as characteristic models of globular proteins and anionic polysaccharides, resp., because of their well-studied molecular characteristics. Hereby, high- and low-methoxy pectins were compared, since the degree of esterification is expected to influence the pectin's properties (e.g. electrical properties, hydrophobicity) and interactions with proteins.

O/W emulsions exhibit a large surface area to volume ratio, whose properties are mainly determined by their interfacial composition. As such, designing the interfacial layer of oil droplets using proteins and polysaccharides as building blocks may tailor the fate of encapsulated hydrophobic ingredients. However, insights into the interfacial protein-polysaccharide (dis)assembly under various environmental conditions have been very limited at present due to the lack of suitable methodologies that can directly access the complex interfacial phenomena.

Individual protein molecules can also be used as a carrier for small hydrophobic molecules (e.g. polyphenols, carotenoids and vitamins), which is mainly ascribed to the ligand-binding properties of the protein. A typical protein case is β-Lg, as discussed

in section 1.5.3. However, most studies in this field only focused on the interactions between β-Lg and hydrophobic compounds at neutral pH, despite the fact that the acidic pH conditions are more relevant to food systems (e.g. in beverages) and after ingestion (e.g. in gastric fluids). Besides, β-Lg molecules tend to aggregate and precipitate in some acidic beverage applications (pH 4-6) due to the proximity of the protein's IEP. To address these issues, β-Lg and pectin can self-assemble into soluble complexes that exhibit good colloidal stability in the pH range. However, it remains unclear to what extent the pH variations and the complexation with anionic pectin affect the ligand-binding properties of the protein. Figure 1.12 illustrates the three parts of this dissertation in order to address two objectives, as explained below.

a) to employ state-of-the-art techniques to understand real-time and in-situ interfacial assembly and disassembly of WPI and LMP under changing environmental conditions (e.g. pH, salt and gastrointestinal fluids).

   In chapter 2, a QCM-D method was developed to investigate the interfacial interactions of WPI and LMP as a function of pH at a hydrophobic surface that was used to mimic the oil-water interface. The obtained findings were further validated by investigating the WPI-LMP interactions at the triglyceride-water interface using a drop shape tensiometry (modified with a subphase exchange system) technique in chapter 3. In Chapter 4, a multiscale approach (including the previously developed methodologies) from the interfacial level to the bulk emulsion level was employed to evaluate the gastric digestion stability of WPI-pectin adsorption layers.

b) to investigate the effect of pH variation and pectin complexation on the hydrophobic binding sites of β-Lg in the bulk (chapter 5)

   In chapter 5, a fluorescent probe method was used to examine the role of pH variations and electrostatic complexation with polysaccharides in the protein-hydrophobic compounds interactions at a molecular level. Three solvatochromic fluorescent probes, including Nile red, retinol and curcumin, were selected as representative models of hydrophobic compounds bound to the inner cavity or/and the outer surface of β-Lg.

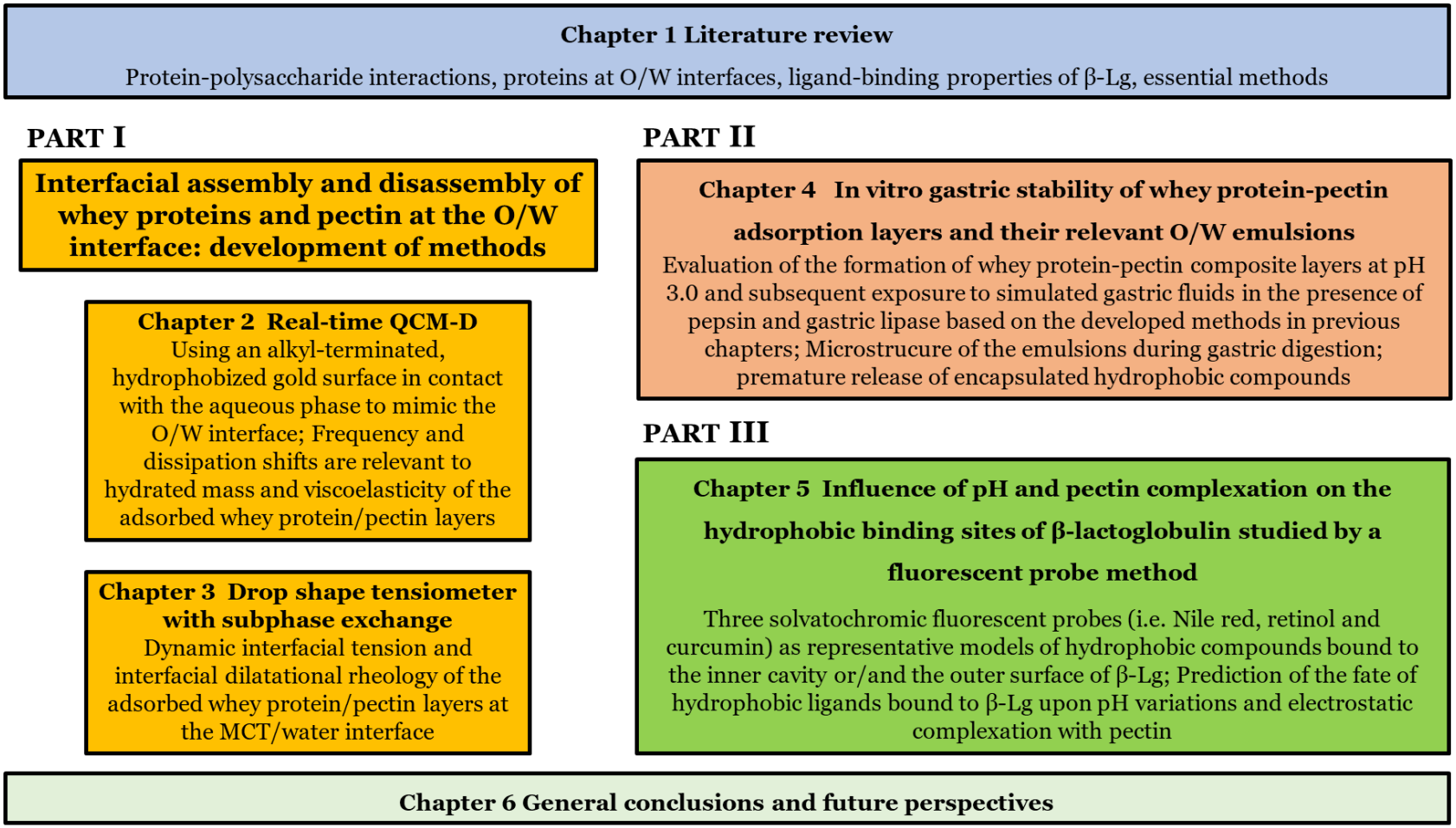

Figure 1.12: Outline of this dissertation

Chapter 2 Electrostatic Interaction Between Whey Proteins and Low-Methoxy Pectin Studied by Quartz Crystal Microbalance with Dissipation Monitoring

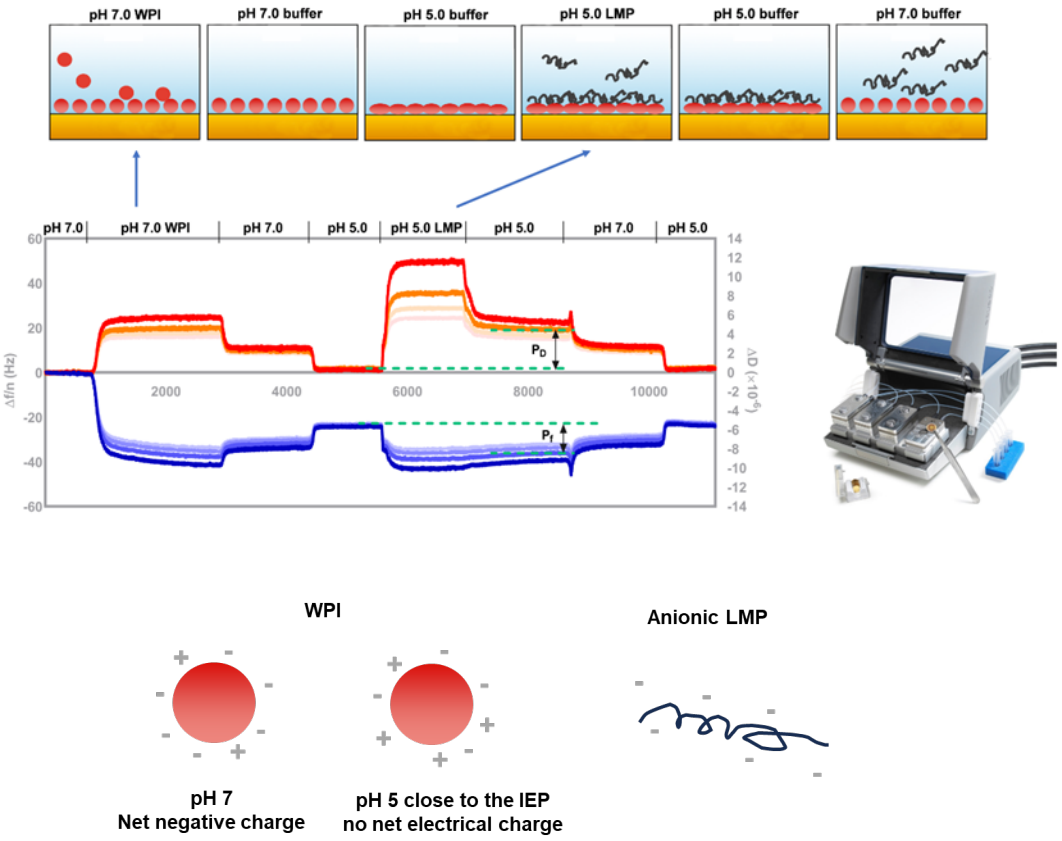

Redrafted from: Li, H., Wu, J., Doost, A. S., Su, J., & Van der Meeren, P. (2021). Electrostatic interaction between whey proteins and low methoxy pectin studied by quartz crystal microbalance with dissipation monitoring. Food Hydrocolloids, 113, 106489. https://doi.org/10.1016/j.foodhyd.2020.106489

Hao Li: Investigation, Conceptualization, Methodology, Software, Writing - original draft, Formal analysis, Visualization. Jianfeng Wu: Writing - review & editing, Formal analysis. Ali Sedaghat Doost: Writing - review & editing, Resources. Jiaqi Su: Writing - review & editing, Paul Van der Meeren: Supervision, Conceptualization, Writing - review & editing, Methodology, Visualization.

Abstract

Electrostatic interaction between proteins and polysaccharides has attracted considerable attention in the design of fluid interfaces with improved performance, e.g. by sequential adsorption. Here, a real-time quartz crystal microbalance with dissipation monitoring (QCM-D) technique was used to investigate the effect of pH on the sequential adsorption of whey proteins and low-methoxy pectin (LMP) on a hydrophobic surface (i.e. alkyl-terminated gold sensor), mimicking the oil-water interface. At neutral pH, whey proteins adsorbed onto the hydrophobic surface and formed a highly hydrated and viscoelastic film. The protein film reversibly became more rigid around its isoelectric point (IEP) due to structural rearrangements. Interfacial complexation of LMP and the pre-adsorbed WPI occurred over a wide pH range (3.0–6.5), but the adsorbed amount of LMP was pH-dependent. Adsorption of LMP increased the viscoelasticity of the pre-adsorbed WPI layer by electrostatic complexation. Especially, some trapped liquid could be released from the interfacial layer due to the relatively strong interaction (e.g. at pH 3.0-4.0). After switching to pH 7.0, the adsorbed LMP was fully detached from the protein layer, suggesting its pH-response behavior. The results indicated that QCM-D is ideally suited to investigate the effect of changing environmental conditions (such as pH) on the characteristics of the adsorbed layer, and to study the interaction between different components by sequential adsorption.

2.1 Introduction

Protein-polysaccharide interactions have received increasing research interest during the last decade due to their potential importance in food engineering and novel food formulations (Dickinson, 2008; Wijaya, Patel, et al., 2017). Among these applications, mixtures of proteins and polysaccharides have been used to prepare dispersions (such as emulsions, and foams) with improved performance (Rodriguez Patino & Pilosof, 2011). For example, the sequential adsorption of polysaccharides onto protein-adsorbed interfaces (also known as the layer-by-layer approach) has been demonstrated to improve the colloidal stability of protein O/W emulsions against a variety of environmental stresses, such as pH changes, thermal processing, elevated ionic strength, and freezing (Guzey & McClements, 2006). Moreover, this approach may alter the interfacial permeability in order to achieve the controlled release of active compounds, as well as prevent destabilization of protein-stabilized droplets during digestion (Benjamin et al., 2012; Scheuble et al., 2014)

Most polysaccharides are more hydrophilic and not effectively surface active. To prepare the bilayer structure, protein-coated droplets should be prepared initially followed by a crucial washing step to remove excess proteins, as complexation in the bulk impedes adsorption kinetics. Subsequently, an oppositely charged polysaccharide is introduced to induce interfacial complexation, which is mainly driven by electrostatic attraction. The amount of polysaccharide added to the primary emulsion is critical, as insufficient polysaccharide may cause bridging flocculation, while excessive polysaccharide may cause depletion flocculation (Cho & McClements, 2009). The pH of the solution may play an important role in the electrostatic attraction-driven interfacial complexation since it determines the degree of ionization of the charged groups in biopolymers. This may further influence the distribution of the polysaccharide at the interface or in the bulk. In this respect, a better understanding of the effect of changing environmental conditions (such as pH) on the interfacial assembly and disassembly of proteins and polysaccharides may provide helpful insights for the rational formulation design of emulsions with tailored functionalities.

Currently, few studies have been successful to investigate real-time protein-polysaccharide interactions at the oil-water interface. In most previous studies, charge

inversion (e.g. zeta potential) has been used to determine adsorption of anionic polysaccharides on protein droplets (Guzey & McClements, 2006). However, charge inversion can not be used as an indicator when the pH is higher than the protein IEP since both the protein and anionic polysaccharide carry a net negative charge. Some common methods (e.g. centrifugation and chemical quantification) can be used to separate and quantify the adsorbed/unadsorbed anionic polysaccharide in protein emulsions. However, they are time-consuming and labor-intensive. More recently, Bertsch et al. (2019) used neutron reflectometry to investigate the interfacial complexation of β-Lg and pectin at the air-water interface, but the time resolution of the techniques is limited and only the thickness of the interfacial layer can be obtained.

In this study, a real-time quartz crystal microbalance with dissipation monitoring (QCM-D) technique was used to study the interfacial protein-polysaccharide assembly/disassembly. To mimic the oil-water interface, the surface of a gold sensor was modified with 1-hexadecanethiol to make an alkyl-terminated, hydrophobized surface (Teo et al., 2016). QCM-D is a surface-sensitive technique, which is able to monitor nanogram-level mass changes in the interface organization in real-time and meanwhile provide viscoelastic information about the interfacial film (Reviakine et al., 2011). Detailed information regarding the interfacial film (such as adsorption/desorption, competitive adsorption, swelling/collapse, thickness, and viscoelasticity) may be obtained from the QCM-D technique (Cardoso et al., 2016; Lee et al., 2017; O'Neal et al., 2018). However, few studies have attempted to investigate the inter-/intra interactions between food biopolymers at oil-water interfaces using this technique. Teo et al. (2016) proposed a hydrophobically modified gold sensor to mimic the oil-water interface. The interfacial assembly of two types of protein at the sensor surface was found to be similar to what happened at the real oil-water interface, suggesting that QCM-D may be useful to probe the complex interfacial phenomena of food biopolymers at interfaces. Pinďáková et al. (2019) applied QCM-D to characterize the deposition of cellulose nanocrystals onto a casein layer at pH 3.0 at a silicon dioxide surface. To our knowledge, there has been no systematic QCM-D study investigating protein-polysaccharide electrostatic interactions at an O/W mimicking interface.

In this work, whey protein isolate (WPI, enriched with β-lactoglobulin) and low-methoxy pectin (LMP) were selected as models of globular proteins and anionic

polysaccharides. Since their molecular characteristics have been well studied, this combination is a good model for studying protein-polysaccharide interactions found in soft matter systems such as food emulsions. Initially, the WPI was adsorbed onto the hydrophobic surface at neutral pH. Subsequently, the characteristics of the WPI adsorbed layer were studied both below and above its isoelectric point (IEP). Afterward, LMP was introduced to investigate the interfacial complexation as a function of pH. Finally, the pH-responsive disassembly behavior of the mixed biopolymer layer was explored.

2.2 Materials and Methods

2.2.1 Materials

Whey protein isolate was obtained from Davisco Foods International, Inc. (BiPro, Le Sueur, MN, USA). According to the manufacturer, it contains 92.6% of protein, whereas about 85% of the total protein consists of β-lactoglobulin. Its protein profile was analyzed by SDS-PAGE (Figure A1 in Annexes). Low-methoxy pectin (Unipectine OB700) with a degree of esterification between 33 and 38% was received from Cargill (Ghent, Belgium) and contained 89.6% of dry matter. The average molecular weight of the LMP is 45.6 kDa, as determined from its intrinsic viscosity (i.e. 245 mL/g) in 0.155 M NaCl at 25°C using the Mark-Houwink-Sakurada equation: $[\eta] = K{M_W}^{\alpha}$, with K and α equal to 1.4×10^{-4} and 1.34, resp. Besides, it was also characterized by a broad molecular weight distribution (De Vries et al., 1982; Setiowati et al., 2019). 1-hexadecanethiol (95%) was purchased from Sigma-Aldrich Corp. (St. Louis, MO, USA). Water used for all experiments was purified by a Milli-Q system (Millipore Corporation, USA). All other chemicals were of analytical grade.

2.2.2 Solution preparation

WPI solution (1%, w/w) was prepared by dissolving the WPI powder in 20 mM sodium phosphate buffer (pH 7.0). After stirring at room temperature for 2 h and standing at 4 °C overnight, the WPI solution was filtered using a 0.45 μm mixed cellulose ester (MCE) membrane to remove insoluble material. LMP was dissolved in 20 mM sodium acetate buffer (pH 3.0, 3.5, 4.0, 5.0, or 5.5) or 20 mM sodium phosphate buffer (pH 6.0, 6.5, or 7.0) at a concentration of 0.4% (w/w). The LMP solution was stirred

overnight to facilitate its dissolution, followed by centrifugation at 4000 g for 20 min to remove insoluble materials. The solution pH was readjusted with 1M HCl or NaOH if necessary.

2.2.3 Preparation of self-assembled monolayers (SAMs) on gold

Clean gold-coated crystal sensors (4.95 MHz, QSX 301) placed in a holder were immersed in 2 mM 1-hexadecanethiol in ethanol for at least 20 h to prepare the hydrophobically modified surface at 25 ˚C. Afterward, the gold sensors were thoroughly rinsed with ethanol and dried with clean air. The contact angle of the modified gold sensors with distilled water was determined by drop shape analysis (KRÜSS, DSA)

2.2.4 Cleaning procedures for gold sensors

The gold sensors were treated within a UV/ozone chamber for 10 min and soaked in basic piranha solution which consists of Milli-Q water, 25% ammonia, and 30% hydrogen peroxide mixed at a volume ratio of 5:1:1 at 75 °C for 10 min (Höök et al., 2001; Teo et al., 2016). Subsequently, the sensors were rinsed with Milli-Q water and dried with clean air. The dried sensors were placed in the UV/ozone chamber again for 10 min.

2.2.5 QCM-D protocols

A Q-sense E4 system was used for all experiments. Prior to the measurements, the tubing and sample chamber (Biolin Scientific, Sweden) were cleaned with a 2% soap (Hellmanex II) solution for 40 min with a flow rate of 0.5 mL/min and afterward with Milli-Q water overnight at a flow rate of 0.1 mL/min. The flow rate in the following experiments was also kept constant at 0.1 mL/min. All the QCM-D experiments were performed at 22 °C. The experiment was started by pumping 20 mM buffer solution (pH 7.0) into the QCM-D chamber until a stable baseline was obtained. Subsequently, the WPI solution (1%, w/w) was introduced into the QCM-D chamber and afterward the pH 7.0 buffer was used to remove excess or loosely bound WPI. To investigate the effect of pH on the characteristics of the adsorbed protein layer, it was rinsed repeatedly with pH X and pH 7.0 buffers (with X = 3.0, 4.0, 5.0 or 6.0).

To study the interfacial complexation of WPI and LMP as a function of pH, the adsorbed WPI at pH 7.0 was rinsed with a pH Y buffer (Y = 3.0, 3.5, 4.0, 4.5, 5.0, 5.5, 6.0, 6.5 or 7.0). Subsequently, LMP (0.4%, w/w) dissolved in the corresponding buffer was introduced to contact the WPI layer. Finally, a rinsing step was performed to remove excess LMP. Besides, to compare the characteristic differences in the interfacial film before and after introducing LMP, the frequency change and dissipation change were termed as $P_{f/n}$ and $P_{D,}$ respectively. Since the $\Delta f/n$ and ΔD after rinsing excess LMP were continuously changing (especially for data at pH 3.0-5.0) in a slow way and hard to reach stable values, the average $\Delta f/n$ and ΔD were collected after around 15 min of equilibration time.

Since the shifting of various buffer solutions used for pH adjustment also results in QCM-D response (via slight changes in density or viscosity), a control experiment was performed. A stable baseline was first established by the 20 mM phosphate buffer (pH 7.0). Subsequently, the hydrophobically modified gold surface (without protein or polysaccharide) was contacted with pH Y buffers in sequence. The obtained frequency or dissipation shifts between the pH 7.0 and the pH Y buffers were used to correct the above data. After eliminating the effect of the bulk liquid, the frequency or dissipation shifts were only caused by the changes in the adsorbed layer.

Data analysis was performed using QTools software 30.15.553 (Biolin Scientific). For a rigid adsorbed layer, the linear relationship between normalized frequency change ($\Delta f/n$) and adsorbed mass is given by the Sauerbrey model as described in Section 1.8.1. In this work, the adsorbed mass and shear moduli of the viscoelastic WPI layer were analysed by the Kelvin-Voigt model. Unless stated differently, the density of the protein layer was assumed to be 1200 kg/m^3. Note that the latter model is still not perfect to analyse monolayers of globular proteins or any other discrete nanoscale particles because of the lateral heterogeneity of this type of film (Reviakine et al., 2011). In this work, we mainly focus on the semi-quantitative analysis of the QCM-D data, and it is powerful enough to characterize the interfacial assembly/disassembly of protein and polysaccharide.

2.2.6 Atomic force microscopy (AFM)

The AFM instrument used during all experiments is the nanowizard 4™ with a manual stage (JPK BioAFM, Bruker). All imaging experiments were performed using a triangular cantilever on the DNP-S10 chip (cantilever A) which has a nominal spring constant of 0.35 N/m and a nominal tip radius of 10 nm (Bruker, https://www.brukerafmprobes.com/p-3256-dnp-s10.aspx). All images were acquired in the Quantitative Imaging® mode using a setpoint of 8 nN. All data processing of AFM measurements was performed in the JPK SPM DP software. After preparing the sensor surface, the gold sensors were taken out from the QCM-D chambers and put into a 3 cm petri-dish. Subsequently, the pH 7.0 sodium phosphate buffer was added into the petri-dish to fully immerse the sensors and then scan the sensor surface in the liquid medium.

2.2.7 Statistical analysis

Data were presented as the mean ± standard deviation of at least three independent experiments. Data analysis was conducted with GraphPad Prism 8.0 software (San Diego, USA). The difference between samples was evaluated using one-way ANOVA analysis or t-test analysis. All statements of significance were based on the 0.05 probability level.

2.3 Results and discussion

2.3.1 Adsorption of WPI onto the hydrophobic surface

WPI consists of three principal proteins, i.e. β-lactoglobulin (β-Lg), α-lactalbumin, and bovine serum albumin. All of them are globular proteins with amphiphilic character, which are able to adsorb onto the O/W interface and stabilize oil droplets (Mezzenga & Fischer, 2013). Here, the gold-coated sensors were hydrophobically modified by 1-hexadecanethiol to simulate the O/W interface. The thiol group (SH) of 1-hexadecanethiol molecule can be immobilized onto the gold surface through covalent bond, and a stable self-assembled monolayer (SAM) can be readily formed (Bain et al., 1989; MacCarini et al., 2005). The successful preparation of the SAM on the gold surface was confirmed by a water contact angle of 105±2° (as compared to around 70° before modification), suggesting its hydrophobic nature. Note that the adsorption of proteins here is mainly driven by molecular diffusion, and its timescale is orders of

magnitude longer than typical adsorption times encountered for most emulsifiers during a high-energy emulsification process (e.g. homogenization).

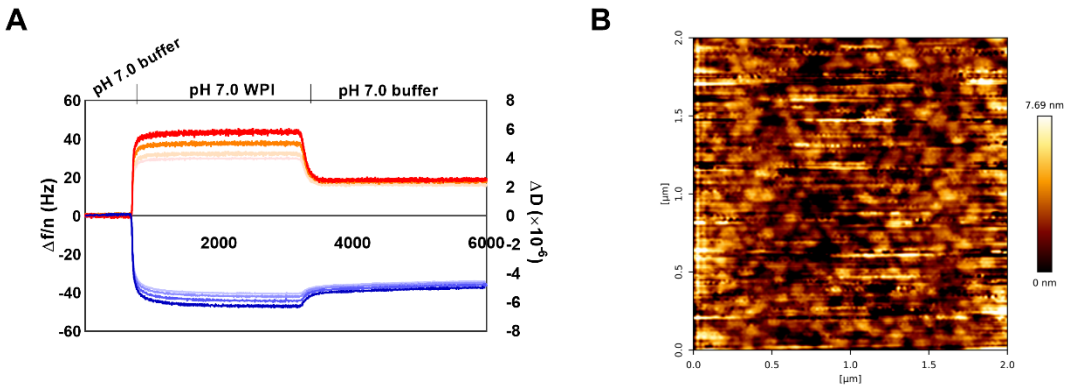

Figure 2.1: (A) Normalized frequency (blue, left axis) and dissipation (red, right axis) shifts as a function of time (s) for the 3rd, 5th, 7th, and 9th overtones (with fading colors for increasing overtones) upon contacting the hydrophobically modified surface with a 1% WPI solution at pH 7.0; (B) AFM image of the WPI-adsorbed surface observed in the 20 mM pH 7.0 sodium phosphate buffer.

Figure. 2.1A shows the frequency and dissipation shifts as a function of time for the 3rd, 5th, 7th, and 9th overtones upon contacting the hydrophobized gold surface with 1% (w/w) WPI solution at pH 7.0. Initially, the baseline was established with a clean pH 7.0 buffer. After introducing WPI, a sudden decrease in normalized frequency Δf/n was observed, reaching -44, -42, -40, and -39 Hz at saturation for the 3rd, 5th, 7th and 9th overtone, respectively. It was also accompanied by increased dissipation, reaching 5.7×10^{-6}, 4.9×10^{-6}, 4.2×10^{-6}, and 3.8×10^{-6} at saturation at the 3rd, 5th, 7th and 9th overtone, respectively. These shifts mostly occurred within the first 50 s. Since the QCM-D response is not only affected by interfacial adsorption but also by the bulk changes (i.e. viscosity and density differences between the baseline buffer and the protein solution), a rinsing step with the pH 7.0 buffer was performed to remove excess or/and loosely bound protein. To simplify the following discussion, only the data of the 5th overtone were considered since the data at the different overtones exhibit a similar trend. Upon rinsing, the Δf/n and ΔD reached -35.8±2.5 Hz and $(2.5\pm0.2)\times10^{-6}$ at the 5th overtone, respectively. Moreover, the overtone-dependency (especially for ΔD) was apparently decreased. Therefore, some loosely bound and excess protein molecules were removed from the measurement chamber, but a considerable amount remained

adsorbed. The rinsing effect can be ascribed to the formation of a second adsorption layer over the first one. The primary protein layer acted as an anchor to the O/W mimicking interface, whereas the outer layers contained some loosely bound protein. This is in line with the mechanism reported by Tcholakova et al. (2002), who described that a second adsorption step happens and results in protein multilayers on the O/W interface when the concentration of β-lactoglobulin in O/W emulsions is above a critical concentration.

Table 2.1: The estimated viscosity, elasticity, thickness and surface load of the WPI layer adsorbed at pH 7.0 after rinsing at pH 7.0 and 5.0, resp., as calculated by the viscoelastic Voigt model (based on 3rd, 5th, 7th, 9th and 11th overtones).

pH	Layer Density (kg/m^3)	Viscosity (mPa.s)	Elasticity (kPa)	Thickness (nm)	Adsorbed mass (mg/m^2)
7.0	1050	4.01±0.42	606±124	7.1±0.4	7.5±0.5
	1100	3.70±0.20	579±117	6.8±0.4	7.5±0.4
	1200	3.51±0.05	547±86	6.5±0.5	7.8±0.6
5.0	1200	5.00±0.26	1004±204	4.5±0.1	5.4±0.1
	1350	4.40±0.22	942±135	4.0±0.1	5.3±0.1
	1400	4.34±0.24	911±140	3.8±0.1	5.4±0.1

Note: *The density and dynamic viscosity of the pH 5.0 acetate buffer (20 mM) at 22°C were 998 kg/m^3 and 0.965 mPa.s, whereas these of the pH 7.0 phosphate buffer (20 mM) at 22°C were 1000 kg/m^3 and 0.967 mPa.s. The kinematic viscosity was determined by Ubbelohde viscometry, and the solution density was measured by an Anton-Paar DMA 5000M density meter. The density of the adsorbed protein layer at pH 7.0 was assumed to be 1050, 1100, and 1200 kg/m^3, respectively. At pH 5.0, the (less hydrated) layer density was assumed to be 1200, 1350, and 1400 kg/m^3, respectively. For both pH conditions, the system baseline was established by the corresponding buffer. The significance of the layer difference between pH 5.0 and pH 7.0 was evaluated by a paired t-test, as discussed below.*

As a rule of thumb, a layer with a ΔD value above 1×10^{-6} can be considered as a viscoelastic layer. In Table 2.1, by fitting the results with the Kelvin-Voigt viscoelastic model (based on overtones 3-11), the estimated adsorbed mass was 7.8±0.6 mg/m^2 at pH 7.0, independent of the assumed layer density. If the layer density is assumed to be 1200 kg/m^3, the layer thickness of 6.5 nm seems to be a monolayer of whey protein isolate. Additionally, the adsorbed protein layer was imaged by AFM (Figure 2.1B), suggesting the formation of a heterogeneous and nano-scale structure. The adsorbed mass was much higher than the typical values of 2.0-2.5 mg/m^2 for a monolayer of adsorbed globular proteins (Setiowati et al., 2017; Tcholakova et al., 2002). This is ascribed to the fact that QCM-D measures hydrated mass, whereas the latter value describes the dry mass obtained by chemical quantification.

Since pH 7.0 is away from the isoelectric point of WPI (i.e. around 5.2), these adsorbed protein molecules are not close-packed due to electrostatic repulsion. Hence, a considerable fraction of mass can be due to trapped liquid. For instance, more than 50% of solvent mass has been reported for other globular proteins (e.g. albumin, lysozyme) in QCM-D results (Ouberai et al., 2014). Regarding the WPI layer at pH 7.0, around 70% of the adsorbed mass may be ascribed to the trapped liquid.

2.3.2 Effect of pH on the adsorbed WPI layer

The solution pH plays a dominant role in electrostatic interactions as it controls the degree of ionization of charged groups in biopolymers. In this section, the characteristics of the adsorbed protein layer upon exposure to various pH conditions were studied. Figure 2.2 shows the normalized frequency and dissipation shifts of the pre-adsorbed WPI layer upon repeated rinsing steps with pH 5.0 (or pH 3.0) and pH 7.0 buffers. Noted that these raw data also include the response from the bulk changes (e.g. density or/and viscosity variations between the different buffers). As such, the Δf/n or ΔD shifts referred to in the following discussion had already been corrected by the bulk effect (see Figure A2 in Annexes), so the data present are only due to changes in the adsorbed layer.

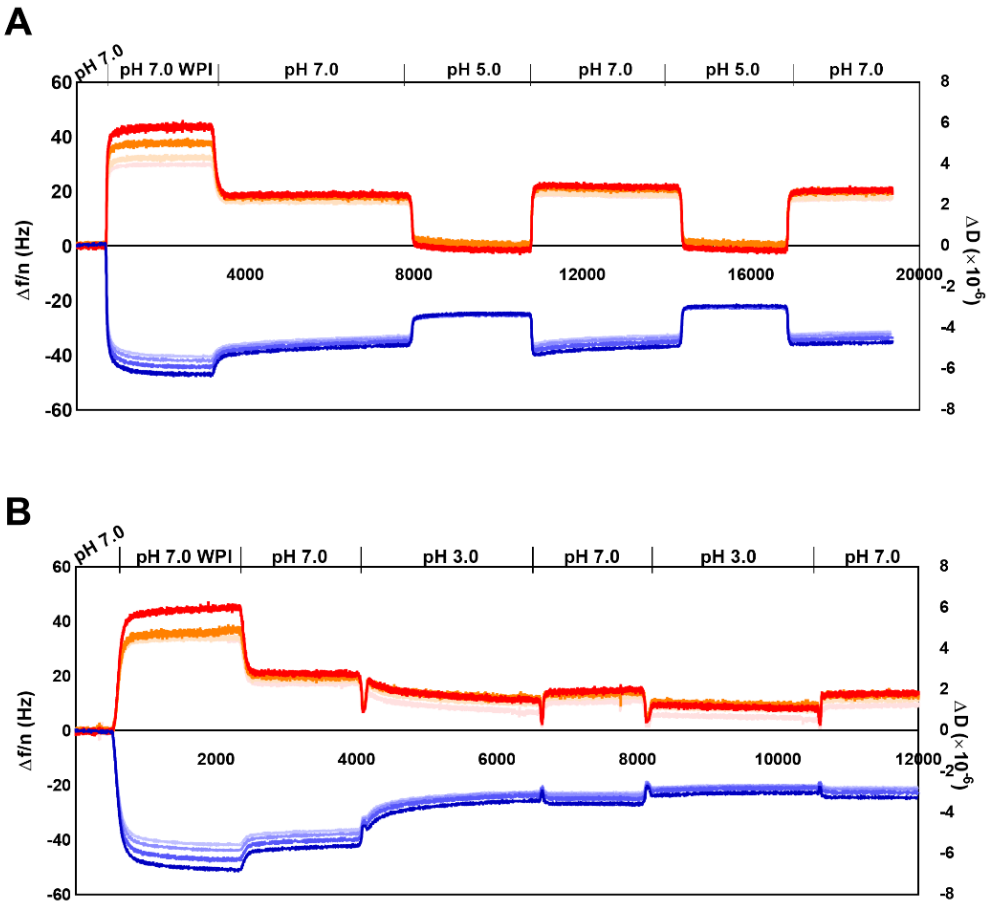

Figure 2.2: Normalised frequency (blue, left axis) and dissipation (red, right axis) shifts as a function of time (s) for the 3rd, 5th, 7th, and 9th overtones (with fading colors for increasing overtones) of a pre-adsorbed WPI layer (at pH 7.0) upon repeated rinsing with a combination of a pH 5.0 buffer and the pH 7.0 buffer (A) or a pH 3.0 buffer and the pH 7.0 buffer (B).

After contacting with the pH 5.0 buffer, the Δf/n increased from -35.1±1.0 Hz to -27.3±1.3 Hz and ΔD dropped from $(2.5\pm0.1)\times10^{-6}$ to $(0.8\pm0.1)\times10^{-6}$. In addition, the extent of overtone dependency at pH 5.0 was also less than at pH 7.0, especially for Δf/n. At pH 5.0, the adsorbed mass was calculated to be 5.3±0.1 mg/m^2, regardless of the assumed layer density. Interestingly, upon rinsing with pH 7.0 buffer again, both Δf/n and ΔD (and their overtone dependency) underwent a reversible change, i.e. comparable to the original level of the WPI layer at pH 7.0. A following rinsing cycle re-confirmed this point. Therefore, these noticeable Δf/n and ΔD shifts upon pH changes were not due to protein desorption but to reversible structural rearrangements

within the adsorbed layer. This phenomenon can be explained by the different amount of water molecules trapped in the WPI layer at different pH levels.

At pH 7.0, whey proteins carry a highly net-negative charge. The repulsive forces between adjacent proteins resulted in a rather loosely adsorbed protein film. As such, a lot of liquid was trapped in the layer. In contrast, the electrostatic repulsion is minimized between the adsorbed protein molecules when the pH approaches the IEP of WPI (i.e. 5.2). The protein molecules tend to aggregate, and the overall layer becomes more compact, and hence a fraction of trapped water molecules will be released from the hydrated layer. As such, the protein layer becomes more rigid, as evidenced by the dropped ΔD. When the pH was brought back to 7.0, the restored $\Delta f/n$ and ΔD corresponded to the re-swelling of the adsorbed layer. The estimated viscoelasticity, thickness and adsorbed mass of the WPI layer at pH 7.0 and 5.0 are summarized in Table 2.1. The estimated viscosity and elasticity values were comparable to that of a β-Lg layer adsorbed onto a hydrophobic PES surface (Liu & Kim, 2009). Besides, the elasticity of the WPI layer at pH 5 was greater than at pH 7.0 based on a paired t-test ($p<0.05$). Further, the table also demonstrates that the assumed layer density had no significant effect on the estimated mass and elasticity of the adsorbed layer.

Besides, similar experiments were also performed at other pH levels (pH 6.0, 4.0, 3.0), both above and below the IEP of WPI. The raw data can be found in Figure A3. When the pH 6.0 buffer was introduced to rinse the WPI layer, the $\Delta f/n$ and ΔD reached 34.1±1.8 Hz and $(2.1\pm0.2)\times10^{-6}$. Likewise, the pH reversibility was also observed. The pH-induced shifts (relative to pH 7.0) were smaller than that at pH 5.0 since the adsorbed layer still carries a net negative charge at pH 6. Upon adjusting to pH 4.0, the $\Delta f/n$ increased to -26.8±2.5 Hz, which was comparable to that at pH 5.0. However, the ΔD decreased to $(1.2\pm0.2)\times10^{-6}$, slightly higher than at pH 5.0. Besides, when the pre-adsorbed WPI layer was exposed to pH 3.0, the $\Delta f/n$ increased to -25.4 ±0.9 Hz and ΔD was about $(2.4\pm0.2)\times10^{-6}$. Additionally, an overtone-dependent response was observed.

These results suggest that the viscoelastic protein layer also became more rigid upon changing from pH 7.0 to 4.0. In contrast, the adsorbed proteins are highly positively

charged at pH 3.0, i.e. two pH units below the IEP of WPI. Therefore, the adsorbed layer can be highly hydrated and viscoelastic, similar to that observed at pH 7.0. To be noted, the absolute values of Δf/n and ΔD became smaller (around 4 Hz and 0.2×10^{-6}) after the first pH cycle (7.0-4.0-7.0), but this became less obvious in the second cycle. This phenomenon was particularly pronounced at pH 3.0, where the absolute values of Δf/n and ΔD at pH 7.0 largely dropped by 14 Hz and 0.6×10^{-6} after the first pH cycle. We speculate that some pre-adsorbed proteins may have desorbed below pH 4.0, which is likely due to the dissociation of β-Lg dimers into monomers (Boland & Singh, 2019).

2.3.3 Interfacial assembly of WPI and LMP at different pH values

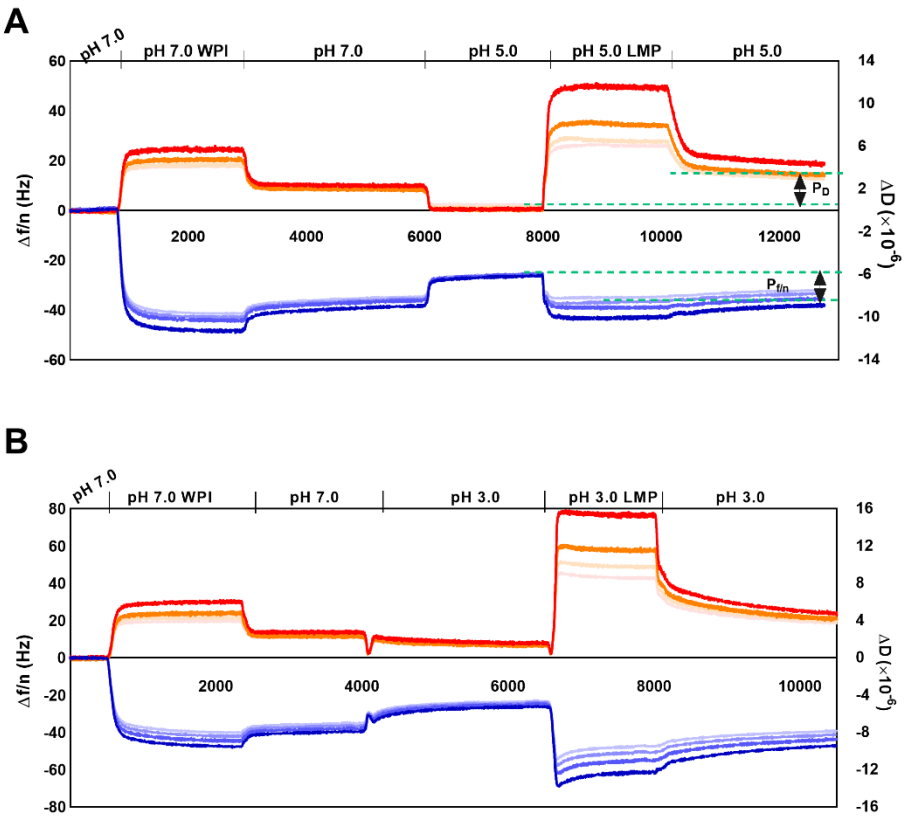

Figure 2.3: Normalized frequency (blue, left axis) and dissipation (red, right axis) shifts as a function of time (s) for the 3rd, 5th, 7th, and 9th overtones (with fading colors for increasing overtones) upon sequential adsorption of WPI (1.0 %, w/w) at pH 7.0 and LMP (0.4%, w/w) at pH 5.0 (A) and pH 3.0 (B) onto a hydrophobically modified surface.

The sequential adsorption of WPI and LMP was investigated over a wide pH range (pH 3.0-7.0). Figure 2.3A depicts Δf/n and ΔD shifts as a function of time for the 3rd, 5th, 7th, and 9th overtones upon contacting the pre-adsorbed protein surface with LMP at pH 5.0. Upon LMP addition, the Δf/n and ΔD shifts greatly rose to -41.1±1.6 Hz and (8.9±0.3)×10^{-6}. Furthermore, the responses became more overtone-dependent, particularly for ΔD. This can be due to the bulk effects or/and some loosely bound LMP. After rinsing, the Δf/n and ΔD shifts dropped to 37.3±1.1 Hz and (4.5±0.5)×10^{-6} after around 15 min, but both of them were still much larger than before introducing LMP (i.e. individual WPI layer at pH 5.0). These results clearly indicate the adsorption of LMP, which leads to an increased adsorbed mass and interfacial viscoelasticity. To better compare these variations as a function of pH, the Δf/n and ΔD shifts before and after introducing LMP were termed as $P_{f/n}$ and P_D. Hence, in Figure 2.4, the $P_{f/n}$ and P_D at pH 5.0 are -10.4±1.1 Hz and (3.5±0.4)×10^{-6}. At pH 7.0, P_D was close to zero and $P_{f/n}$ was even a positive value, suggesting no LMP adsorption. At pH 6.0-6.5, there was some LMP adsorption, but it was limited. At pH 5.0-5.5, the variations of $P_{f/n}$ and P_D became more pronounced. Below pH 5.0, however, the $P_{f/n}$ and P_D variations around pH 4.0 became smaller than at their neighboring pH values. Furthermore, the $P_{f/n}$ at pH 3.0-3.5 was much greater than at all other tested pH levels.

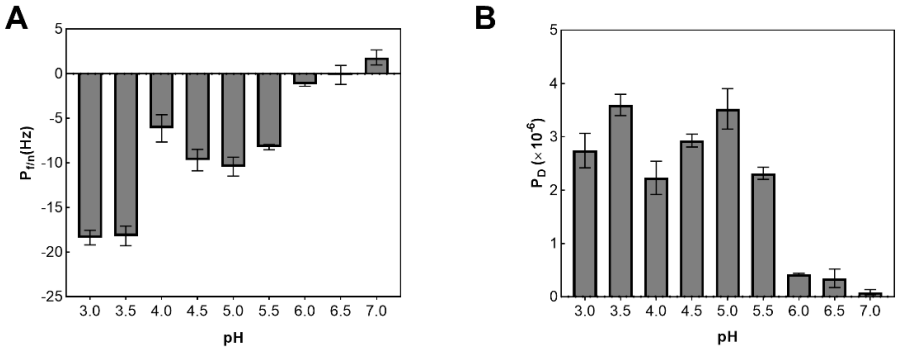

Figure 2.4: The frequency change ($P_{f/n}$, Hz) (A) and dissipation change (P_D, ×10^{-6}) (B) of the WPI layer before and after contacting LMP as a function of pH. In all cases, WPI was first adsorbed at pH 7, and then rinsed by a sequence of the pH 7 buffer, followed by a buffer of the intended pH, after which LMP was adsorbed and rinsed at the latter pH. The data come from the 5th overtone.

It can be concluded that the LMP adsorption happened over a wide pH range from 3.0 to 6.5, i.e. both below and above the IEP of WPI. In this range, the lower the pH, the more favorable for the electrostatic deposition of LMP. Above the IEP, WPI carries a net negative charge but still contains positively charged patches (due to the high pKa of lysine), which are binding spots for the anionic LMP. Below pH 5.0, WPI and LMP carry opposite charges, whereby the electrostatic attraction between them is more favorable. Therefore, the smaller variations at pH 4.0 were unlikely due to less LMP adsorption, but to a stronger electrostatic complexation. This will produce a compact adsorbed layer, resulting in the release of trapped water molecules.

With regard to the raw data, there is a special dip for the $\Delta f/n$ immediately after LMP addition at pH 4.0, which may be interpreted as the fast adsorption of LMP and subsequently the release of trapped water. Likewise, at pH 3.0, both $\Delta f/n$ and ΔD shifts rapidly enhanced and then slowly dropped (Figure 2.3B). Even after rinsing, the absolute values of $\Delta f/n$ and ΔD continued to become smaller with time. However, these phenomena were not observed above pH 5.0 (Figure A4). The stronger interfacial complexation below pH 5.0 may lead to more structural rearrangements within the interfacial layer.

To be noted, the LMP also can adsorb onto the hydrophobic surface at either pH 3.0 or 7.0 in the absence of WPI (Figure A5), which may be due to the presence of hydrophobic methyl-esterified galacturonic acid units and the protein moiety in its molecular structure (Schmidt et al., 2015). However, the LMP did not directly adsorb onto the hydrophobic surface in the presence of WPI. This point can be known from Figure A5, when the mixture of WPI and LMP was introduced to the hydrophobic surface at pH 7.0 (where no complexation occurred, as discussed later). Both the $\Delta f/n$ and ΔD shifts after the rinsing step were well consistent with that in Figure 2.1A ($p>0.05$), suggesting that only the WPI existed on the hydrophobic surface. Therefore, during the sequential adsorption experiments, LMP could only interact with the pre-adsorbed protein molecules instead of the hydrophobic surface.

2.3.4 pH-responsive adsorption/desorption of LMP

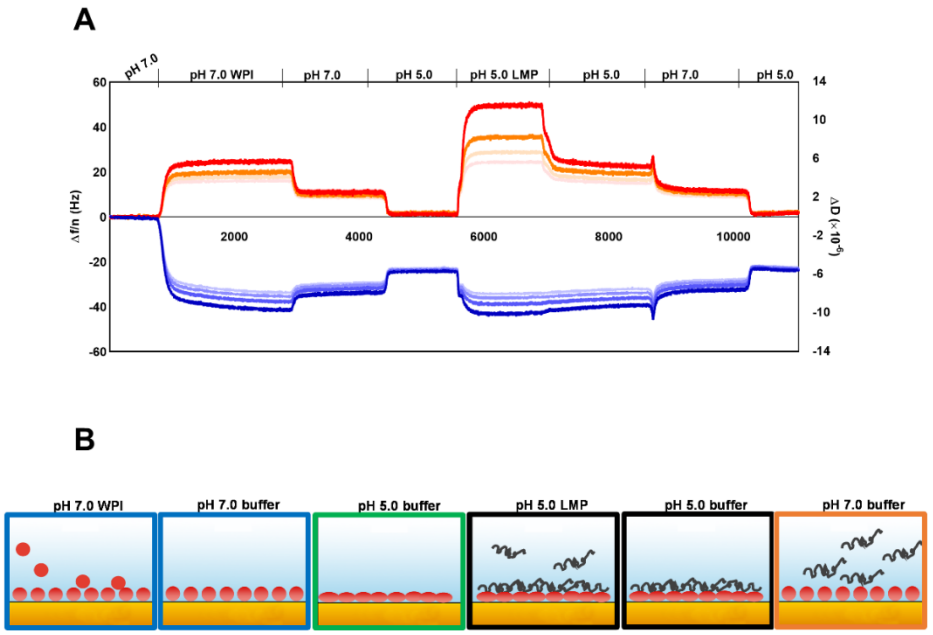

Figure 2.5: (A) Sequential adsorption of WPI (1.0 %, w/w) and LMP (0.4%, w/w) onto the hydrophobically modified surface at pH 5.0; After removing excess LMP, the mixed layer was rinsed sequentially by pH 7.0 buffer and pH 5.0 buffer. Normalized frequency (blue, left axis) and dissipation (red, right axis) shifts as a function of time (s) for the 3rd, 5th, 7th, and 9th overtones (with fading colors for increasing overtones). (B) Schematic representation of the sequential adsorption and pH-response behavior.

In this section, the WPI/LMP bilayers prepared at acidic pH conditions (pH 3.0-5.0) were then exposed to pH 7.0 (i.e. by rinsing them with the pH 7.0 buffer), to determine the reversibility of the LMP adsorption. At pH 7.0, the two biopolymers are strongly negatively charged. In Figure 2.5A, upon exposure to pH 7.0, a sharp dip and peak were observed for the Δf/n and ΔD shifts, respectively. Subsequently, both Δf/n and ΔD were converted to a similar extent of overtone-dependency and magnitude as the original WPI layer at pH 7.0. The final rinse step with pH 5.0 buffer confirmed that the adsorbed layer had similar properties as the WPI layer. This was supported by the estimated surface load (i.e. the hydrated mass) in Table 2.2 as well.

As discussed previously, no LMP adsorption on the WPI layer was observed at pH 7.0. Therefore, the adsorbed LMP molecules at pH 5.0 could be fully detached from the primary protein layer upon rinsing with the pH 7.0 buffer since the pH no longer

favored interfacial complexation. Meanwhile, the compact protein layer trapped more water molecules and became swelling. The pH-responsive desorption at pH 7.0 was also observed for the WPI/LMP bilayers prepared at pH 3.0 and 4.0 (Figure A6). These results also imply that the conformational changes of the protein during interfacial complexation with LMP may be reversible or non-destructive. Figure 2.5B gives a schematic diagram of the pH-responsive structural rearrangements of the WPI layer, as well as the pH-triggered adsorption/desorption of LMP.

Table 2.2: Hydrated mass of the adsorbed WPI and WPI/LMP layers at different conditions

	Hydrated mass (mg/m^2)
WPI at pH7 after rinsing	7.8 ± 0.6^{b}
WPI layer rinsed with pH5 buffer	5.8 ± 0.3^{c}
Adsorption of LMP and rinsing at pH5	9.8 ± 0.5^{a}
Rinsing with pH7 buffer	7.0 ± 0.4^{b}
Rinsing with pH5 buffer	5.2 ± 0.2^{d}

Note: different letters indicate significant differences ($p<0.05$).

Recently, Bertsch et al. (2019) compared the interfacial thickness of the β-Lg/LMP bilayer at pH 4.0 and pH 7.0 using neutron reflectometry and indicated that the adsorbed LMP at pH 4.0 may desorb from the primary protein layer at 7.0, in line with our QCM-D results. In fact, neutron reflectometry is not easily available and its time-resolution is lower than QCM-D (Skoda, 2019). By using QCM-D, information about the adsorbed material (such as adsorption/desorption, structural rearrangements, and interfacial viscoelasticity) can be obtained in real-time.

The pH-dependent WPI-LMP interactions at the hydrophobic surface are similar to those of β-Lg /carboxyl polysaccharides interactions in aqueous solutions (i.e. in the absence of the hydrophobic surface). For instance, a kinetic study using small-angle light scattering suggested that the formation of β-Lg/LMP complexes was initiated at pH 6.4 upon acidification from pH 7 downwards (Girard et al., 2004). Likewise, a

calorimetric study focusing on β-Lg/alginate interactions reached similar conclusions (Harnsilawat et al., 2006).

2.4 Conclusions

In this chapter, a QCM-D technique was employed to investigate the sequential adsorption of WPI and LMP at the interface between a hydrophobic and an aqueous phase. To that end, gold-coated crystal sensors were hydrophobically modified to mimic the oil-water interface.

From the obtained results, it was clear that WPI adsorbed onto the surface and formed a viscoelastic layer at neutral pH, which can be described as a heterogeneous and highly hydrated layer. When the pH of the continuous phase approached the IEP of WPI, the adsorbed protein layer became more densely packed and less hydrated due to the structural rearrangements. Furthermore, those changes were found to be reversible.

As far as interfacial WPI-LMP interactions are concerned, the adsorption of LMP onto the pre-formed WPI layer was observed over a wide pH range from pH 3.0 to 6.5, i.e. both below and above the IEP of WPI. Above pH 6.5, both WPI and LMP were highly negatively charged, and hence no interfacial complexation occurred. In contrast, the LMP adsorption was more favorable upon lowering the pH from 6.5 to 3.0. Below pH 5.0, WPI and LMP have opposite charges, in which the interfacial complexation became stronger and was accompanied by more structural rearrangements. Hereby, some trapped liquid could be released from the adsorbed layer (especially at pH 4.0). At pH 7.0, the adsorbed LMP molecules were fully detached from the primary WPI layer because of pH-induced charge inversion. These results suggested the excellent suitability of QCM-D to investigate the effect of (changing) environmental conditions on the characteristics of the adsorbed layer, and to study the interaction between different components by sequential adsorption. The findings may contribute to the design of multilayer emulsions. The pH-responsive adsorption/desorption behavior of LMP is also useful for developing pH-sensitive colloids or delivery systems.

Last but not least, it should be kept in mind that the frequency and dissipation response of QCM-D is not only affected by changes in the interfacial layer, but also by changes in the bulk liquid properties (such as viscosity and density). Additionally, to obtain

accurate quantitative information, data-analysis is always complicated for heterogeneous, viscoelastic layers (Johannsmann et al., 2008). To circumvent these problems, it is valuable to use QCM-D combined with other state-of-the-art techniques. For example, pairing QCM-D and ellipsometry allows one to estimate both the wet mass and dry mass of the interfacial film, and thus could be helpful to study the properties of adsorbed materials in more detail.

Chapter 3 Sequential Adsorption of Whey Proteins and Low Methoxy Pectin at the Oil-Water Interface: An Interfacial Rheology Study

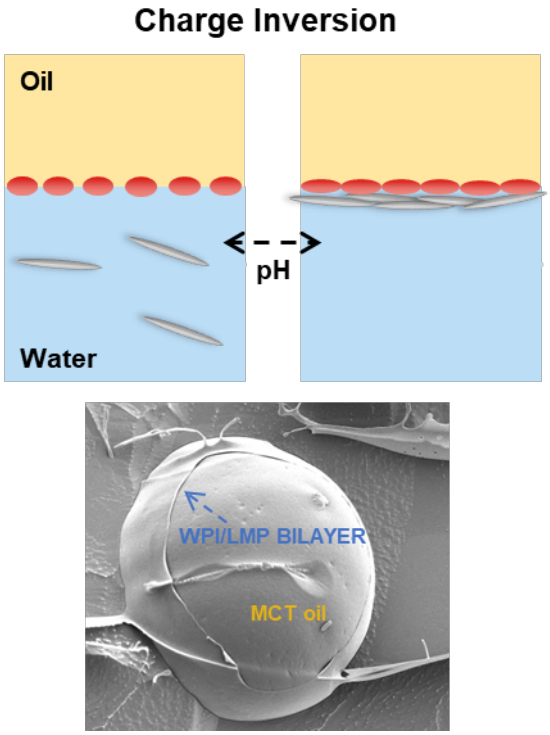

Redrafted from: Li, H., & Van der Meeren, P. (2022). Sequential adsorption of whey proteins and low methoxy pectin at the oil-water interface: an interfacial rheology study. Food Hydrocolloids, 128, 107570.
https://doi.org/10.1016/j.foodhyd.2022.107570

Hao Li: Investigation, Conceptualization, Methodology, Software, Writing - original draft, Formal analysis, Visualization. Paul Van der Meeren: Supervision, Conceptualization, Writing - review & editing, Methodology, Visualization.

Abstract

Protein-polysaccharide bilayers have attracted a growing interest in the design of emulsion stabilizers with improved performance. An in-depth understanding of their interfacial properties is crucial for rational interfacial design. Here, the sequential adsorption of whey protein isolate (WPI) and low methoxy pectin (LMP) at the oil-water interface as a function of pH was investigated with a modified drop tensiometer allowing external phase exchange. Residual WPI in the bulk phase could accumulate at the interface (i.e. pre-formed WPI film at pH 7.0) when the pH was adjusted to be close to its iso-electric point, leading to a reduced interfacial tension and increased surface concentration. However, the interfacial tension was hardly influenced by successive pH changes and LMP addition if the excess protein was washed away beforehand. A maximum interfacial dilatational elasticity was reached when the pH was close to the isoelectric point of WPI, corresponding to the minimum hydration degree. Deposition of LMP significantly increased the interfacial viscoelasticity of the pre-adsorbed WPI layer, but its magnitude varied with pH. Additionally, during the large-amplitude oscillatory cycles, the bilayer structures displayed a more linear rheological response than the single WPI layer. Moreover, the adsorbed LMP at acidic pH conditions exhibited pH-responsive desorption upon exposure to neutral pH, as evidenced by the restored interfacial viscoelasticity. Compared with the individual WPI layer, the more rigid and thicker WPI/LMP bilayer could better protect O/W emulsions from flocculation and coalescence.

3.1 Introduction

Similar to low molecular weight surfactants, many food proteins are able to stabilize air-water or oil-water interfaces by reducing the interfacial tension (McClements, 2004, 2015). Moreover, proteins tend to unfold at the interfaces and form a viscoelastic network, which can be seen as a two-dimensional hydrogel (Murray, 2002). It has been reported that the rheological properties of the adsorbed layers at fluid interfaces may be relevant to the stability of foams or emulsions (Murray, 2002, 2011). For instance, interfacial films with a larger elasticity can better protect emulsion droplets from film rupture (e.g. coalescence) and disproportionation, as well as prolong the lifetime of foams (Miquelim et al., 2010; Peng et al., 2017; Romoscanu & Mezzenga, 2005). Besides, recent studies have shown that stronger interfacial films may be more resistant to surfactant-induced competitive displacement and possibly limit lipolysis in the upper gastrointestinal (GI) tract (Cai, 2020; Roth et al., 2000; Scheuble et al., 2016b). Thus, the interfacial viscoelasticity could be tailored to meet the needs of different applications. However, the interfacial elasticity of individual protein networks is sometimes inadequate to provide mechanical stability to emulsion droplets, e.g. during the production of emulsion-templated microcapsules, oil powders, or oleogels (Mezzenga, 2018). The broken film during food processing may result in the leakage of hydrophobic liquids.

Protein-polysaccharide interactions, through either conjugation (Maillard reaction, enzymatic cross-linking) or electrostatic interactions, have attracted a growing interest in the design of interfacial structures with applications in the food and pharmaceutical industries (Li et al., 2022). Their electrostatic interactions are the focus in this work since non-covalent complexation may enable the design of delivery systems with environmental responsiveness. In this manner, the protein-polysaccharide mixed layers can be prepared by either pre-formed electrostatic complexes or by sequential adsorption (also known as “layer-by-layer” electrostatic deposition) (Guzey & McClements, 2006). In principle, the latter case could be a more feasible approach to reinforce the oil-water interface without interfering with the formation of dense protein networks (Ganzevles et al., 2006).

The preparation and colloidal stability of protein-polysaccharide multilayer emulsions have been extensively reported in recent years. Moreover, these emulsions were applied to encapsulate, protect, and control the release of bioactive compounds from the interior phase (McClements, 2012).

However, it cannot be excluded that the claimed emulsion stability and functional properties originate at least partly from bulk depletion and coacervation (Fischer, 2013). Therefore, these studies cannot replace direct investigations of the adsorption layer. To the best of our knowledge, there is still a lack of useful insights about the interfacial properties of protein-polysaccharide bilayers at the oil-water interface, e.g. related to their rheology, real-time assembly, morphology, as well as environmental stress-responsive behaviors. Besides, most studies in this field only focused on the influence of various polysaccharides on the interfacial dilatational rheology of pre-formed protein films at one specific pH and observed either significant or insignificant results (Ganzevles et al., 2007; Ganzevles et al., 2006). In this study, we investigated to what extent changing pH conditions influenced the interfacial dilatational rheology in both the protein and polysaccharide layers.

The interfacial rheological properties can be investigated by interfacial shear rheology and dilatational rheology (Sagis & Fischer, 2014). Interfacial shear rheology is typically performed on a rotational rheometer equipped with bi-conical disk or double-wall ring geometries, which are placed at the planar oil-water or air-water interface (with a constant area). The dilatational properties may be determined using a Langmuir trough, in which the interface is compressed or expanded by an oscillatory motion of the barriers of the trough, whereby the effect of the deformation on the surface pressure is determined using a Wilhelmy plate. Nowadays, the dilatational properties are frequently determined by drop shape tensiometry, where the area of a droplet can be expanded or compressed (i.e. deformation or strain) in a controlled way (e.g. sinusoidal oscillations), leading to changes in surface or interfacial pressure (i.e. stress) (Sagis, 2011; Sagis & Fischer, 2014). Measurements of the dilatational rheology of interfacial layers are of particular interest because these are more likely to be involved in real emulsion/foam formation and destabilization phenomena (Berton-Carabin et al., 2016; Dan et al., 2013; Hinderink et al., 2021; Maldonado-Valderrama & Rodríguez Patino, 2010; Romoscanu & Mezzenga, 2005).

In this study, the sequential adsorption of WPI and LMP at the medium-chain triglycerides (MCT)/water interface was investigated with a modified drop tensiometer allowing external subphase exchange. The effect of pH on the protein layer properties (previously adsorbed at neutral pH) and subsequent LMP adsorption (i.e. at pH conditions both below and above the iso-electric point of WPI) were characterized by dynamic interfacial tension and dilatational rheology. The interfacial structure of emulsion droplets was visualized using scanning electron microscopy (Cryo-SEM). Lastly, we compared the coalescence stability of WPI emulsions and WPI/LMP bilayer emulsions.

3.2 Materials and Methods

3.2.1 Materials

As described in section 2.2.1, whey protein isolate and low-methoxy pectin (Unipectine OB700) were obtained from Davisco Foods International, Inc. (BiPro, Le Sueur, MN, USA) and Cargill (Ghent, Belgium), resp. Medium-chain triglycerides (MCT) were obtained from Go-Keto, containing 60% of C8 and 40% of C10. Florisil® (60–100 mesh for chromatography) was purchased from VWR (Ghent, Belgium). All other chemicals were of analytical grade. Deionized water was used for all experiments.

3.2.2 Sample preparation

WPI powder was dissolved in 20 mM sodium phosphate buffer (pH 7.0; ionic strength (I) = 43 mM) at a concentration of 0.01% (w/w). After stirring for 2 h at room temperature and overnight hydration at 4 °C, the WPI dispersion was passed through a 0.45 μm mixed cellulose ester (MCE) membrane filter to remove any insoluble materials.

MCT oil was mixed with 5% (w/w) florisil and mildly stirred overnight at room temperature to remove surface active ingredients, and the supernatant was collected and stored at 4 °C for further use. After overnight stirring, LMP was dissolved in the corresponding buffer (pH 3.0-7.0; I=43 mM) at a concentration of 0.01% (w/w). The density of the MCT oil and various buffers was measured at 25 °C by an Anton Paar DMA 5000 M density meter (Table 3.1).

Table 3.1: Density of MCT oil, WPI solution and various buffers at 25.00±0.01 ˚C

Sample	pH	Ionic strength (mM)	Density (kg/m^3)
MCT oil	-	-	943.8
0.01% WPI (w/w)	7.0	-	999.6
20 mM sodium phosphate buffer	7.0	43	999.5
	3.0	17 (+ 26 mM NaCl)	999.9
20 mM sodium acetate buffer	4.0	3 (+ 40 mM NaCl)	999.2
	5.0	13 (+ 30 mM NaCl)	999.1

3.2.3 Drop shape tensiometry

The dynamic surface tension was measured with a modified drop tensiometer allowing external phase exchange (Teclis, Tracker, France), using a 50 mL thermostatted optical glass cuvette containing two magnetic stirrers, in combination with the Windrop software (Teclis, France). The temperature was controlled at 25 °C by a Julabo circulator. A rising MCT oil drop (20 μL) was formed at the tip of a U-shaped needle with a diameter of 1.61 mm, which was surrounded by 40 mL of 0.01 wt.% WPI solution. The surface tension was recorded every 5 s. The WPI was allowed to adsorb from the bulk to the interface for at least 13 h before the area deformation was applied and the continuous phase was changed.

A peristaltic pump (Ismatec, Germany) with two Teflon tubes was used to exchange the continuous phase in the cuvette at a flow rate of 11 mL/min. The inlet tube was placed close to one bottom corner of the cuvette, and the outlet tube was placed at its diagonal position across the cuvette. To investigate the effect of pH on the interfacial properties, the continuous phase was replaced by a 5-fold volume of protein-free pH 7.0 buffer (i.e. about 200 mL) and subsequently by a 5-fold volume of fresh pH 3.0, 4.0 or 5.0 buffers. To confirm the effectiveness of the protein removal via the phase exchange, the intrinsic fluorescence of WPI (i.e. excitation wavelength set at 280 nm and maximum emission intensity at 336 nm) was used to check the residual protein content in the cuvette. For protein concentrations from 0.0001 to 0.01 wt.% at pH 7.0, the fluorescence intensity of WPI had a linear relationship with the protein

concentration (R^2=0.9997). Accordingly, about 99% of the protein in the cuvette had been removed after a 5-fold volume pH 7.0 buffer rinsing. Subsequently, the further 5-fold volume buffer rinsing used for pH adjustments (i.e. in total 10-fold volume) could essentially exclude the influence of protein in the bulk phase.

To examine the sequential adsorption of LMP onto the WPI layer as a function of pH, the continuous phase was exchanged with 150 mL of 0.01 wt.% LMP solution at different pH levels. Upon equilibration for an extra 10 h, the free LMP was rinsed with 200 mL clean buffer. After each rinsing step, the interfacial rheology as a function of time was measured. To explore the reversibility of the interfacial complexation, the continuous phase further was replaced with a 5-fold volume of pH 7.0 buffer.

3.2.4 Interfacial dilatational rheology

To investigate the dilatational rheology of the interfacial film, an amplitude sweep was performed with a motor-driven syringe at a frequency of 0.01 Hz or 0.1 Hz (i.e. by increasing or decreasing the volume of the oil drop sinusoidally). The volume increase/decrease corresponded to a 0-20% of the surface area change. Each measurement was carried out for at least 5 sinusoidal cycles, whereby the mid-two or three cycles were used to calculate the interfacial rheology by the Windrop software (Teclis, France). Between each measurement at different amplitudes, there was a 10 min stop for relaxation. The response of the interface to such strain dA/A is reflected by a variation in interfacial tension γ (i.e. stress). As shown in Equations (3.1) and (3.2) below, the viscoelastic modulus E is a complex number, with a real part $E_d{}'$ (the storage modulus, elasticity) and an imaginary part $E_d{}''$ (the loss modulus, viscosity). θ is the phase difference between the stress and strain.

$$E = \frac{d\gamma}{dA/A} = \frac{d\gamma}{dInA} \qquad (3.1)$$

$$E = E_d{}' + iE_d{}'' = |E|\cos\theta + i|E|\sin\theta \qquad (3.2)$$

3.2.5 Emulsion preparation and characterization

3.2.5.1 Emulsion preparation

4 g of MCT oil was added into 20 mL of WPI solution (0.5 wt.%, pH 7.0) in a 60 mL sample container. The mixture was homogenized using an Ultra-turrax T25 (IKA,

Germany) at the highest speed (24,000 rpm) for 4 min to prepare WPI-coated droplets (i.e. about 16 wt.% oil). After standing at room temperature (about 20 ˚C) for 4 hours, 10 mL of the emulsion samples (in a 15 mL graduated falcon tube) was mildly centrifuged at 70×g for 1 hour. To remove excess WPI, the subnatant was removed carefully with a 10 mL syringe equipped with a long needle, and the cream layer was re-dispersed in 9 mL of the pH 3.0 buffer, and the centrifugation step was repeated. Subsequently, the cream layer was dispersed in 9 mL of pH 3.0 LMP solution (0.5 wt.%) or pH 3.0 buffer (as control), which was followed by 1 h mild stirring. This LMP concentration was selected because serious (bridging) flocculation happened at lower LMP concentration (e.g. at 0.1-0.2 wt.%). For better imaging of the interfacial structure of the emulsion droplets, the excess LMP in the continuous phase was also replaced with the pH 3.0 buffer. The ionic strength of the buffers used in emulsion preparation was also fixed at 43 mM (Table 3.1).

3.2.5.2 Particle size distribution and zeta-potential

The droplet size distribution of the emulsions was measured directly after preparation, as well as after 12 days of storage at 4 °C using static light scattering by a MasterSizer 3000 equipped with a Hydro MV unit (Malvern, U.K.). The obscuration value was fixed between 5 and 10% with a stirring speed of 1500 RPM in the phosphate buffers (pH 3.0 or 7.0). Since a bimodal distribution was obtained for the WPI-stabilised emulsion at pH 7.0 after 12 days of storage, measurements were also performed upon 10-fold dilution of the original WPI emulsion in 1% SDS solution. Moreover, the latter sample was measured both before and after ultrasonication for 2 min at 10% of the total power in the Hydro MV unit. The zeta potential (ζ) of the emulsion droplets was determined using a Zetasizer 3000 (Malvern Panalytical Ltd, Malvern, U.K.) after 1000 times dilution by the pH 3.0 buffer. Each individual measurement was an average of three runs.

3.2.5.3 Cryo-scanning electron microscopy

The interfacial structure of the WPI emulsion at pH 7.0 and of the WPI/LMP bilayer emulsion at pH 3.0 was visualized with cryo-SEM. The samples were placed in the slots of a stub, plunge-frozen in liquid nitrogen, and transferred into the cryo-preparation chamber (PP3010T cryo-SEM preparation system, Quorum Technologies, UK), where

they were freeze-fractured, sublimated (30 min for WPI emulsion and 1 hour for bilayer emulsion) and subsequently sputter-coated with Pt and examined with a JEOL JSM 7100F SEM (JEOL Ltd, Tokyo, Japan).

3.2.5.4 Ultracentrifugation

To investigate the coalescence stability, the emulsions samples (containing about 16 wt% oil phase) were subjected to ultracentrifugation at 20,000 RPM (i.e. 48,200 g) and 20 ˚C for 1 hour in a Sorval RC-5B centrifuge. The oiling-off due to the film rupture was visualized.

3.2.6 Data analysis

Data were presented as the mean ± standard deviation of at least four independent experiments. The difference between samples was evaluated using one-way ANOVA using GraphPad Prism 9.3 software (San Diego, USA).

3.3 Results and Discussion

3.3.1 Effect of pH on the pre-adsorbed WPI layer properties

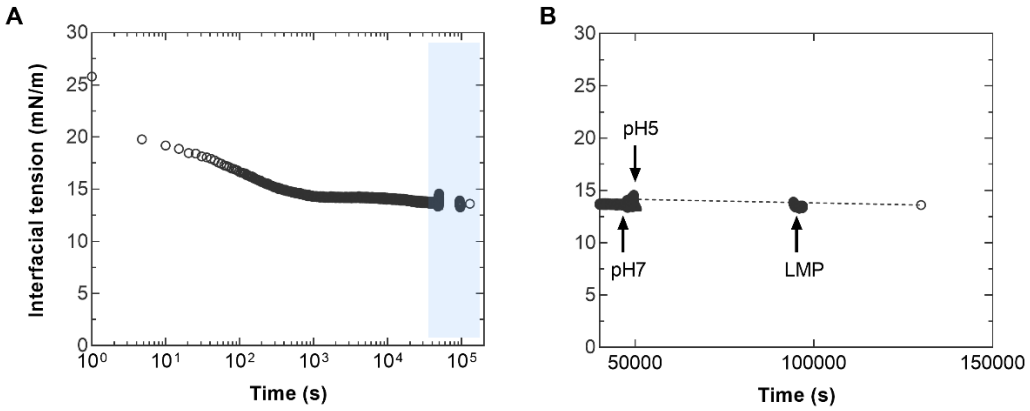

Figure 3.1: Interfacial tension as a function of time (in a logarithmic scale) for the sequential adsorption of 0.01% WPI (at pH 7.0) and 0.01% LMP (at pH 5.0) onto a MCT oil droplet (a) and a zoom of the time window when the LMP solution was entered (in a linear scale) (b). The protein film was formed at pH 7.0, followed by rinsing steps with pH 7.0 and pH 5.0 buffers. Afterwards, the LMP was introduced at pH 5.0, and a final rinsing step was performed. The dashed line was plotted to demonstrate that the interfacial tension was almost constant during the measurements.

At 25 ˚C, the interfacial tension of the MCT oil-water interface was 25.80.4 mN/m, close to previous results (Bergfreund, Bertsch, et al., 2021). No significant changes were observed within hours, suggesting the absence of surface-active impurities. Figure 3.1A shows the dynamic interfacial tension of the oil-water interface as a function of time (with a logarithmic scale) during the sequential adsorption of WPI and LMP. The initial sharp reduction within a few seconds suggested the rapid adsorption of WPI. After that, the interfacial tension was slowly reduced to 13.60.5 mN/m after about 13 hours (Table 3.1), which still went down in a rather slow way. The two major fractions of WPI (i.e. β-lactoglobulin and α-lactalbumin) are both globular proteins, which can unfold at the hydrophobic interface and expose their more hydrophobic segments towards the oil phase. Meanwhile, the unfolding may lead to increased

protein-protein interactions (e.g. through hydrophobic interaction or probably formation of disulphide bonds between protein molecules), and enable the formation of an inter-connective film or network (Dickinson & Matsumura, 1991). This process is also referred to as aging or surface denaturation, which may take several hours or days depending on the structural stability of the globular proteins (Bergfreund, Diener, et al., 2021).

Table 3.2: Interfacial tension of MCT oil against different types of continuous phase

Type of continuous phase vs MCT oil droplet	Interfacial tension (mN/m)
pH 7.0 buffer	25.8 ± 0.4^{a}
pH 7.0 WPI (0.01%, w/w)	13.6 ± 0.5^{b}
WPI directly rinsed with pH 5.0 buffer	12.1 ± 0.2^{c}
WPI sequentially rinsed with pH 7.0 and pH 5.0 buffers	13.2 ± 0.3^{b}
WPI sequentially rinsed with pH 7.0 buffer, pH 5.0 buffer and pH 5.0 LMP (0.01%, w/w)	13.2 ± 0.5^{b}
WPI sequentially rinsed with pH 7.0 buffer, pH 4.0 buffer and pH 4.0 LMP (0.01%, w/w)	13.6 ± 0.3^{b}

Note: different letters indicate significant differences ($p<0.05$).

Subsequently, the interfacial tension was unaffected by the pH 7.0 buffer rinsing, suggesting the irreversible adsorption of WPI. However, when the continuous phase was directly exchanged with the pH 5.0 buffer, a significantly lower interfacial tension was observed at 12.1±0.2 mN/m after a few minutes (Table 3.2). To be noted, if an additional pH 7.0 rinsing step was performed to remove excess WPI before adjusting to pH 5.0 buffer, the reduction was less pronounced. The lower interfacial tension at pH 5.0 can be due to more protein adsorption (Burgess & Sahin, 1997; Graham & Phillips, 1980). If enough protein is present, generally, the maximum surface load can be observed around its iso-electric point, where protein multilayers can even be formed (Engelhardt et al., 2013; Tcholakova et al., 2005). Likewise, after adjusting to pH 5.0 (i.e. close to the IEP of WPI, at around 5.2), the residual protein molecules in the aqueous phase tended to accumulate and became more densely packed at the interface

due to the reduced electrostatic repulsion between them. However, after previously removing the un-adsorbed WPI, the influence of pH changes (from pH 7.0 to pH 3.0-5.0) on the interfacial tension was marginal.

Besides, both the subphase type (e.g. oil hydrophobicity) and the nature of the protein could alter the interfacial properties (Bergfreund et al., 2018; Bergfreund et al., 2021). To have a better understanding of the WPI layer properties at the MCT oil-water interface, the interfacial dilatational rheology (at a fixed area amplitude of 2.6% and a frequency of 0.01 Hz) as a function of aging time was measured after the pH adjustments (in Figure 3.2). As far as the area amplitude is concerned, lower values (e.g. less than 1%) considerably influence the accuracy and reproducibility of measurements by drop tensiometry, and the dilatational moduli cannot be calculated correctly. Besides, the more complex non-linear response at higher amplitudes makes data analysis more complicated (Sagis & Scholten, 2014). To be noted, when the area amplitude was between 1.5 and 4%, we found that the dilatational moduli of the WPI layer were independent of the applied strain (Figure 3.2). Besides, the dilatational elasticity was gradually reduced with the increase of amplitude, and the non-linear response became more pronounced. Similar results were also reported by Ho et al. (2018) and Schröder et al. (2017). Hence, a 2.6% of deformation was set to study the effect of pH on protein layer properties, which can provide a good balance between a good instrument signal and a linear rheological response. Additionally, this point was confirmed by the symmetric Lissajous plots in Figure 3.3 (i.e. the response of surface pressure under applied strain). A low frequency was chosen to avoid the formation of surface waves, and also to facilitate the comparison with published data which also adopted this frequency (Kieserling, Alsmeier, et al., 2021; Sagis & Fischer, 2014). In fact, the interfacial rheology at 0.1 Hz was also investigated (in Figure 3.4). Whereas the elastic modulus was slightly higher that at 0.01 Hz, the obtained results exhibited a similar trend. Hence, we only showed the results obtained at 0.01 Hz.

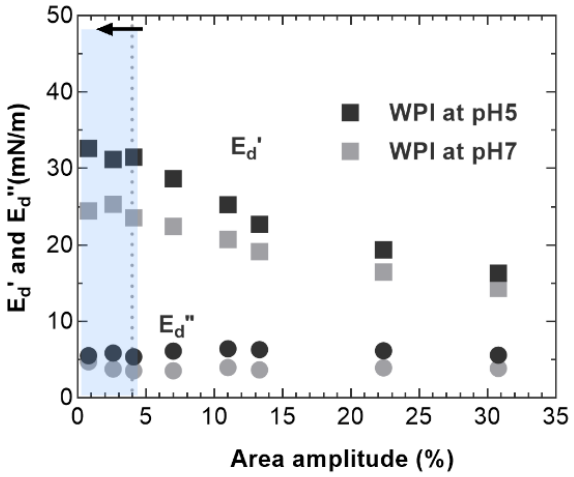

Figure 3.2: The interfacial dilatational rheology of the different adsorbed layers was measured as a function of amplitude and represented as interfacial dilatational elastic modulus E_d' (squares) and viscous modulus E_d" (circles). The protein film was pre-prepared at pH 7.0 (aging 13 hours), followed by rinsing steps with pH 7.0 and 5.0 buffers. Upon adjusting to pH 5.0, the amplitude sweep was performed after one hour aging.

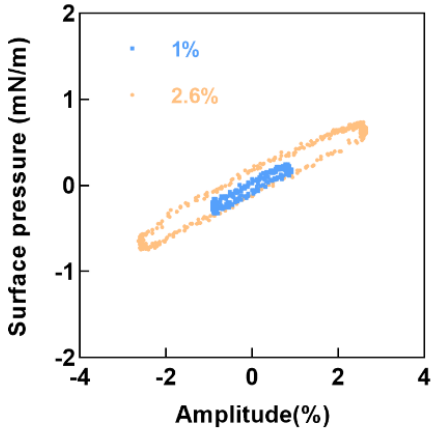

Figure 3.3: Lissajous plot of surface pressure versus area amplitude for a WPI layer (pH 7.0) at amplitudes of 1.0% (blue) and 2.6% (yellow), at a frequency of 0.01 Hz.

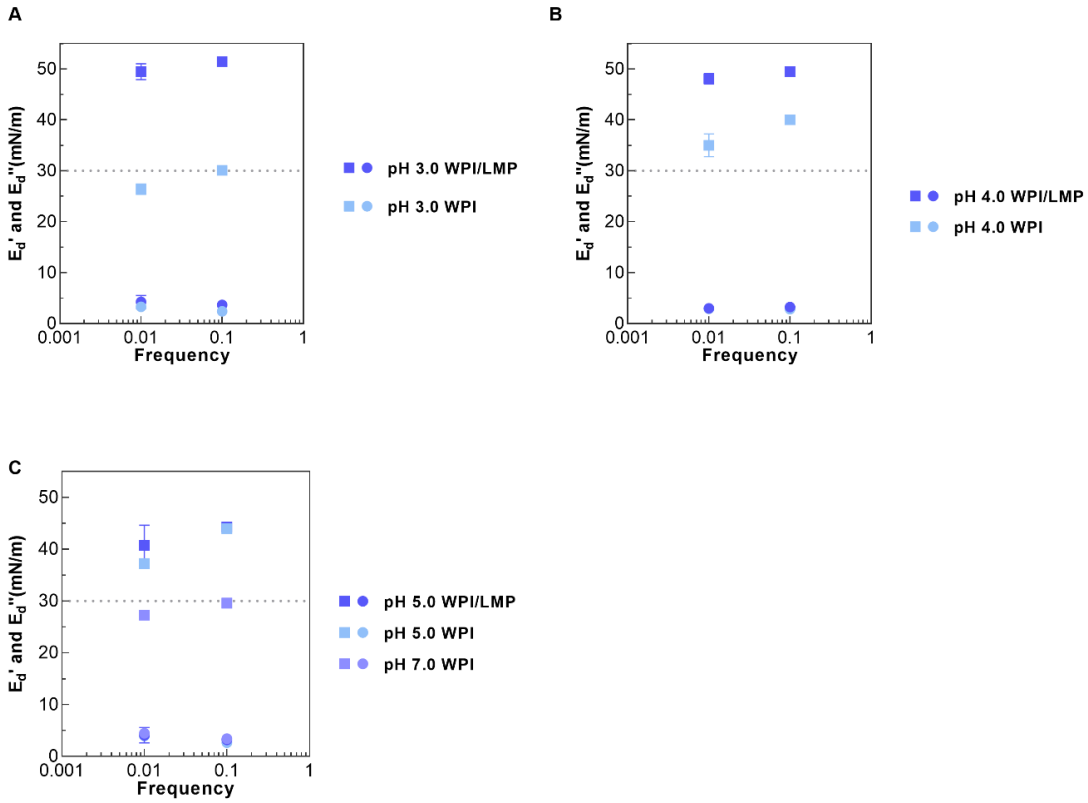

Figure 3.4: Interfacial dilatational rheology of the different adsorbed layers as a function of applied frequency (at a fixed area amplitude of 2.6%) and represented as interfacial dilatational elastic modulus E_d' (squares) and viscous modulus E_d" (circles). In all cases, the protein film was pre-adsorbed at pH 7.0 (about 13 hours), followed by rinsing steps with pH 7.0 and pH 3.0-5.0 buffers. After 12 hours, LMP was introduced at the corresponding pH, and a rinsing step was performed 10 hours later.

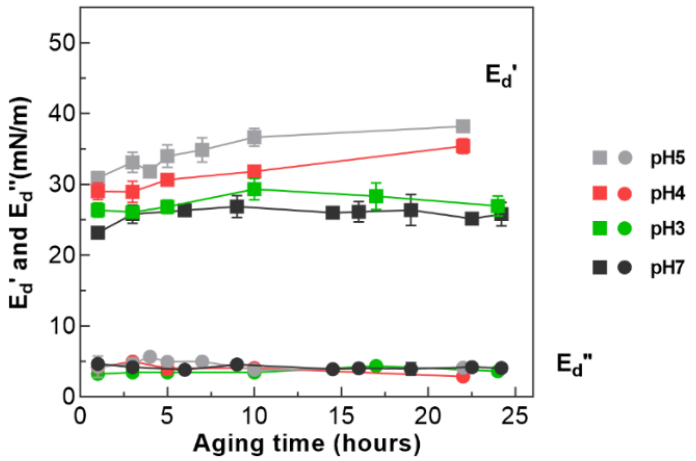

Figure 3.5: Interfacial dilatational rheology of the pre-adsorbed WPI layer (at pH 7.0) upon exposure to different pH values, measured at an area amplitude of 2.6% and a frequency of 0.01 Hz, and represented as the interfacial elastic modulus E_d' (squares) and the interfacial viscous modulus E_d" (circles). The interfacial rheology of the WPI layer at pH 7.0 was measured within 24 hours. For the three cases at pH 3.0-5.0, the protein film was pre-adsorbed at pH 7.0 for about 13 hours, followed by rinsing steps with pH 7.0, and then with pH 3.0, 4.0 or 5.0 buffers. All of them are independent experiments.

For all tested pH conditions, the interfacial elastic modulus E_d' was much higher than the interfacial viscous modulus E_d", suggesting that the adsorbed WPI film was mainly elastic. At pH 7.0, the elastic modulus E_d' gradually increased within the first 3-4 hours, and then levelled off at around 26 mN/m. Similar kinetics of a β-lactoglobulin film at the MCT-water interface were also observed by interfacial shear rheology (Kieserling et al., 2021). In the pH 3.0-5.0 buffers used for pH adjustments, a different amount of sodium chloride was added to set the total ionic strength to 43 mM (i.e. consistent with the pH 7.0 buffer) to exclude the possible influence of ionic strength changes. As shown in Figure 3.5, the highest elastic modulus E_d' was observed at pH 5.0, followed by pH 4.0 and 3.0. Because the excess WPI had been removed, no extra protein adsorption could have occurred. Hence, the significantly increased modulus at pH 5.0 (i.e. around the IEP) must be due to increased protein-protein interactions as a result of reduced electrostatic repulsion between adjacent protein molecules. It should be noted that the elastic modulus E_d' at pH 5.0 continued to increase slowly during the 22 hours of the

test. Similar phenomena were also observed at pH 4.0. In contrast, when the pH value was adjusted to pH 3.0 (i.e. much lower than the IEP), the elastic modulus was comparable to that at pH 7.0, which was due to the electrostatic repulsion between adjacent protein molecules (i.e. far away from IEP). As the differences between the viscous moduli E_d" at different pH conditions were very small, they were not discussed in detail here. Similarly, a previous work studied the pH effect on the interfacial shear rheology of a β-Lg layer at the oil-water interface and observed a maximum shear elasticity around the protein's IEP (Rühs et al, 2012). This was also the case for a β-Lg layer at the air-water interface (Engelhardt et al., 2013).

3.3.2 Adsorption/desorption of LMP onto/from the pre-adsorbed WPI layer

The solution pH plays a dominant role in the electrostatic properties of biomacromolecules as it controls the ionization degree of charged groups (e.g. -NH_2 and -COOH). Hence, the sequential adsorption of LMP onto the preformed WPI layer was studied over a wide pH range (3.0-7.0). Before pH adjustments and LMP addition, the excess WPI was washed out by a fresh pH 7.0 buffer to avoid the electrostatic complexation in the bulk. In Table 3.2, the pH adjustments and successive LMP addition at pH 3.0-5.0 only slightly decreased the interfacial tension (i.e. within 1 mN/m)**.** Although some pectin samples were reported to be able to reduce the oil-water interface tension (e.g. due to the existence of minor protein moieties), they lack effective surface activity compared to the protein used. Similar phenomena were also observed in the sequential adsorption of other protein-polysaccharide combinations (Corstens et al., 2017; Scheuble et al., 2014).

Besides, the interfacial dilatational rheology was studied both before and after LMP addition. Hereby, the protein layer was allowed to age for about 13 hours at the tested pH before LMP adsorption. After introducing LMP and 10 hours of equilibration, the excess LMP was removed by subphase exchange. In Figure 3.6, the amplitude sweep was performed for different interfacial layers. A significant increase of the elastic modulus E_d' after adding LMP suggested the interaction of LMP with the protein layer. For instance, at an amplitude of 2.6%, the elastic modulus E_d' of the WPI layer at pH 3.0 increased from 26.4±1.0 to 48.9±1.2 mN/m. Similar but slightly smaller

enhancements were also observed at pH 4.0 (i.e. from 34.9±2.2 to 48.1±1.0 mN/m). Both of them cannot be ascribed to the aging effect of the primary protein layer, as shown in Figure 3.5. At pH 3.0-4.0, the two biopolymers carry opposite charges. Hereby, the existence of electrostatic attraction facilitated the adsorption of anionic LMP. Besides, even for large amplitude oscillatory measurements, the interfacial elasticity of the WPI/LMP bilayer was still appreciably higher than that of the individual WPI layer.

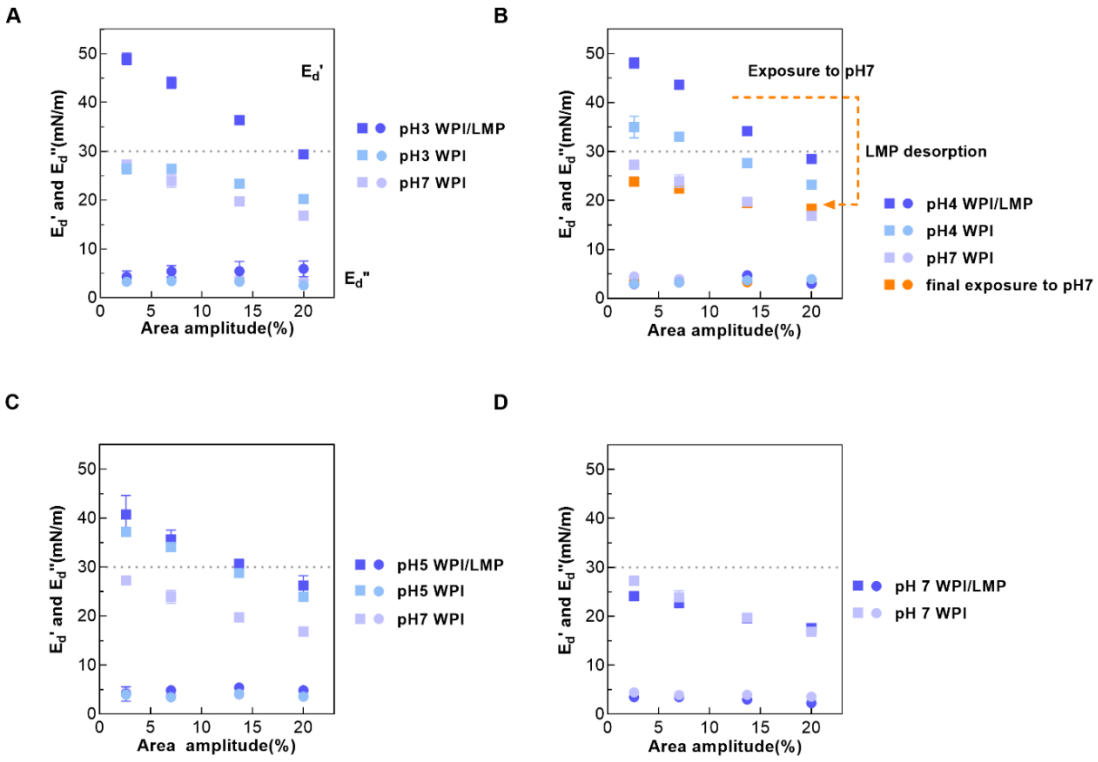

Figure 3.6: Interfacial dilatational rheology of the different adsorbed layers was measured as a function of amplitude and represented as interfacial dilatational elastic modulus E_d' (squares) and viscous modulus E_d" (circles). In all cases, the protein film was pre-adsorbed at pH 7.0, followed by rinsing steps with pH 7.0 and pH 3.0-5.0 buffers. Subsequently, LMP was introduced at the corresponding pH, and a rinsing step was performed. To study the desorption of LMP, a final rinsing step with a pH 7.0 buffer was used.

However, much smaller changes (i.e. from 36.9±0.7 to 40.7±3.9 mN/m), as well as a large deviation of E_d' (i.e. 3.9 mN/m) among independent repetitions were observed at pH 5.0, which suggested only a limited or insignificant increase. Besides, a 5-fold

higher LMP concentration (i.e. 0.05 wt.%) was also tested to determine the effect of LMP concentration but the same results were observed (data not shown). In fact, the elastic modulus was comparable to that of the individual protein film after aging for 22 hours at pH 5.0 (Figure. 3.5). Even though pH 5.0 is close to the IEP of WPI, the protein molecules still contain positively charged patches, which enable the adsorption of the anionic LMP, as confirmed by the QCM-D measurements in chapter 2. Similar results (i.e. insignificant changes of the interfacial dilatational rheology) were also reported for the adsorption of carboxylated pullulan onto a pre-formed β-lactoglobulin film at the air-water interface at pH 4.5, but they did not investigate the adsorption at more acidic pH conditions (Ganzevles et al., 2007).

To investigate the possible non-linear behaviour during large amplitude oscillatory cycles, the "Lissajous figures" were plotted to analyse the dynamic changes in the interfacial film during extension/compression. Generally, a purely elastic behaviour exhibits a linear shape, whereas a purely viscous response shows a spherical shape. Elliptic plots indicate a linear viscoelastic response, whereas asymmetric shapes point to a non-linear response (Sagis & Fischer, 2014). As depicted in Figure 3.7A-D, both the WPI and WPI/LMP bilayer stabilized interfaces exhibited narrow shapes at 20% deformation, suggesting that the response was predominantly elastic. The plots of the WPI layer seemed more asymmetric than the bilayer structures (i.e. formed at pH 3.0-5.0). To quantitatively describe these Lissajous plots, the S-factor during extension/compression was determined for all systems: S=0 for a linear elastic response, S>0 for interfaces displaying strain hardening, and S<0 for interfaces displaying strain softening (Sagis & Fischer, 2014). As depicted in Figure 3.7E, the WPI layer exhibited strain-softening during extension, which can be due to the disconnection of the interfacial microstructure. Conversely, the increased surface coverage upon compression led to a jammed state (i.e. strain-hardening) (Schröder et al., 2017).

In contrast, upon LMP adsorption, the Lissajous plots of the bilayer structure (especially at pH 3.0-4.0) showed an appreciably higher slope during extension/compression cycles. Since the slope is related to the dilatational elasticity, these observations confirmed the results in Figure 3.6. Besides, relatively symmetric plots were observed for the bilayer structures, indicating a more linear rheological

response during the oscillation cycles. Additionally, the values of the S-factor (either during extension or compression) were closer to zero when decreasing the pH from neutral to acidic conditions where the deposition of LMP is more favourable. The linear response (e.g. less strain-softening during extension than for the single WPI layer) also implied that the interfacial layers were more resistant to collapse at large deformations.

Hence, it can be concluded that the deposition of LMP onto the protein-coated oil-water interface indeed increased the interfacial viscoelasticity, whereby the magnitude was largely dependent on the pH conditions. It should be noted that the interfacial elasticity of the bilayers at the three pH conditions was in the range of 40-51 mN/m (i.e. at an amplitude of 2.6%), which was only slightly higher than that of the individual WPI layer at pH 5.0 where the maximum elastic modulus was observed (around 38 mN/m). One speculation is that the interfacial viscoelasticity is mainly governed by the protein-protein interactions in the primary protein layer, whereby the deposition of anionic LMP can deplete the positive charges and reduce the repulsion between adjacent protein molecules. Additionally, there would be less repulsive forces between the adsorbed LMP molecules when the pH was close to its $pK_{a,}$ which to some extent could also strengthen the interfacial layer.

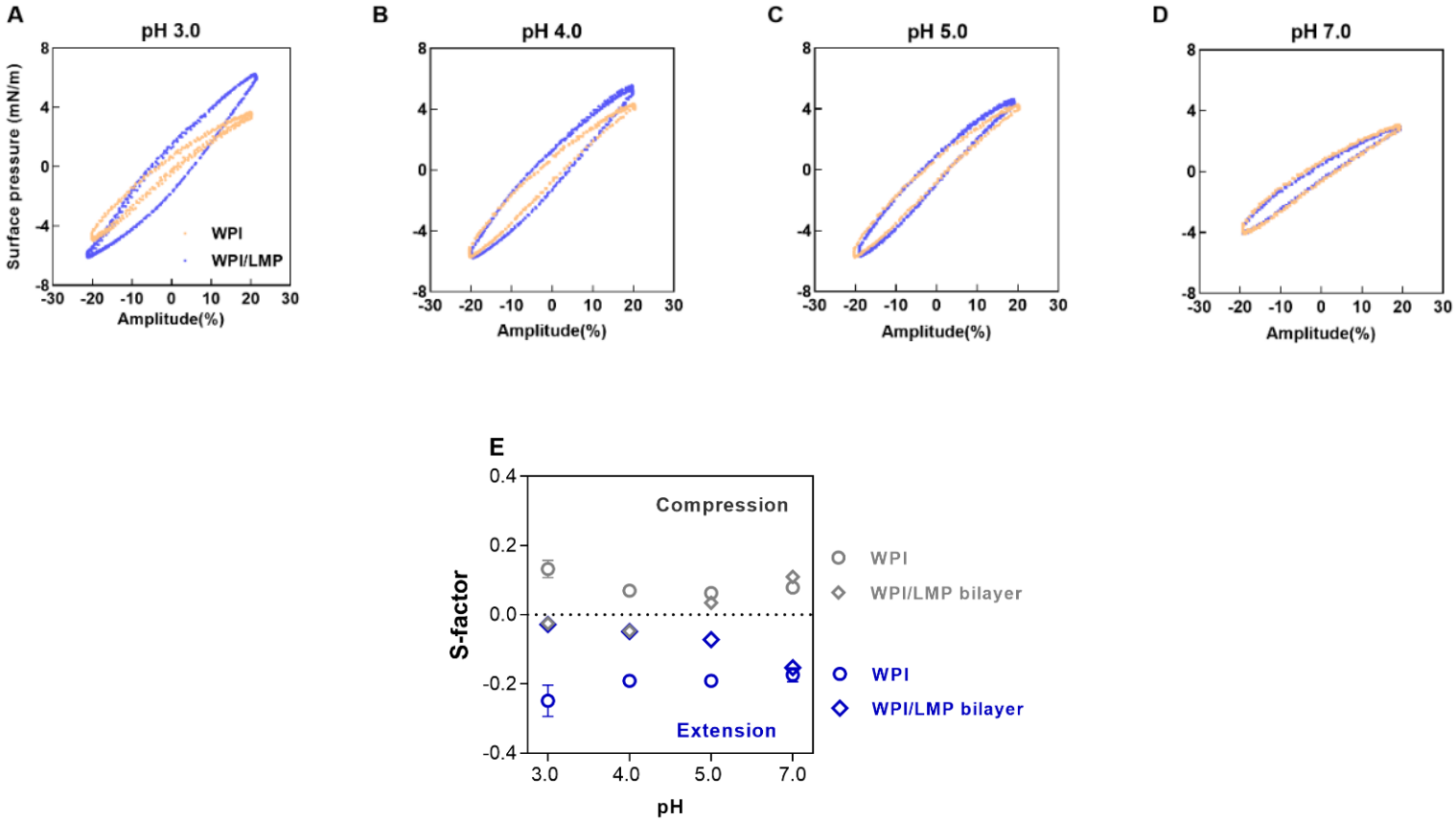

Figure 3.7: Lissajous plots of surface pressure versus area amplitude (up to 20%) for a WPI layer (yellow) and WPI/LMP bilayer (blue) at various pH conditions (A-D), and the S-factor in extension (blue)/compression (grey) of MCT-water interfaces stabilized by a WPI layer (circles) or WPI/LMP bilayer (diamonds) as a function of pH (E).

Additional evidence of the formation of an appreciably elastic film after WPI/LMP adsorption can be visualized in the photographs of the oil droplets upon partially withdrawing the interior oil (Figure 3.8). For WPI/LMP bilayer coated droplets, obvious wrinkles can be observed on the surface of the droplets when the volume was decreased gradually (e.g. from initially 20 μL to below 8 μL). Meanwhile, the sphere-like droplets acquired a "pear-like" shape. Individual WPI stabilized droplets also exhibited similar phenomena, but the wrinkles were less obvious even at pH 5.0 where the maximum interfacial elasticity was observed. In contrast, the clean oil-water interface always had a spherical shape, irrespective of the droplet volume, upon shrinking a pre-formed interface.

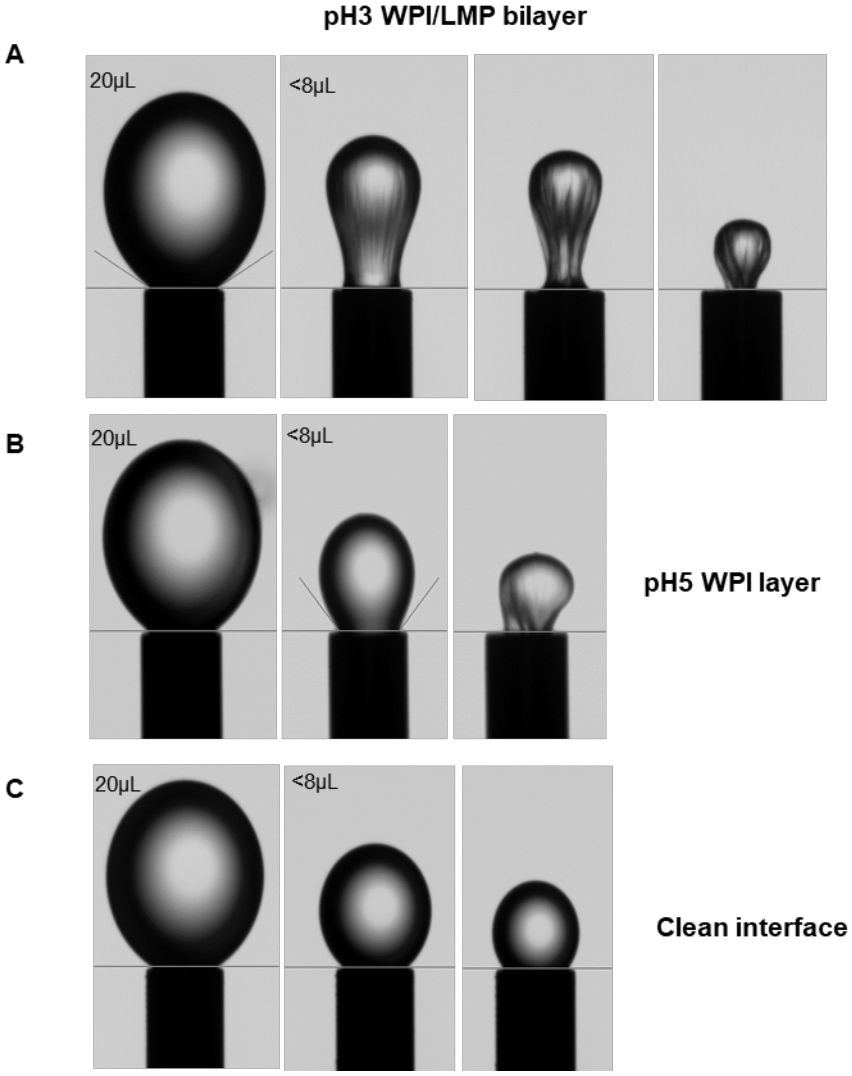

Figure 3.8: Photographs of a WPI/LMP coated MCT oil droplet (A,B) and a clean oil droplet (C) formed on a needle tip. The volume of the oil droplets (initially 20 μL) was gradually reduced through the motor-driven syringe (-0.2 μL/s).

At pH 7.0, both WPI and LMP carry highly negative charges. Nevertheless, positively charged patches are present, considering the high pK_a value (about 10.5) of the lysine residues in whey proteins. As shown in Figure 3.6D, the addition of LMP at pH 7.0 did not boost the elastic or viscous modulus of the pre-adsorbed WPI layer at all tested deformations. Instead, a slight reduction was observed at small deformations, which can be due to a structural hysteresis during the rinsing steps. Besides, the Lissajous plot of the WPI layer basically overlapped with that after LMP addition at pH 7.0 (Figure. 3.7D). Hereby, it can be concluded that no LMP adsorption occurred at pH 7.0. These results clearly show that the interfacial complexation was not favoured at pH conditions that are at least some pH units above the protein's IEP, which is due to the strong intermolecular electrostatic repulsion.

The pH-dependent interfacial rheology also suggested that the interfacial deposition was mainly driven by electrostatic interactions, which determined the binding affinity between the protein and the anionic polysaccharide. To test the reversibility of the interfacial complexation, the WPI/LMP bilayer formed at pH conditions below the IEP of WPI was further exposed to pH 7.0 (i.e. rinsed by the pH 7.0 buffer). As shown in Figure 3.6B, upon rinsing, the interfacial elastic modulus E_d' went down appreciably at all tested deformations (e.g. from about 48.1 mN/m to 23.8 mN/m at an amplitude of 2.6%). The resulting E_d' values were comparable to or even slightly smaller than that obtained at pH 7.0 for the pre-adsorbed WPI layer. Similar phenomena were also observed for the WPI/LMP bilayer prepared at pH 5.0 and 3.0 (data not shown). These results pointed to the desorption of the LMP layer from the pre-adsorbed WPI layer due to the charge inversion upon exposure to pH 7.0. These results are well consistent with the QCM-D results in chapter 2.

3.3.3 Characterization of WPI emulsion and WPI/LMP bilayer emulsion

The particle size distribution (PSD) of the emulsion droplets stabilized by WPI (at pH 7.0) or WPI/LMP (at pH 3.0) is shown in Figure 3.9. Their comparable PSD directly after preparation (day0) and the inversion of the zeta-potential (from +23.5 to –5.6 mV) at pH 3.0 upon LMP addition suggested the adsorption of LMP onto the WPI-coated droplets, as well as the absence of flocculation. Moreover, the interfacial structure of the droplets was visualized by Cryo-SEM (Figure 3.10). To enable the

observation of the interfacial film, the sublimation time was optimized to slightly shrink the oil droplets. Indeed, the WPI/LMP bilayer film was thicker than the individual WPI film.

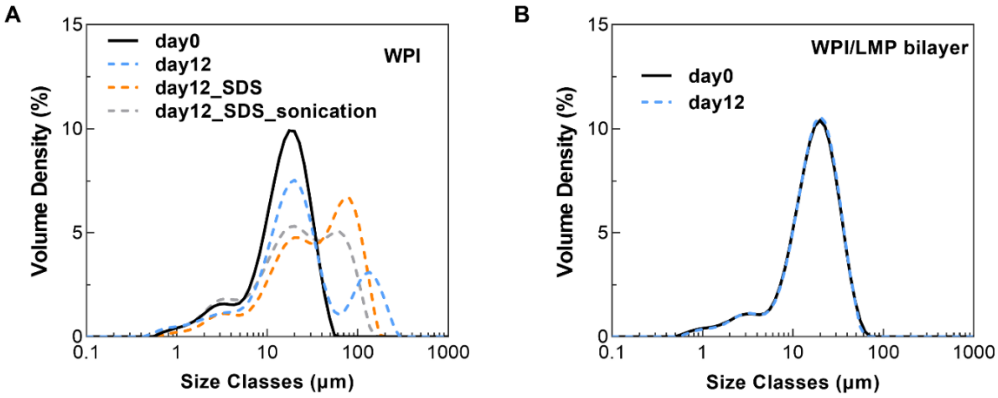

Figure 3.9: Particle size distribution of emulsions (16% MCT oil) stabilized by (A) WPI at pH 7.0 and (B) WPI/LMP (bilayer) at pH 3.0 upon dilution in the corresponding buffer or in a pH 7.0 buffer containing 1% SDS (day12_SDS); the latter sample was also subjected to ultrasonication (day12_SDS_ultrasonication)

After 12 days of storage at 4˚C, no PSD change can be observed for the bilayer emulsion, whereas larger size particles (e.g. over 100 μm) were observed in the WPI-stabilized emulsion at pH 7.0. The emergence of an additional mode at large diameters was also observed in WPI-stabilized emulsions at pH 3.0 (data not shown). In order to investigate whether these larger structures were due to flocculation or coalescence, the effect of dilution in an aqueous SDS solution and/or ultrasonication on the PSD was investigated. It was reported that SDS can break aggregates by eliminating bridging flocculation and hydrophobic interactions (Setiowati et al., 2017). It should be noted that the effect of SDS on protein-coated droplets may be complicated especially at acidic pH conditions (Demetriades & McClements, 2000). Hence, only the results of dilution in SDS for the WPI emulsion at pH 7.0 are shown. As depicted in Figure 3.6, the SDS treatment could not fully break these large aggregates. A subsequent ultrasonication treatment was also used, which can be a stronger way to physically break aggregates. However, these big aggregates were still not broken down. Therefore, these results suggested that the larger droplet sizes were either due to strong (largely irreversible) aggregation or coalescence in the WPI-stabilized emulsion. In fact, both

phenomena are not independent from each other as severe aggregation during storage also can unavoidably lead to an increased probability to coalesce. Similar coalescence (or oiling-off) phenomena of WPI-coated droplets during storage were observed by Matsuyama et al. (2021). Therefore, the LMP coating effectively prevented aggregation and coalescence of WPI-coated droplets during storage.

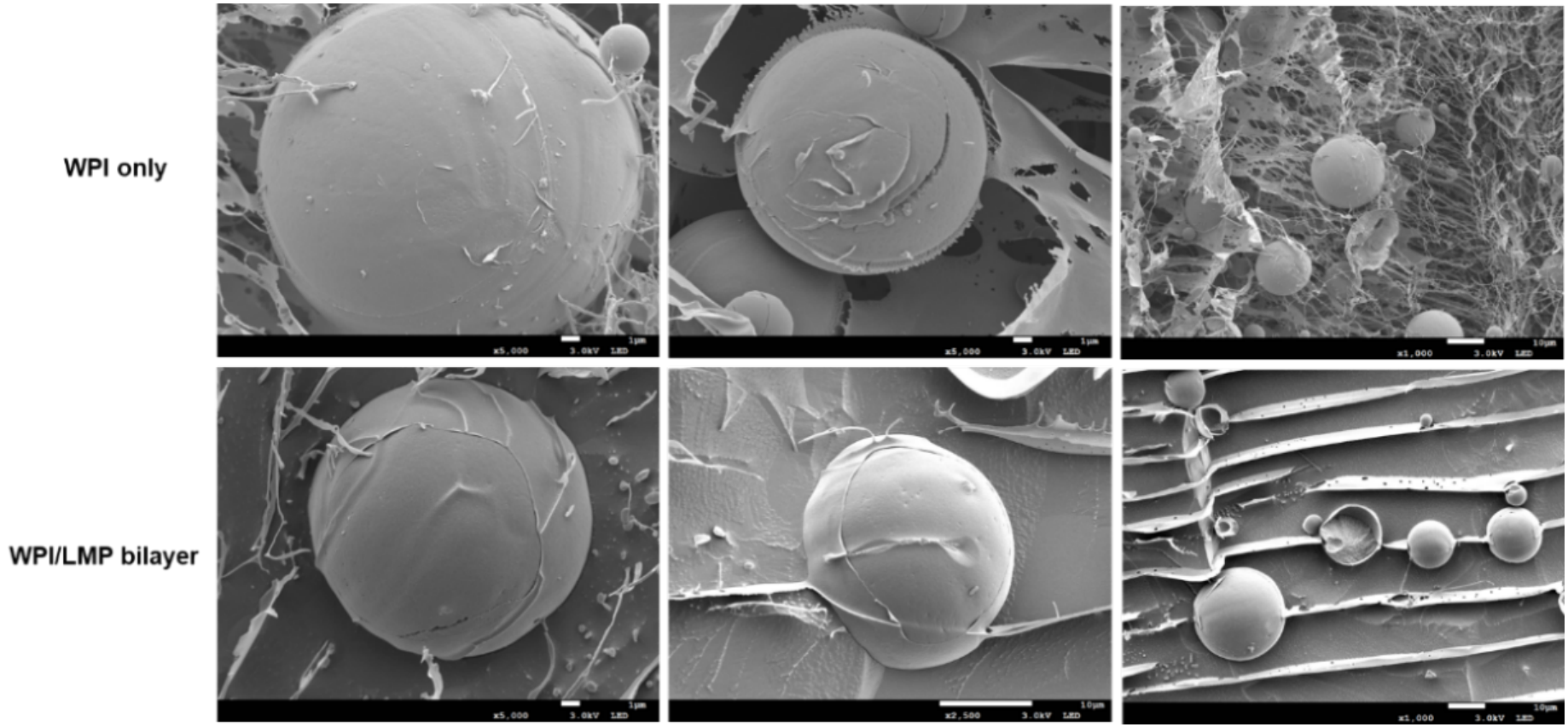

Figure 3.10: Cryo-SEM images of WPI and WPI/LMP stabilized emulsion. The images from left to right indicate different magnifications for each sample.

Figure 3.11: Visual appearance of WPI (left) or WPI/LMP bilayer (right) emulsions at pH 3.0 after ultracentrifugation (at 48,200×g, for 60 min). The yellow circle is used to highlight the oiling-off phenomenon.

Moreover, the emulsion samples were also subjected to ultracentrifugation (at 48,200×g for 60 min). This high centrifugation force compresses the cream layer and pushes the droplets against each other. Hereby, the droplets are squeezed together much more strongly and hence the chance to induce coalescence is much higher than in the gravity field. When the pressure is above the yield stress of the interfacial materials, it will cause the rupture of the interfacial film and lead to oiling off. As shown in Figure 3.11, the WPI emulsion showed obvious oiling off after ultracentrifugation (either at pH 3.0 or 7.0), whereas no oiling-off was observed in the bilayer emulsion. Additionally, a solid-like cream layer was formed in the latter case. These results confirm the better mechanical properties of the bilayer, which can be ascribed to its higher interfacial elasticity and thickness.

3.4 Conclusions

We investigated the effect of pH on the sequential adsorption of WPI and LMP at the MCT oil-water interface through dynamic interfacial tension and interfacial

dilatational rheology. For the pre-formed protein layer at pH 7.0, successive pH changes and LMP addition hardly influenced the interfacial tension provided that the excess protein in the continuous phase was washed away. The maximum interfacial viscoelasticity was reached when the pH was close to the IEP of WPI because of increased protein-protein interactions (i.e. reduced electrostatic repulsion). The deposition of LMP onto the protein-coated oil-water interface could significantly increase the interfacial viscoelasticity, but the magnitude of this effect was largely dependent on the solution pH value. Besides, a more linear rheological response of the bilayer structures than of the individual WPI layer was observed during large amplitude oscillatory cycles, especially at pH 3.0-4.0. No LMP adsorption was observed at pH 7.0 due to the strong electrostatic repulsion. Moreover, the adsorbed LMP showed a pH-responsive desorption behaviors upon exposure to neutral pH, as evidenced by the restored interfacial elasticity. The thicker WPI/LMP layers could be visualized by cryo-scanning electron microscopy (Cryo-SEM). The composite layer not only effectively prevented the irreversible aggregation and/or coalescence of lipid droplets during storage, but also exhibited outstanding mechanical properties to avoid film rupture during ultracentrifugation. This work can provide useful insights into the design of interfacial structures with improved performance by globular proteins and anionic polysaccharides. The pH-responsive interfacial complexation may be used to design functional delivery systems for bioactive ingredients. Besides, these results also proved that interfacial rheology is a useful tool to study the biopolymer interactions at fluid interfaces, whereby the methodology can be easily extended to other systems. Whereas the present work only discussed the interfacial dilatational rheology characteristics, interfacial shear rheology with subphase exchange could be an additional valuable tool to further understand the sequential adsorption of proteins and oppositely charged biopolymers.

Chapter 4 Designing Gastric Stable Adsorption Layers by Whey Protein-Pectin Complexation at the Oil-Water Interface

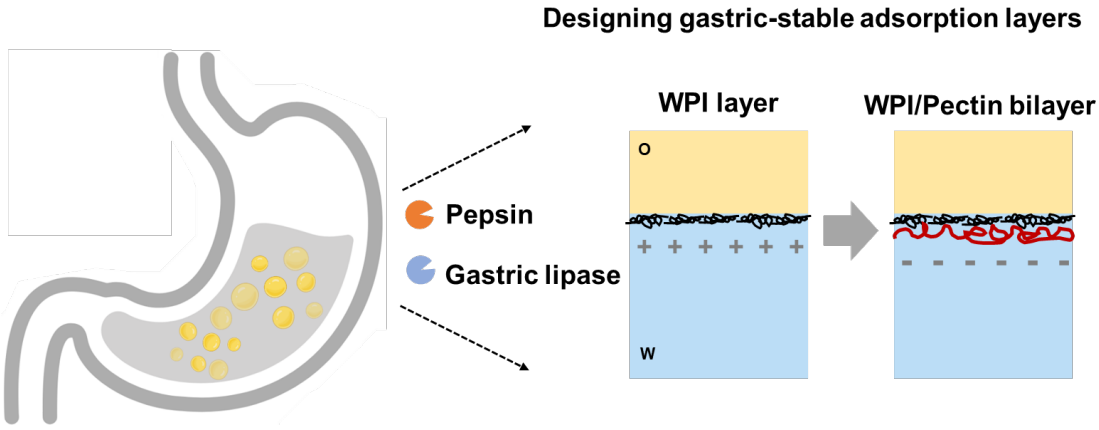

Abstract

This chapter aims to design gastric-stable emulsions with food-grade biopolymers, using a novel multiscale approach. The adsorption layer formation at the oil-water interface was based on opposite charge interactions between whey proteins and pectin (with different esterification levels) at pH 3.0 by a sequential adsorption method. The interfacial assembly and disassembly (interfacial complexation, proteolysis, and lipolysis) during in vitro gastric digestion were evaluated using a quartz crystal microbalance with dissipation monitoring, zeta potential, dynamic surface tension, and interfacial dilatational rheology. Besides, the evolution of the particle size and microstructure of bulk emulsions during the digestion was investigated by static light scattering and light microscopy. Compared with whey protein isolate (WPI)-stabilized emulsions, the presence of an additional pectin layer can prevent or at least largely delay gastric destabilization (giving rise to coalescence or/and oiling off). Especially, the esterification degree of the pectin used was found to largely affect the emulsion stability upon gastric digestion.

4.1 Introduction

Oil-in-water (O/W) emulsions are overwhelmingly present in foods, pharmaceuticals, and personal care products, where they are frequently used as delivery systems for lipophilic ingredients (Luo et al., 2020; McClements et al., 2007). As an ideal delivery system, it is required that the encapsulated functional ingredients can be released from the lipid droplets on demand during the life cycle of the emulsions (e.g. from food processing to after ingestion).

In emulsion systems, oil and water phases are separated by a narrow region, the oil-water interface, which is dominated by emulsifiers to ensure the metastability of the system. Despite the fact that this interface is very thin (in the nanometer range), it represents a large surface area and controls to a great extent the physicochemical stability of emulsions (Berton-Carabin et al., 2018). Thus, interfacial design is a promising way to tailor the functional properties of emulsion systems. The purpose of this study was to design gastric stable adsorption layers using food biopolymers that would enable lipid droplets to survive the harsh gastric digestion conditions (e.g. acid pH, pepsin, gastric lipase), and ultimately be released in the small intestine.

Food proteins exhibit an excellent surface activity in the stabilization of the oil-water interface, whereby submicron or even nanoemulsions can be easily produced. However, the protein layer at the O/W interface is usually vulnerable to pepsin proteolysis. For instance, β-lactoglobulin, a primary protein fraction in milk whey, is resistant to pepsin in bulk solution but can be easily broken down by pepsin once adsorbed onto the oil-water interface due to protein unfolding (MacIerzanka et al., 2009).

Besides, lipolysis by gastric lipase produces free fatty acids, which are highly surface active and may displace proteins from the O/W interface (Scheuble et al., 2016). The role of gastric lipase has long been neglected for in vitro digestion experiments since human gastric lipase is not commercially available. Sassene et al., (2016) compared different gastric lipase alternatives for in vitro models of gastric digestion. More recent studies (including the INFOGEST protocol) have suggested that rabbit gastric lipase could be a suitable alternative (Acquistapace et al., 2019; Brodkorb et al., 2019). In fact, in vivo studies have demonstrated that there is a significant amount of lipolysis that may occur in the stomach, which can account for 10 to 30% of the total amount of

lipids that are cleaved in the digestive tract (Armand, 2007; Malagelada et al., 1979; Pilichiewicz et al., 2006). The rupture of the interfacial membrane and lipolysis will affect the stability of emulsions (leading to flocculation/coalescence) and may impact the stability and release of encapsulated bioactive ingredients (Nguyen et al., 2019; Steingoetter et al., 2015). In some cases, insoluble fatty acids produced by gastric lipolysis could also build up at the interface of the emulsion droplets (Pafumi et al., 2002). Additionally, the work of Golding et al., (2011) demonstrated that the nature of the interfacial membrane dictates if the emulsion undergoes simple aggregation or gastric coalescence in both in vitro and in vivo studies.

As discussed in Chapter1, the combination of polysaccharides with proteins could be an effective strategy to modify and extend the functional performance of proteins. Here, it is hypothesized that the indigestibility of polysaccharides could protect the protein-coated droplets during gastric digestion so that a gastric stable emulsion can be made. Since most polysaccharides are not effectively surface active, we used a layer-by-layer technique to allow the adsorption of anionic pectin onto a previously formed protein layer.

The formation of a bilayer or multilayer onto emulsion droplets using proteins and polysaccharides has been extensively reported to improve the colloidal stability of the droplets against pH (e.g. around the isoelectric point) and ionic strength variations and to retard lipid oxidation during storage (Guzey & McClements, 2006; Tian et al., 2021). However, concerning their gastric stability, the role of an additional polysaccharide layer is still not fully elucidated. Despite the fact that some relevant studies already existed (Araiza-Calahorra & Sarkar, 2019; Sabet et al., 2021; Xu et al., 2014), most of them evaluated the gastric stability of multilayer emulsions using only particle size analysis (e.g. light scattering, microscopy). Emulsion digestion is actually a complicated interface phenomenon (Maldonado-Valderrama, 2019). The obtained information from these previous studies may be speculative since it cannot be excluded that the claimed stability or functionalities originate from the bulk coacervation or/and depletion. No more detailed information (e.g. proteolysis kinetics, leakage of the oil core) can be acquired. More importantly, the role of gastric lipase was not taken into account in their in vitro digestion protocols, although gastric lipase has been demonstrated to exhibit a synergistic effect with pepsin on the gastric stability of

protein-stabilised emulsions (Golding et al., 2011). Accordingly, the formulation design (especially the choice of polysaccharide) for gastric-stable emulsions remains empirical.

This work aims to elucidate the influence of pectin adsorption on the gastric stability of WPI-coated droplets. Simulated gastric fluids were prepared according to the well-recognized INFOGEST protocol. The digestive enzymes were derived from rabbit gastric extracts so that the combined effect of pepsin and gastric lipase could be evaluated. Since the degree of esterification in pectins can largely influence their physiochemical properties (e.g. electrical properties, gelation properties), both high- and low-methoxy pectin were investigated. A novel multiscale approach was used to provide insights into the gastric digestion of protein/polysaccharide emulsions. First, the in-situ interfacial assembly of WPI and pectin was investigated by quartz crystal microbalance with dissipation monitoring and zeta-potential analysis. Second, the real-time proteolysis and lipolysis at the O/W interface were studied on a single droplet via a modified drop shape tensiometer equipped with a subphase exchange setup. This technique has been demonstrated to study the digestion of a single protein layer at the oil-water interface (Maldonado-Valderrama, 2019), and it is extended to study the properties of the bilayer structures. Besides, the drop shape tensiometer enables to determine the lipolysis kinetics of triglycerides (Labourdenne et al., 1994; Scheuble et al., 2016). Finally, the evolution of the particle size, zeta potential, and microstructure of a bulk emulsion during gastric digestion was monitored and quantified.

4.2 Materials and Methods

4.2.1 Materials

As described in sections 2.2.1 and 3.2.1, WPI and LMP were obtained from Davisco Foods International, Inc. (BiPro, Le Sueur, MN, USA) and Cargill (Ghent, Belgium). HMP with a DE of 68% (average molecular weight 55.8 kDa) was received from Cargill (Ghent, Belgium), and was used without further purification. As described in section 3.2, medium-chain triglycerides (MCT) were obtained from Go-Keto. Rabbit gastric extracts (RGE15) were purchased from Lipolytech (Marseille, France), including around 15 U/mg gastric lipase and 500 U/mg pepsin. Curcumin (95%, B21573) was

obtained from Alfa Aesar (Germany). Deionized water was used for all experiments. All other chemicals were of analytical grade.

4.2.2 Dynamic interfacial tension and dilatational rheology

4.2.2.1 Stock solution preparation

WPI was dissolved in 20 mM sodium phosphate buffer (pH 7.0; ionic strength= 43 mM) at a concentration of 0.1% (w/w). After stirring for 2 h at room temperature and overnight hydration at 4 °C, the WPI dispersion was passed through a 0.45 μm mixed cellulose ester (MCE) membrane filter to remove any insoluble materials. LMP was dissolved in deionized water at a concentration of 0.1% (w/w) after overnight stirring. 0.02% (w/w) of NaN_3 was added into the biopolymer solutions. They were diluted 10-fold by buffers at the tested pH conditions before using.

The simulated gastric fluid (SGF) used for subphase exchange was prepared according to the INFOGEST protocol, including 0.257 g/L KCl, 0.063 g/L KH_2PO_4, 1.05 g/L $NaHCO_3$, 1.379 g/L NaCl, 0.012 g/L $MgCl_2$, 0.024 g/L $(NH_4)_2CO_3$, 0.011 g/L $CaCl_2.(H_2O)_2$, and 1g/L RGE (i.e. containing 15 U/mL lipase and 500 U/mL pepsin). This amount of enzymes was lower than applied during bulk emulsion digestion, but was more than sufficient for observing digestion on a single droplet; it was chosen to avoid a high solution turbidity.

4.2.2.2 In vitro digestion at the oil-water interface

The dynamic interfacial tension was measured with a modified drop tensiometer allowing external phase exchange (Teclis, Tracker, France), as described in section 3.2.3. The temperature was controlled at 37 °C by a Julabo circulator.

The WPI was allowed to adsorb from the bulk to the interface for around 15,000 s before the area deformation was applied and the continuous phase was replaced by a 5-fold volume of protein-free pH 7.0 buffer (i.e. about 200 mL) and subsequently by a 5-fold volume of fresh pH 3.0 phosphate buffer (20 mM). To prepare a WPI-pectin bilayer film, the continuous phase was further exchanged with 150 mL of 0.01 wt.% LMP or HMP solution in pH 3.0 buffer, followed by 1 hour of equilibration to allow pectin adsorption. Similar protocols were also used to prepare the adsorption layers at pH 5.0.

To investigate the role of SGF on the properties of the pre-formed WPI layer or bilayer, the continuous phase was exchanged with 200 mL of SGF (without RGE), followed by 0.5 hour of equilibration. Finally, 40 mL of 1 g/L RGE in SGF was introduced to study gastric digestion at the oil-water interface.

The dilatational moduli of the interfacial film at the end of each stage were determined at 0.05 Hz (i.e. by increasing or decreasing the volume of the oil drop sinusoidally) at an area amplitude of 5%.

4.2.3 QCM-D and zeta-potential

The sequential adsorption of WPI and pectin at a hydrophobic surface was investigated at pH 3.0 by a Q-sense E4 system (Biolin Scientific, Sweden).The QCM-D protocol was described in section 2.2. The temperature during running samples was set at 25.0 °C. Gold-coated crystal sensors (4.95 MHz, QSX 301) were modified with 2 mM 1-hexadecanethiol in absolute ethanol for at least 20 h to hydrophobize the surface at 30 °C. The hydrated mass of the adsorbed layer was estimated by fitting the frequency and dissipation shifts (based on the 3rd to 11th overtones) with the viscoelastic Kevin-Voigt model using QTools software 30.15.553 (Biolin Scientific). The dynamic viscosity and density of the continuous phase are input parameters for the fitting and were determined to be 0.915 mPa.s and 999.5 kg/m^3 at 25.0 °C, respectively.

The zeta-potential of WPI (1 wt.%) and LMP or HMP (0.1 wt.%) as a function of pH was measured with a Zetasizer 3000 (Malvern Panalytical Ltd, Malvern, U.K.)

4.2.4 Emulsion preparation and characterization

4.2.4.1 Emulsion preparation

1 wt.% WPI solution was prepared in 10 mM sodium phosphate at pH 3.0. 5 g of MCT oil was added into 45 g of 1 wt.% WPI solution. Subsequently, the mixture was homogenized at 24,000 RPM for 4 min to prepare the WPI emulsion. To remove the excess of non-adsorbed protein, the emulsion was centrifuged at 70 g for 1 h. The obtained subnatant was removed by a syringe equipped with a long needle, and then replaced with the same amount of the pH 3.0 buffer. Subsequently, the cream layer was dispersed in the buffer by inverting the centrifuge tubes several times. Since some

large droplets emerged after the centrifugation step, the WPI-stabilized emulsion was further homogenized at 24,000 RPM for 4 min.

To prepare WPI/pectin bilayer emulsions, 10 g of the washed WPI emulsion was added dropwise into 15 g of 0.5 wt.% pectin solution (adjusted to pH 3.0) under continuous stirring. The excess pectin was also removed by the centrifugation/redispersion steps: the cream layer was dispersed in 19 g of the pH 3.0 buffer. Hence, the final emulsion contained ca. 5 wt.% of MCT oil.

4.2.4.2 In vitro gastric digestion of emulsion

The in vitro gastric digestion of emulsions was performed according to the INFOGEST method, which is a standardized digestion protocol with international consensus presented by Brodkorb, et al. (2019). The prepared SGF contained 0.514 g/L KCl, 0.126 g/L KH_2PO_4, 2.10 g/L $NaHCO_3$, 2.758 g/L NaCl, 0.024 g/L $MgCl_2$, 0.048 g/L $(NH_4)_2CO_3$, 0.022 g/L $CaCl_2(H_2O)_2$, and 8g/L RGEs (i.e. containing 120 U/mL rabbit gastric lipase and 4000 U/mL rabbit pepsin). The SGF was adjusted to pH 3.0 with 6 M HCl at 37 °C. 3 mL of the emulsions was mixed with 3 mL of the SGF (i.e. both in the presence and absence of RGE) in a 15 mL falcon tube. The mixtures were incubated at 37 °C in a water bath under mild orbital shaking. The particle size, zeta-potential, microstructure and interfacial composition of the emulsion droplets as a function of time (i.e. after 0 min, 10 min, 30 min, 60 min, and 120 min) during digestion were determined according to the following protocols.

4.2.4.3 Particle size and zeta-potential of emulsion droplets

The particle size of the emulsion droplets was measured before and after in vitro gastric digestion using static light scattering by a MasterSizer 3000 equipped with a Hydro MV unit (Malvern, U.K.). The obscuration value was fixed between 5 and 10% with a stirring speed of 2600 rpm in mixtures of the pH 3.0 phosphate buffer and the SGF (i.e. mixed in an equal volume). The zeta potential (ζ) of the emulsion droplets was determined using a Zetasizer 3000 (Malvern Panalytical Ltd, Malvern, U.K.) after 1,000 times dilution by the buffer-SGF mixtures mentioned above. Each individual measurement was an average of three runs.

4.2.4.4 Microscopy observation

The microstructure of the emulsions before and after in vitro gastric digestion was observed by a CX40 optical microscope (Olympus GmbH, Hamburg, Germany) equipped with an Axiocam ERc5s camera (ZEISS, Germany). The observation was done at a magnification of 100X (i.e. 10X ocular lens and 10X objective lens). Briefly, one drop of the emulsions was placed on a glass slide and covered with a round cover slide to prevent the flow of droplets during observation.

4.2.5 Release of encapsulated curcumin

Curcumin-loaded emulsions were prepared according to the protocol described in section 4.2.4. Curcumin was dissolved in MCT oil at a concentration of 0.05 wt.% by incubation in a water bath at 50˚C for 10 min and subsequent 1 min of ultrasound treatment at room temperature (ca. 20 ˚C). The standard curve for curcumin quantification was set as absorbance values at 425 nm of curcumin diluted in MCT oil in the concentration range from 0.0000625 to 0.0005 wt.%.

The migration of curcumin from emulsion droplets was determined by using a membrane-free model and MCT oil was used as a release medium (Beicht et al., 2013; Wilson et al., 2021). 5 mL of MCT oil was gently placed on top of 2 mL digestion samples (i.e. already adjusted to pH 7 with NaOH to deactivate the enzymes) in 15 ml falcon tubes. The lower phase but not the upper phase was mildly stirred for 5 min, followed by centrifugation at 1,000 g for 12 min. Subsequently, the curcumin amount in the upper phase was quantified upon suitable dilution using an ultraviolet-visible spectrophotometer. The migration rate of curcumin (%) was expressed as the amount of migrated curcumin relative to the total curcumin input during emulsion preparation.

4.2.6 Data analysis

Data were presented as the mean ± standard deviation of at least three independent experiments. The difference between samples was evaluated using one-way ANOVA using GraphPad Prism 9.3 software (San Diego, USA).

4.3 Results and Discussion

4.3.1 Interfacial assembly of WPI and LMP/HMP

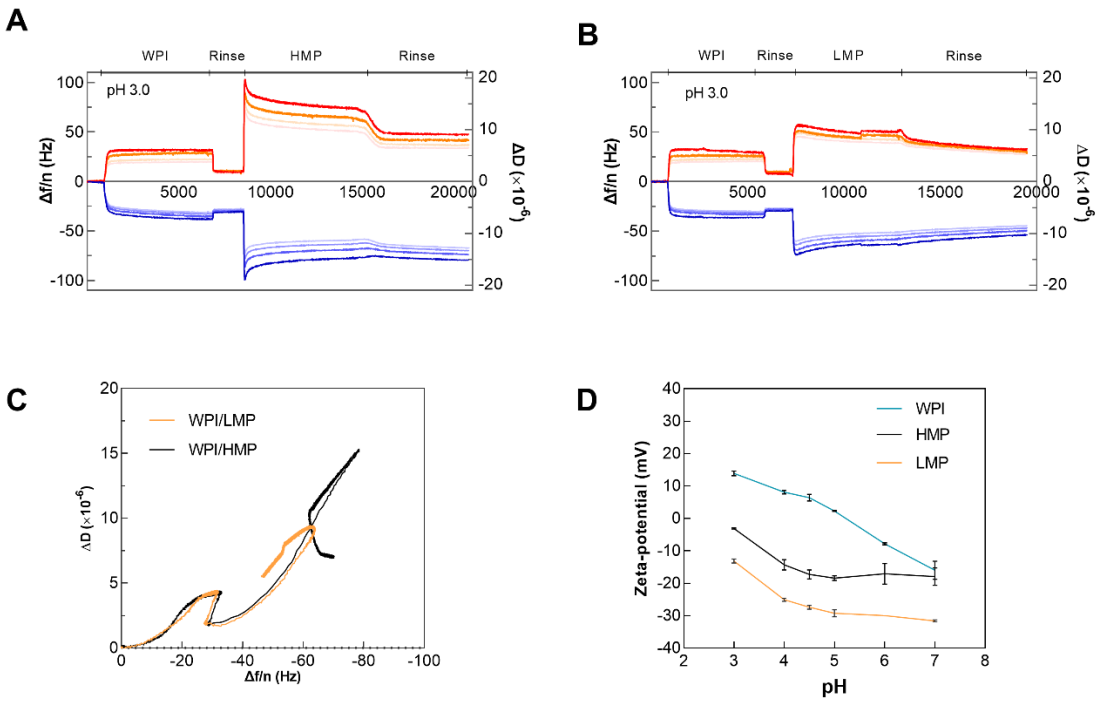

Figure 4.1: The 3rd, 5th, 7th, and 9th overtones of the normalized frequency (Δf/n) and dissipation shifts (ΔD) (with fading colors for increasing overtones) as a function of time during the sequential adsorption of WPI and HMP (A) or LMP (B) at pH 3.0; ΔD versus Δf/n plot at the 7th overtone (C); Zeta-potential of WPI, HMP and LMP as a function of pH (D).

The interfacial assembly of WPI and pectin was tested at pH 3.0 by QCM-D. The alkyl-terminated hydrophobic surface exhibited a water contact angle of 105±2° and was used to mimic the oil-water interface. Initially, the WPI solution was introduced to allow adsorption. After removing excess or loosely bound proteins by a rinsing step, the pectin solution was fed to interact with the pre-formed protein layer and afterwards a rinsing step was carried out. Figures 4.1A and B depict the frequency (Δf/n) and dissipation shifts (ΔD) as a function of time during the sequential adsorption. WPI led to a decreased frequency and increased dissipation. Taking the 5th overtone as an example, the values reached -28±1 Hz and $(1.9\pm0.1)\times10^{-6}$ after rinsing, resp., suggesting a mass uptake (due to WPI adsorption) onto the hydrophobic surface. By fitting the experimental data with the Voigt model (Reviakine et al., 2011), a wet mass

of 6.3±0.8 mg/m^2 was obtained. This value was much higher than the typical surface load (dry mass) of a WPI monolayer (ca. 2 mg/m^2) (Setiowati et al., 2017), which implied that the WPI layer at pH 3.0 entrapped about 70 wt.% of water. Comparable hydration degrees were also observed for other globular proteins (e.g. lysozyme and albumin) (Ouberai et al., 2014). Upon the introduction of 0.1 wt.% pectin, it can be observed that both types of pectin caused enhanced $\Delta f/n$ and ΔD shifts both before and after the rinsing step, suggesting the adsorption of pectin onto the protein layer. Besides, the HMP caused more pronounced shifts than the LMP.

Before the rinsing step, the absolute values of these shifts initially increased to a peak value and then decreased gradually, which was thought to be due to slow rearrangements within the interfacial layer and the removal of water molecules. These rearrangements were more obvious in the ΔD versus $\Delta f/n$ plot (which was based on the 7th overtone in Figure 4.1C), in which the time effect is eliminated. Upon rinsing, the $\Delta f/n$ and ΔD shifts for WPI-LMP reached -61.5±2.5 Hz and (8.0±0.5)×10^{-6} at the 3rd overtone, -55.1±1.0 Hz and (7.9±1.0)×10^{-6} at the 5th overtone, and -51.0±0.5 Hz and (7.7±0.3)×10^{-6} at the 7th overtone. In contrast, the values for WPI/HMP at the three overtones were -77.5±1.5 Hz and (9.6±0.6)×10^{-6}, -71.0±0.5 Hz and (8.1±0.1)×10^{-6}, and -67.0±0.2 Hz and (7.0±0.1)×10^{-6}, respectively. This also corresponded to a higher hydrated mass for the WPI/HMP bilayer, i.e. about 30 wt.% higher relative to the WPI/LMP case (in Table 4.1). Especially, it was observed that the response of ΔD was more overtone-dependent for WPI/HMP, which indicates more liquid-like characteristics.

This different behavior can be explained from the zeta-potential as a function of pH behavior as illustrated in Figure 4.1D: as compared with HMP, the LMP used had more anionic groups and thus could more strongly (electrostatically) interact with the oppositely charged protein molecules. As a further consequence, the LMP formed a denser composite layer, whereas the adsorbed HMP most probably adopted a more extended conformation (e.g. neutral chains) into the aqueous phase. Besides, the higher adsorbed mass of HMP may be also partly explained by the higher average molecular weight of the HMP compared to the LMP.

Table 4.1: Hydrated mass of the adsorbed WPI and WPI/pectin layers at pH 3.0

Samples	Hydrated mass (mg/m²)
WPI layer	6.3±0.8[c]
WPI/LMP bilayer	15.2±1.0[b]
WPI/HMP bilayer	20.4±0.6[a]

Note: different letters indicate a significant difference ($p<0.05$)

4.3.2 In vitro gastric digestion at the O/W interface

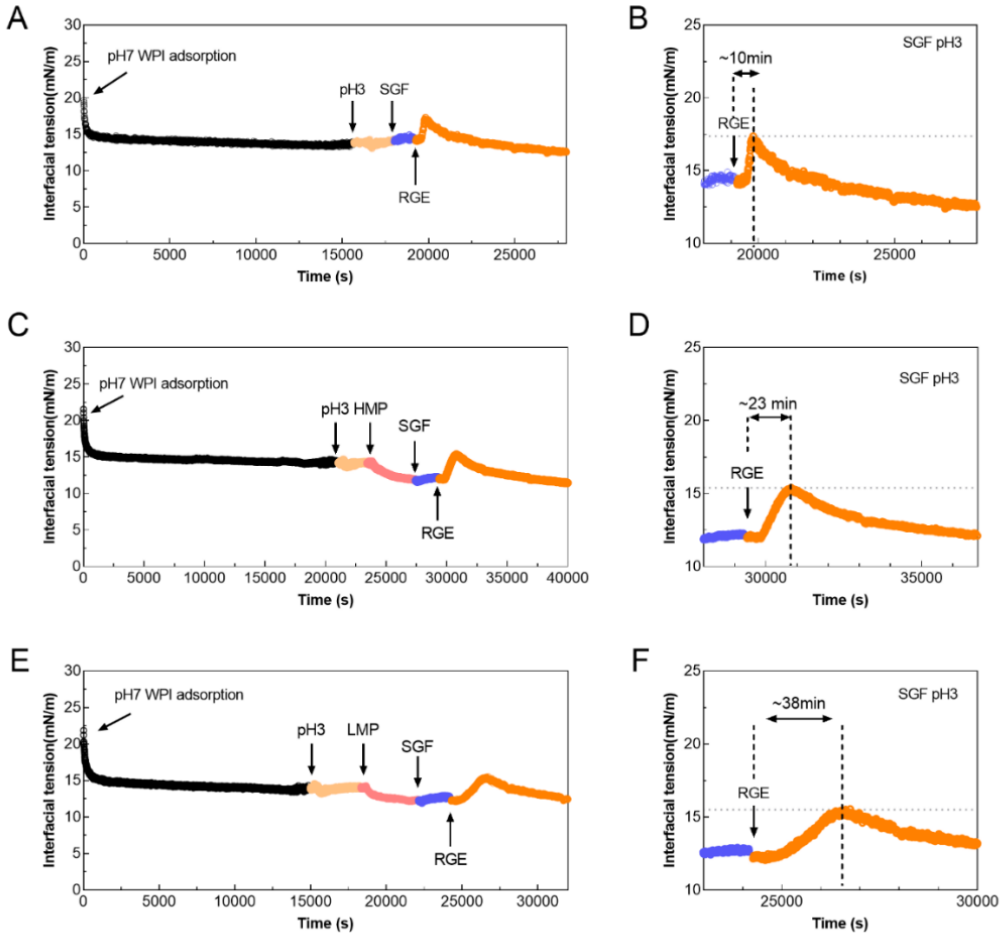

Figure 4.2: Interfacial tension as a function of time for the sequential adsorption of 0.01% WPI (at pH 7.0) and 0.01% pectin (at pH 3.0) onto a MCT oil droplet, followed by successive rinsing steps of SGF (without or with RGE), showing the adsorption and digestion of an interfacial WPI layer (A, B), a WPI/HMP bilayer (C, D), and a WPI/LMP bilayer (E, F). Panels B, D, and F are zoom-in windows of their left

counterparts, focusing on the digestion phase. All measurements were performed at 37˚C. RGE and SGF refer to rabbit gastric extracts and simulated gastric fluids, respectively.

The evolution of interfacial layer during the simulated gastric digestion was evaluated by interfacial tension and dilatational rheology. In Figure 4.2, the WPI interfacial layer was prepared after 3 h of adsorption for equilibrium, as discussed in chapter 2, followed by a rinsing step to remove excess proteins in the bulk. The protein adsorption lowered the interfacial tension of MCT/water from 25.8±0.4 to 13.6±0.5 mN/m. Subsequently, the subphase pH was adjusted to pH 3.0, which did not affect the interfacial tension.

In order to prepare WPI/pectin bilayers, an LMP or HMP solution was introduced to the pre-formed WPI layer at pH 3.0, followed by a rinsing step to remove loosely bound or/and excess pectin. The interfacial tension was only slightly reduced (around 1mN/m) for both LMP and HMP, which is expected since the pectin is less (or not) surface active relative to the proteins. In contrast, the interfacial elastic modulus (E') was apparently enhanced, where the E' increased from 30.4±0.6 mN/m (for the WPI only) to 42.2±0.2 mN/m for WPI/HMP and to 50.8±1.7 mN/m for WPI/LMP.

As a result of electrostatic attraction, the anionic pectin adsorbs on top of the positively charged protein layer at pH 3.0, thus neutralizing positive charges and facilitating intra-/inter protein interactions, resembling the role of a cross-linker. As discussed above, LMP contained more negative charges, and hence could interact with the protein layer more strongly, forming a more compact composite layer than HMP, in line with the QCM-D results in Section 4.3.1.

Upon exposure to SGF, the interfacial tension was essentially constant for both WPI and WPI/pectin layers in the absence of rabbit gastric extract (RGE). Additionally, the E_d' was slightly enhanced (e.g. for the WPI layer and WPI/HMP layer), which may be due to the electrostatic screening effect because of the enhanced ionic strength. This also implied that most pectins remained adsorbed. In contrast, in the presence of RGE (i.e. including pepsin and gastric lipase), for the experiments on WPI, there was a progressive increase in interfacial tension from 13.6±0.5 to 17.5±0.2 mN/m over 10 min. The interfacial tension was then decreased slowly during the rest of the digestion.

A similar pattern in interfacial tension was observed for the WPI/HMP and WPI/LMP bilayers, but the first increase was slower and with a smaller magnitude, e.g. from 12.5±0.2 to 15.5±0.2 mN/m in 23 min for WPI/HMP but in 38 min for WPI/LMP. The increase in interfacial tension was ascribed to the proteolysis by pepsin, corresponding to a partial break-up of interfacial protein networks. In the meantime, the gastric lipase may also adsorb onto the O/W interface and lead to lipolysis, as discussed below.

As the WPI layer is highly positively charged at pH 3.0, the adsorption of pepsin to the oil-water interface is favored since pepsin exhibits a net negative charge at this pH (Andreeva & James, 1991). With respect to the bilayer structures, it seems that the pepsin still hydrolyzed interfacial proteins, but to a lesser extent since the pepsin adsorption is not favored due to charge inversion upon anionic pectin adsorption. Besides, the steric hindrance effect of the adsorbed pectin chains might play a crucial role as well since a thicker hydrated layer was formed.

Moving now to the interfacial dilatational moduli (Figure 4.3), for the WPI layer, the E_d' was only slightly decreased after 30 min but remained constant around 30 mN/m during the rest of the digestion phase. For WPI/pectin bilayers, the E_d' gradually decreased over 60 min and then fluctuated between 32 and 35 mN/m, and the E_d" increased with the digestion, suggesting the break-down of the interfacial protein network by pepsin. Note that this effect was not due to the desorption of pectins, as discussed below in bulk experiments.

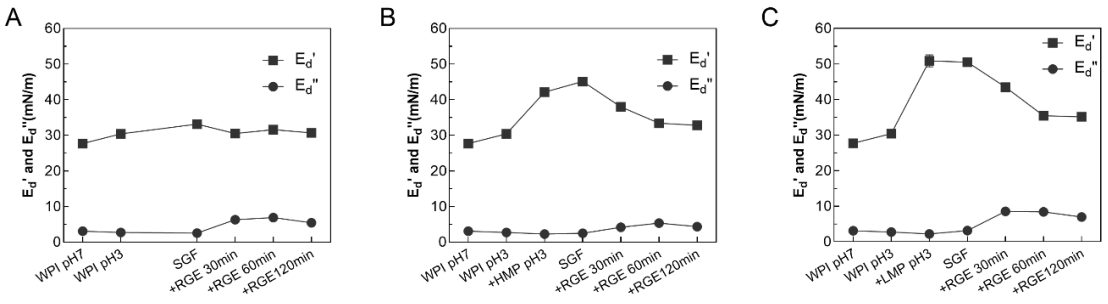

Figure 4.3: Interfacial dilatational rheology of the pre-adsorbed WPI layer (at pH 7.0) upon exposure to different environmental conditions, including no pectin (A), HMP (B) or LMP (C), measured at an area amplitude of 5% and a frequency of 0.05 Hz, and represented as the interfacial elastic modulus E_d' (squares) and the

interfacial viscous modulus E_d" (circles). All measurements were performed at 37°C and pH 3.0.

For the individual WPI layer, it is expected that the breakdown of the interfacial film leads to an apparently reduced E_d', whereby the observed phenomena can be due to the adsorption of hydrolyzed peptides and enzymes onto the MCT/water interface. To further elucidate this process, similar protocols were also performed at pH 5.0. Here, the WPI layer is close to its IEP (i.e. around 5.2 in Figure 4.1). The pepsin exhibits a much smaller enzyme activity but the activity of gastric lipase becomes much stronger (Salelles et al., 2021; Sams et al., 2016). This pH can also simulate the early stage of gastric emptying depending on the meal type (Amara et al., 2019).

In Figure 4.4, the pepsin still hydrolyzed the interfacial proteins at pH 5.0 but in a slower way than at pH 3.0. The Interfacial tension gradually went up to 16.4±0.2 mN/m in 30 min and then decreased. Meanwhile, E_d' largely decreased from 35.1±0.7 mN/m to 13.1±1.0 mN/m in 30 min and then increased with time. This confirmed our hypothesis of the initial breakdown of the interfacial network and the subsequent re-formation of the interfacial network by the adsorption of digestive products and enzymes. With respect to the digestion of the WPI-LMP bilayer at pH 5.0, its interfacial tension went up to a maximum value in a slightly slower way than that of the WPI layer, but the magnitude of their maxima was comparable. The E_d' values also supported the delayed interfacial proteolysis in the presence of LMP at pH 5.0. On the one hand, our previous studies have demonstrated that the LMP adsorption onto the pre-formed layer WPI is more favorable upon lowering the pH from 7.0 to 3.0. In the pH 3.0-5.0 region, the WPI and LMP carry opposite charges and the interfacial complexation is favorable. However, even in the pH 5.0-6.5 region, there is a net electrostatic attraction between positive patches of the whey proteins and anionic LMP, and LMP adsorption still occurs, despite the fact that the overall charge density has the same sign above the protein's IEP In fact, only at pH values above 6.5, there is no LMP adsorption on the WPI layer, or LMP desorption from a previously formed WPI-LMP bilayer. On the other hand, the maximum interfacial tension during the digestion was around 1 mN/m greater at pH 5.0 as compared to that of the bilayer at pH 3.0. These results suggested that there was still a protective effect of the additional pectin layer at pH 5.0, but the effect was less strong than that at pH 3.0 (Benjamin, Silcock, et al., 2012). As a further

consequence, the WPI-pectin bilayer emulsions will be mainly appropriate for acidic food products with a pH range of 3.0 and 4.0 (i.e. in the presence of strong interfacial complexation) in order to maximize their stabilization performance. In this scenario, consumption of these products (e.g. in a fasted state) does not raise the gastric fluid pH to 5 or higher. Nevertheless, in future studies, it is highly advisable to perform dynamic in vitro or in vivo digestion studies (dynamic pH changes) to evaluate the performance of the bilayer systems further.

Since the interfacial layer is mainly solid-like, the viscous modulus is not discussed in detail. For all cases, the E_d" slightly increased with digestion, and then decreased.

In addition to the adsorption of surface-active peptides and enzymes, the gradually reduced interfacial tension can also be due to the adsorption of lipolysis products at the oil-water interface to some extent. The lipolysis of triglycerides by gastric lipase will indeed produce mono- and diglycerides, as well as free fatty acids, which are surface-active and expected to displace some proteins from the interface and reduce the interfacial tension and interfacial elasticity. This effect has been proven pronounced for long-chain polyunsaturated fatty acids (Labourdenne et al., 1994; Reis et al., 2008). However, for medium-chain fatty acids, most lipolysis products at the oil-water interface may be released in the aqueous phase instead of being dissolved in the oil core and subsequently adsorbed onto the O/W interface.

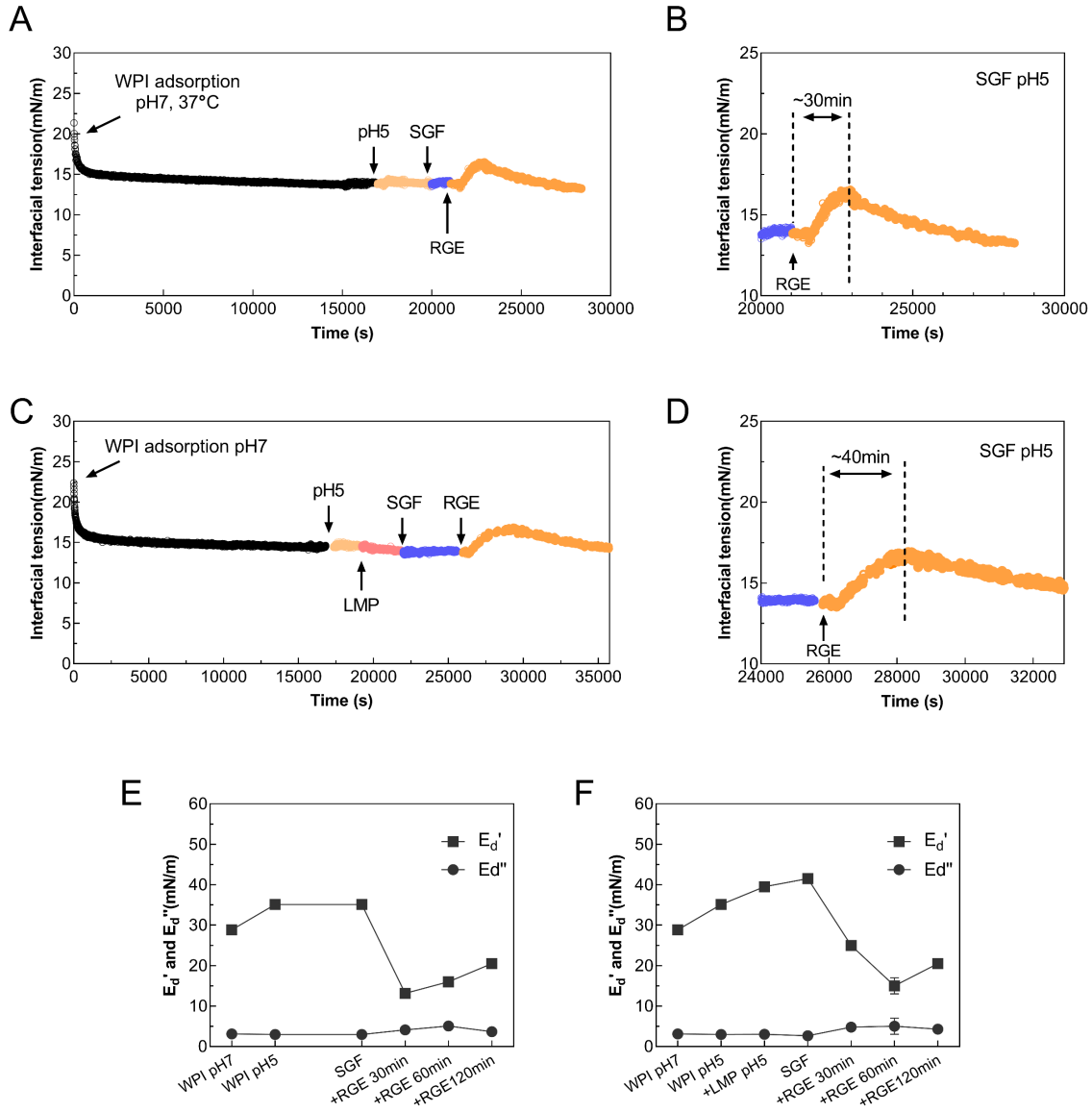

Figure 4.4: Interfacial tension as a function of time for pre-adsorbed WPI layer (A) and WPI/LMP bilayer (C) upon exposure to SGF (before or after RGE addition) at pH 5.0 and 37 °C; Panels B and D are zoom-in windows of their left counterparts, focusing on the digestion phase; Interfacial dilatational rheology of the pre-adsorbed WPI layer (at pH 7.0) upon exposure to different environmental conditions, including no pectin (E) and in the presence of LMP (F), measured at an area amplitude of 5% and a frequency of 0.05 Hz, and represented as the interfacial elastic modulus E_d' (squares) and the interfacial viscous modulus E_d" (circles).

In a nutshell, the introduction of pectin (with different degrees of esterification) increased the mechanical strength of the pre-formed protein layer at pH 3.0, which

was due to electrostatic attraction-driven interfacial complexation. Furthermore, during simulated gastric digestion, the additional pectin layer apparently delayed the breakdown of the interfacial protein network by pepsin and reduced the extent of proteolysis, possibly due to the combined effect of charge inversion and steric hindrance of pectin chains. The interfacial events relevant to gastric lipase might overlap with complex adsorption/desorption phenomena and are complicated to be evaluated by interfacial tension/rheology. To further evaluate the role of pectin, in vitro gastric digestion was also performed for bulk emulsions.

4.3.3 In vitro gastric digestion of bulk emulsions

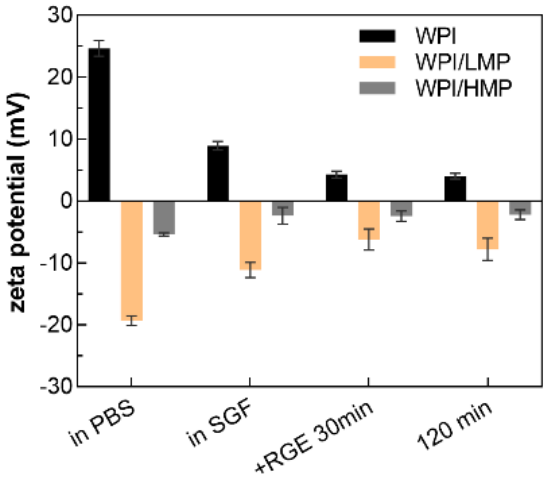

Figure 4.5: Evolution of the zeta potential of WPI, WPI/LMP, and WPI/HMP coated droplets before and after in vitro gastric digestion (at pH 3.0). Note: PBS is 10mM sodium phosphate buffer solution at pH 3.0.

In Figure 4.5, the charge inversion of WPI-coated droplets (from positive to negative) upon pectin addition at pH 3.0 clearly suggested forming an additional pectin layer. As expected, the adsorbed LMP layer contained more negative charges than the HMP layer.

The evolution of the particle size (distribution) for emulsion droplets stabilized by a WPI layer or a WPI/pectin bilayer was recorded during the simulated gastric digestion (Figure 4.6). The particle size distribution (PSD) of WPI-coated lipid droplets is characterized by an increasing contribution of larger particles during gastric digestion.

In addition to the emulsion droplet flocculation caused by the increased ionic strength in SGF, the increased droplet size was primarily due to the proteolysis by pepsin, whereby the broken interfacial film caused droplet coalescence and oiling off. Large oil droplets (i.e. a transparent oil phase) were indeed observed after 120 min of gastric digestion, as visualized in the microscopic images in Figure 4.7.

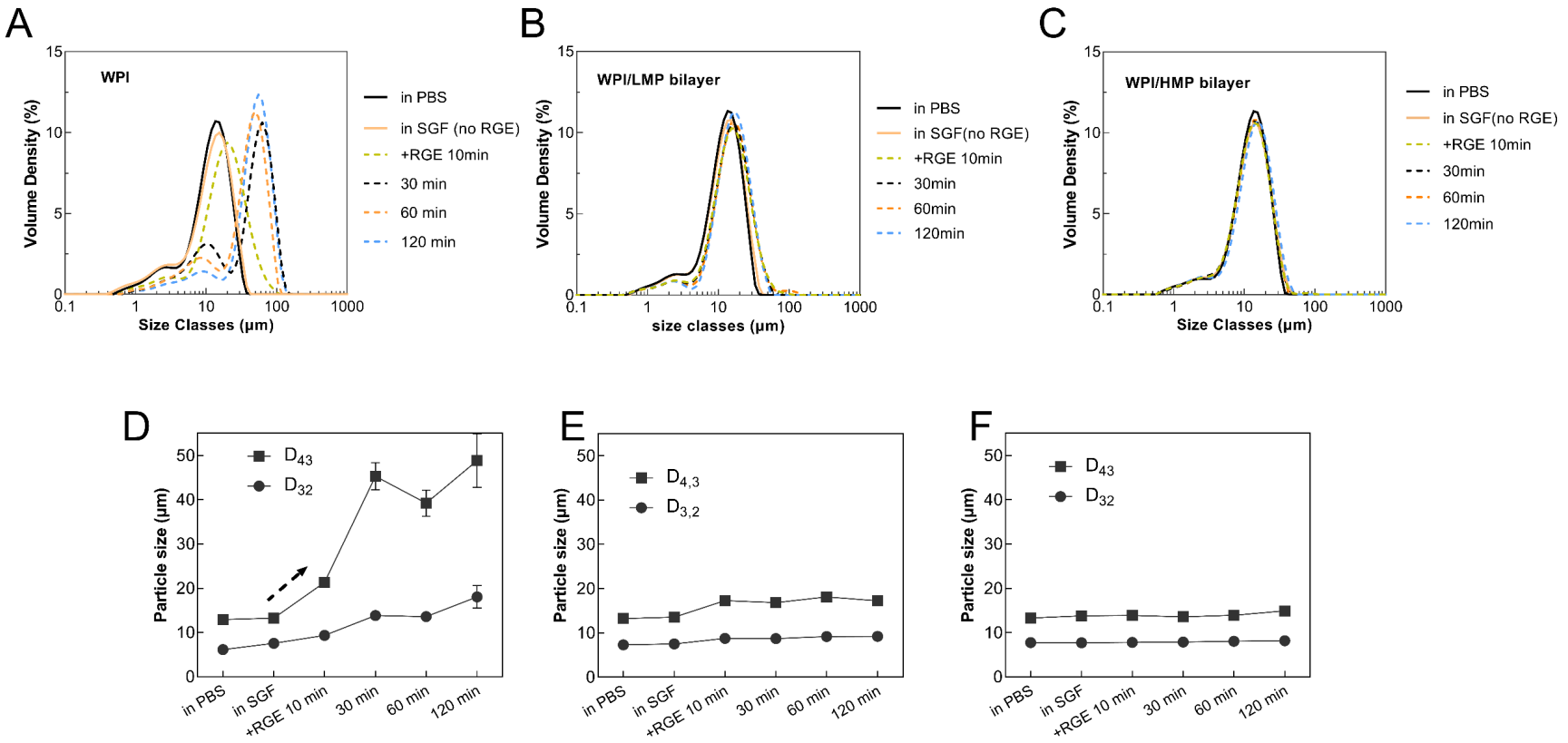

Figure 4.6: Evolution of the volume-weighted particle size distribution (A-C) and average size (D_{43} and D_{32}; D-F) of WPI (A,D), WPI/LMP (B,E), and WPI/HMP (C,F) coated droplets before and after in vitro gastric digestion.

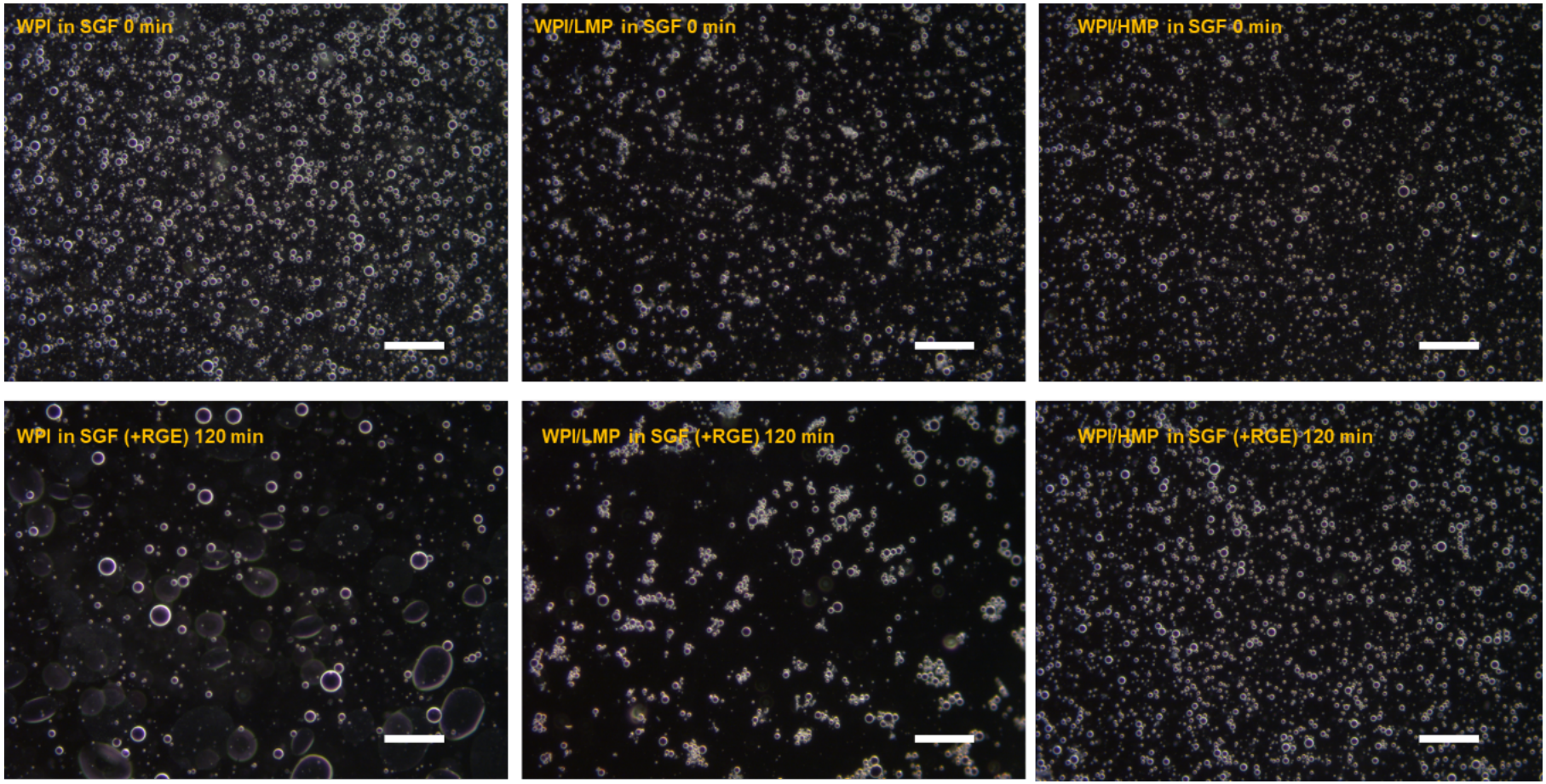

Figure 4.7: Microscopic images of WPI-, WPI/LMP-, and WPI/HMP-coated emulsion droplets before (0 min) and after in vitro gastric digestion (120 min). Note: no enzymes were added at 0 min. Scale bar: 20 μm

In contrast, for WPI/LMP-coated droplets, the PSD only slightly shifted to larger size classes. The $D_{4,3}$ and $D_{3,2}$ increased from 13 to 17 μm and from 7.3 to 9.2 μm, respectively, after 10 min of gastric digestion. Subsequently, the particle size essentially kept unchanged. For WPI/HMP bilayer-coated droplets, the particle size distribution remained basically unchanged within the first 60 min. After 120 min of gastric digestion, the $D_{4,3}$ and $D_{3,2}$ increased from 13 and 7.7 μm to 15 and 8.2 μm, resp.

Besides, the microscopic images in Figure 4.7 showed that the WPI/LMP-coated droplets underwent severe droplet flocculation in SGF, whereas this phenomenon was less obvious for the WPI/HMP-coated droplets. This discrepancy can be due to the fact that the LMP had a higher level of free carboxyl groups, which can be cross-linked by Ca^{2+} or Mg^{2+} (through the "egg-box" model) present in the SGF, thus forming droplet clusters (Cao et al., 2020). In this scenario, the lipid droplets can be very weakly bound with each other within these clusters, which can be easily broken down by the continuous stirring applied during particle size analysis by static light scattering. Furthermore, the flocculation became more pronounced in the presence of RGE.

With respect to the zeta-potential (Figure 4.5), the WPI-coated droplets and bilayer-coated droplets still kept their charge sign but with a smaller absolute value, as compared with the initial droplets. The variation in the ionic strength, binding of counter-ions to the droplet surface, protein displacement by other substances, hydrolysis of protein, and the presence of pepsin can all be relevant with respect to the reduced magnitude of the zeta-potential.

In order to quantitively evaluate the protective effect of adsorbed LMP or HMP on the encapsulated oil core, a certain amount of fresh MCT oil was used as an acceptor medium to quantify the migration rate of encapsulated curcumin from the oil core (In Figure 4.8), which can be a facile way to evaluate the quality of emulsions during the digestion process. In the control group, there was no presence of RGE or physical centrifugation, and the encapsulation efficiency of curcumin was around 95%. At the start of the digestion (0 min), the centrifugation caused the migration of more than 20% of the entrapped curcumin for WPI-coated droplets. After adding RGE, significantly more curcumin migrated during the digestion, reaching 50% after 30 min and over 80% after 120 min.

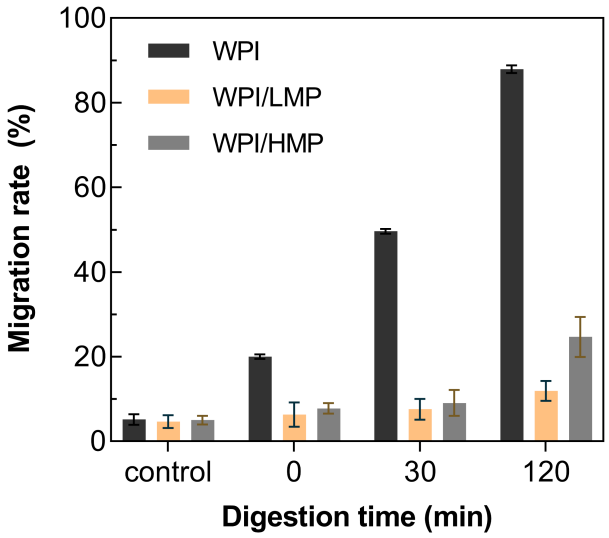

Figure 4.8: Migration rate (%) of curcumin from the oil core to an external MCT oil acceptor medium upon in vitro gastric digestion.

In contrast, the bilayer emulsions were basically unaffected by the centrifugation step, which can be ascribed to the better mechanical strength of their interfacial layer. During the initial 30 min of digestion, no obvious curcumin migration was observed for either WPI/LMP or WPI/HMP. However, at the end of 120 min digestion, around 25 % of curcumin migrated for WPI/HMP emulsions, whereas this value was only about 12% for WPI/LMP emulsions.

These results suggest that the additional pectin layer can greatly retard the destabilization of protein-coated droplets during gastric digestion. The better performance of WPI/LMP than WPI/HMP can be ascribed to the more rigid interfacial layer, as was also seen from the lower dissipation in QCM-D measurements, as well as the higher interfacial elasticity as observed in interfacial dilatational rheology. Besides, it was reported that pepsin exhibits a net negative charge in the pH range of 1.08 to 4.57 (Andreeva & James, 1991). The WPI/LMP bilayer has more negative surface charges, which should electrostatically repel pepsin. These more rigid characteristics may be due to the stronger electrostatic interaction between WPI and LMP (as compared to HMP), as well as to the divalent cations (Ca^{2+} or/and Mg^{2+}) induced cross-linking of LMP chains in SGF.

The different emulsion qualities may impact gastric emptying as well as the release of lipophilic ingredients (Steingoetter et al., 2015). However, it should be noted that in vivo studies have shown that coarse, gastric-unstable emulsions could undergo re-emulsification during antral-pyloric transit (Steingoetter et al., 2015). Besides, the peristalsis movement in the stomatch may also affect the emulsion digestion stabilty.

4.4 Conclusions

In summary, we investigated the influence of pectin adsorption on the gastric stability of WPI-coated droplets. Both LMP and HMP were able to adsorb onto the WPI layer at pH 3.0 through electrostatic interactions, leading to charge inversion and increased viscoelasticity of the interfacial layer. For the obtained bilayer structures, WPI/HMP adopted a more extended conformation into the aqueous phase, whereas the WPI/LMP formed a compact composite layer. This was primarily due to the different degrees of esterification of the pectins, corresponding to varying charge densities. Interfacial proteolysis led to the break-down of the interfacial protein network, as evidenced by the increased interfacial tension and decreased interfacial dilatational elasticity. In the presence of pectin, the proteolysis was largely delayed (especially for LMP) and its magnitude was reduced. In a later phase, the adsorption of digestive products (e.g. peptides, fatty acids) led to a decreased interfacial tension.

During the gastric digestion of emulsions, extensive coalescence and oiling-off occurred for the WPI-stabilised emulsion. For the WPI/pectin bilayer emulsions (containing either LMP or HMP), no apparent coalescence was observed. However, severe droplet flocculation was observed for the WPI/LMP emulsion, which was thought to be due to the presence of divalent cations in SGF. The WPI/HMP emulsion was essentially stable to flocculation during simulated gastric digestion.

This work may provide useful insights into the formulation design of gastric-stable emulsions with food-grade biopolymers. As our studies in Chapters 2 and 3 have demonstrated that the adsorbed pectin exhibits pH-responsive desorption at pH 7, it follows that WPI/pectin bilayer emulsions/microcapsules may be ideal delivery systems to the small intestine. Last but not least, since both protein-polysaccharide electrostatic interactions and the activity of gastric enzymes are highly pH-dependent,

it is of great interest in future studies to employ dynamic in vitro digestion models or in vivo studies to further evaluate this type of system.

Chapter 5 Influence of pH and Low/High-Methoxy Pectin Complexation on the Hydrophobic Binding Sites of β-Lactoglobulin Studied by a Fluorescent Probe Method

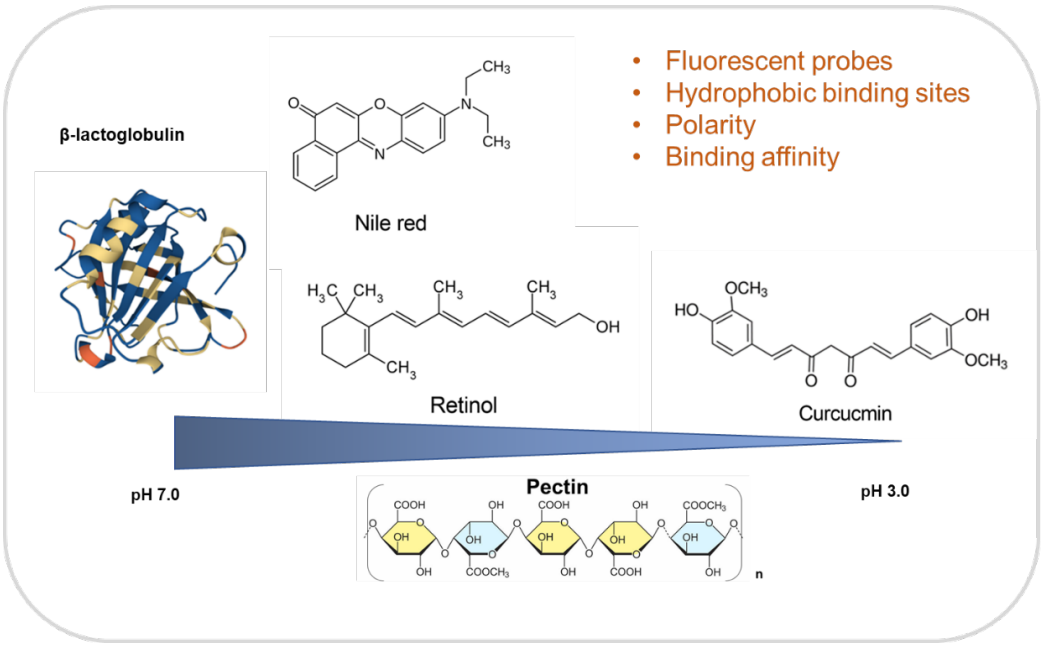

Redrafted from: Li, H., Wang, T., Su, J. and Van der Meeren, P., 2022. Influence of pH and low/high-methoxy pectin complexation on the hydrophobic binding sites of β-lactoglobulin studied by a fluorescent probe method. Food Hydrocolloids, 133, p.108020. https://doi.org/10.1016/j.foodhyd.2022.108020

Hao Li: Investigation, Conceptualization, Methodology, Software, Writing - original draft, Formal analysis, Visualization. Teng Wang, Jiaqi Su: Writing - review & editing. Paul Van der Meeren: Supervision, Conceptualization, Writing - review & editing, Methodology, Visualization.

Abstract

β-lactoglobulin (β-Lg)-polysaccharide soluble complexes formed in a specific pH range through electrostatic interactions have attracted a growing interest in the design of food-grade encapsulation systems for hydrophobic compounds, which is mainly ascribed to the ligand-binding properties of β-Lg. However, it remains unclear whether pH-induced conformational changes in β-Lg and its electrostatic complexation with anionic pectin affect their ability to bind hydrophobic compounds.

Here, a fluorescent probe method was employed to provide useful insights into this field. Three solvatochromic fluorescent probes (i.e. Nile red, retinol and curcumin) were selected as representative models of hydrophobic compounds that were bound to the inner cavity or/and the outer surface of β-Lg. Binding with β-Lg or β-Lg/pectin complexes largely enhanced the fluorescence of the hydrophobic probes. Especially, the polarity difference of different binding sites on β-Lg was revealed by the fluorescence spectra of β-Lg-Nile red as a function of pH. Both Nile red and retinol were bound more favorably to β-Lg at neutral pH than at acidic pH, possibly due to the accessibility of the inner cavity in the former case. Upon acidification, the gradual reduction in fluorescence intensity of the pre-formed protein-ligands complexes (i.e. at pH 7.0) was ascribed to the dissociation between Nile red (or retinol) and the inner cavity of β-Lg. β-Lg-curcumin interactions were less affected by pH variations, suggesting curcumin mainly binding to the outer surface of β-Lg. For the three tested hydrophobic compounds, the formation of soluble complexes between β-Lg with pectin had no adverse effects on their interactions with the protein. These results may provide useful insights into the binding of hydrophobic compounds to β-Lg or β-Lg/pectin complexes. The methodology may also be extended to study the encapsulation performance of other biopolymers or particles.

5.1 Introduction

β-lactoglobulin (β-Lg) belongs to the lipocalin family of proteins that are able to accommodate hydrophobic or amphiphilic molecules in their inner cavity (Sawyer & Kontopidis, 2000). One or two binding sites for hydrophobic or amphiphilic compounds may also exist on its external surface. The complexation of β-Lg with various bioactive compounds has been proved, such as vitamins, carotenoids, fatty acids, polyphenols, peptides and synthetic drugs (Li et al., 2022; Livney, 2010). These interactions are generally spontaneous, and the driven forces may involve hydrophobic interaction, hydrogen bond, and electrostatic interaction. Many bioactive compounds found in foods and pharmaceuticals benefit from complexation (or encapsulation) with proteins, as discussed in section 1.5.3.

Native β-Lg molecules undergo pH-responsive structural rearrangements/aggregation in an aqueous solution. Between pH 4.0 and 5.2, β-Lg molecules aggregate into larger oligomeric structures due to the proximity of their isoelectric point (IEP 5.2). Consequently, secondary aggregation results in highly turbid solutions and even protein precipitation, which limits the functionality of β-Lg (Li et al., 2022; Ron et al., 2010). Electrostatic complexation with anionic polysaccharides has been used to improve the colloidal stability of protein particles, endowing them with improved electrostatic repulsion and steric hindrance (Li, Wang, Hu, et al., 2022; Ron et al., 2010). Generally, proteins and anionic polysaccharides are mixed at a pH above the IEP of the proteins at which they have the same charge sign, and subsequently soluble complexes are formed spontaneously in a specific pH window upon acidification.

In terms of the binding of bioactive compounds to the inner cavity of β-Lg, it is recognized that the so-called Tanford transition (i.e., protonation/deprotonation of Glu89) controls the entrance to the hydrophobic cavity of β-Lg (Uhrínová et al., 2000). Under neutral to slightly basic conditions, the protein is in an “open” state, allowing the entering of small molecular compounds. At pH below 6.2, the E-F loop moves to occlude the entrance, resulting in a “closed” conformation (Uhrínová et al., 2000). Most studies in this field only focused on the interactions between β-Lg and bioactive compounds at neutral pH (Bohin et al., 2012; Cheng et al., 2018; Liang et al., 2007; Zhu et al., 2019), despite the fact that the acidic pH conditions are more relevant to

food systems (e.g. in beverages) and after ingestion (e.g. in gastric fluids). For instance, it is unclear to what extent the conformation changes of β-Lg at acidic pH affect the binding affinity and whether the acidification influences the pre-formed protein-hydrophobic compound complexes obtained at neutral pH. Furthermore, with regard to the electrostatic interaction between β-Lg with anionic polysaccharides, it has been shown that the formation of complexes influences the folding/unfolding states of the native conformation of β-Lg (Benjamin, Lassé, et al., 2012; Burova et al., 2022), which may affect the hydrophobic binding sites of β-Lg.

In this study, a fluorescent probe method was used to examine the role of pH variations and electrostatic complexation with polysaccharides in protein-hydrophobic compounds interactions at a molecular level. Three solvatochromic fluorescent probes (In Figure 5.1A), including Nile red, retinol, and curcumin, were selected as representative models of hydrophobic compounds bound to the inner cavity or/and the outer surface of β-Lg. Nile red is a polarity-sensitive fluorescent dye, as evidenced by its variable fluorescence spectra in various organic solvents or biological tissues (Teo et al., 2021). Especially, Nile red has a long working wavelength range (e.g. 500-700 nm) that is away from wavelengths at which many biomolecules absorb light. Accordingly, the inner filter effect of co-existing biopolymers or compounds can mostly be eliminated compared to the protein fluorescence quenching method. Moreover, the interference of light scattering of large particles in the fluorescence measurements is also much smaller at longer wavelengths.

In an aqueous solution, Nile red is basically insoluble and exhibits little fluorescence. However, once the dye-binding vehicles (e.g. proteins with hydrophobic binding sites) are present, leading to largely enhanced fluorescence intensity and an apparent blue shift of maximum emission (Sackett & Wolff, 1987). Moreover, the fluorescence of Nile red is relatively stable to pH changes. According to Sackett & Wolff, (1987). the fluorescence of Nile red is unaffected by pH between 4.5 and 8.0. Recently, some studies have extended its application to pH 2.5-4.0 (Polverini et al., 2006; Sturm et al., 2021). Only in very acidic environments does Nile red become protonated, which may cause a red-shift of its fluorescence spectrum (Moreno & Levy, 2000).

In terms of the β-Lg/Nile red interactions at neutral pH, molecular simulations and tryptophan fluorescent quenching experiments have suggested that one β-Lg could bind 1 or 2 Nile red molecules, and the primary binding site is in the inner cavity (Brown, 1993; Olsen et al., 2020). Considering the high sensitivity of Nile red fluorescence to the polarity of the surrounding environment, it was hypothesized that the hydrophobic binding sites on β-Lg could be identified and examined (i.e. with different polarities within the cavity or on the external surface) through the fluorescent probe method. Moreover, the fate of pre-formed β-Lg-Nile red complexes upon external stimuli (e.g. pH changes) could be acquired by monitoring the fluorescent spectra during pH titration. Regarding retinol and curcumin, they were employed as representative hydrophobic compounds to further validate and complement the findings (Benjamin, Lassé, et al., 2012; Patra & Barakat, 2011). Both low- and high-methoxy pectin (with different charge densities) were selected since they have different binding affinities to the protein. Besides, the ester groups of pectin may interact with β-Lg through hydrogen bonds or hydrophobic interactions (Girard et al., 2002). Not limited to the three hydrophobic probes, the obtained results may provide useful or generic insights into the binding of hydrophobic compounds to β-Lg.

5.2 Materials and Methods

5.2.1 Materials

β-Lg (over 85% purity) enriched BiPro whey protein was obtained from Davisco (Le Sueur, MN, USA). The protein was further purified to remove denatured or insoluble protein aggregates and salts according to Jung et al. (2008). Briefly, the protein solution (10%, w/w) was dissolved in deionized water. After overnight hydration, the pH was lowered to 4.6 by 6 M HCl, and the mixture was centrifuged at 11,500 RPM (15,200 g) for 1 h at 20 °C in a Sorval RC-5B centrifuge. The clear supernatant was collected and dialyzed with a 10 kDa membrane (Spectra/Por® regenerated cellulose (RC) membrane) against pH 4.6 deionized water for 12 h and against pH 2.0 water for 12 h. The protein solution was then freeze-dried and stored at room temperature for future use. β-Lg (90%) from bovine milk, retinol (95%, R7632) and Nile red (N3013) were purchased from Sigma-Aldrich Corp. (St. Louis, MO, USA). Curcumin (95%, B21573) was obtained from Alfa Aesar (Germany). LMP and HMP (AYD 2560SB) were

received from Cargill (Ghent, Belgium), as described in section 4.2. Deionized water was used for all experiments. All other chemicals were of analytical grade.

5.2.2 Sample preparation

β-Lg stock solution was prepared in deionized water (containing 0.02 wt.% sodium azide) at a concentration of 8 mg/mL following 2 h of stirring and overnight hydration at 4 °C. LMP or HMP stock solutions were dissolved in the pH 7.0 buffer at a concentration of 1.2 mg/mL after overnight stirring. The prepared solutions were passed through a 0.45 μm mixed cellulose ester (MCE) membrane filter to remove insoluble materials. The protein stock solution was diluted in pH 3.0, 4.5 or 7.0 buffers (20 mM salt including 10 mM sodium phosphate and 10 mM sodium acetate) for further use, followed by pH adjustment to the desired value with 0.6 M HCl or 1M NaOH if necessary. For clarification, preliminary experiments revealed that the slight ionic strength difference had little effect on binding. Nile red and curcumin were dissolved in DMSO at 100 μM. Retinol was dissolved in DMSO at 132 μM. These dyes were stored at 4 °C if not in use.

5.2.3 Fluorescence and UV/visible spectroscopy

The fluorescence spectra were recorded by a Cary Eclipse spectrometer with four-clear sided quartz cuvettes. At a detector voltage of 600 V, the emission spectra of Nile red were collected between 560 and 750 nm using an excitation wavelength of 550 nm. An excitation wavelength of 340 nm was selected for retinol and the emission spectra were collected between 350 and 650 nm. For curcumin, the detector voltage was set to 800 V or 600 V, the excitation wavelength was 425 nm, and the emission spectra were collected between 435 and 650 nm.

To investigate the effect of pH on the binding of dyes to the protein, the concentration of the dyes was fixed at 1.2 μM for Nile red and curcumin, and at 1.6 μM for retinol. At these low concentrations, the inner filter effect of the dyes can be ignored. The protein concentration ranged from 0.025 mg/mL to 1.6 mg/mL (i.e. corresponding to 1.25-80 μM β-Lg, as confirmed by the absorbance values at 280 nm. The fluorescence spectra were recorded immediately after direct mixing and after 60 min to achieve equilibrium. All the measurements were performed at room temperature (20 °C).

To study the effect of acidification and pectin (LMP or HMP) addition on the protein-dye binding, the dyes were previously added into the diluted protein solution at pH 7.0 (both in the presence or absence of pectin). The pH value was slowly lowered by 0.6 M HCl from 7.0 to 3.0. The mass ratio of protein to polysaccharide was fixed at 1:1. In a control group, same volume of the pH 7.0 buffer was used to replace the pectin solution. In the experiments with Nile red and curcumin, the total biopolymer concentration was 0.8 mg/mL (i.e. 0.4 mg/mL protein and 0.4 mg/mL pectin). However, for retinol, the total biopolymer concentration was 0.2 mg/mL (i.e. 0.1 mg/mL protein and 0.1 mg/mL pectin). These biopolymer concentrations were selected after preliminary experiments to balance the (desired) fluorescence intensity and the (undesired) light scattering to some extent.

The background fluorescence over pH 3.0-7.0 (i.e. the intensity of the protein itself in absence of pectin) was negligible compared to the dye fluorescence. For the mixtures of β-Lg and pectin, the contribution of the background fluorescence intensity due to protein/polysaccharide interactions at pH 4.5–7.0 was also marginal. However, insoluble β-Lg/pectin complexes were formed below pH 4.5 (especially the LMP), where the stronger β-Lg/pectin interactions led to increased solution turbidity. Consequently, the light scattering resulted in stronger background fluorescence intensity. Therefore, the results shown had already been corrected by subtracting background fluorescence from the raw data. Nevertheless, the data at pH 3.0–4.5 in the presence of pectin should be treated with care, as discussed below. The turbidity changes for 0.4 mg/mL β-Lg (with and without 0.4 mg/mL pectin) upon lowering the pH from 7.0 to 3.0 were displayed as the absorbance values at 425 nm. The binding affinity of protein-dye complexes was analyzed according to the Langmuir-type equation 5.1:

$$F = \frac{F_{MAX} \times C}{(1/K) + C} \qquad (5.1)$$

Where F is the fluorescence intensity of protein-dye mixtures; $F_{MAX}$is the saturation fluorescence intensity of dyes; C is the concentration of β-Lg (μM); K is the association constant and $1/K$ is indicated as the dissociation constant (K_d).

5.2.4 Statistics

Data were obtained from at least three independent experiments and shown as mean ± standard deviation. The difference between samples was evaluated using one-way ANOVA. The non-linear regression was done in GraphPad Prism 9.3 software (San Diego, USA).

5.3 Results and Discussion

5.3.1 Binding of Nile red with β-Lg

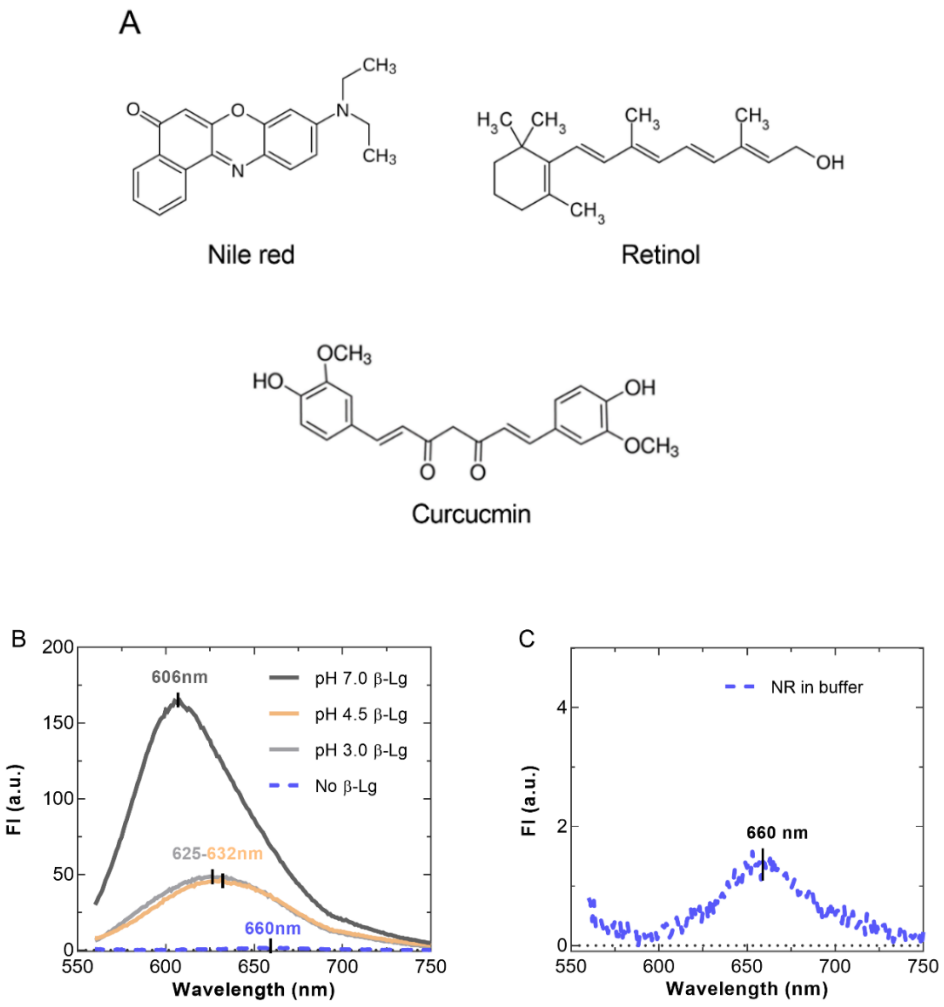

Figure 5.1: Chemical structure of Nile red, retinol and curcumin (A); Fluorescence intensity (FI) of 1.2 μM Nile red in the presence or absence of β-Lg (0.6 mg/mL, 30 μM) at various pH values (B). The Panel C is a zoom-in window of the Nile red spectrum in 20 mM phosphate/acetate buffer (pH 7.0) without β-Lg.

Nile red is a polarity-sensitive probe which generally exhibits a greater quantum yield and a shorter maximum emission wavelength in less polar solvents (Sackett & Wolff, 1987; Teo et al., 2021). In an aqueous environment (i.e. a highly polar solvent), Nile red is basically insoluble (or highly aggregated), and its maximum fluorescence intensity (FI) was extremely low (e.g. FI below 2 in Figure 5.1B and C) at a maximum emission wavelength (λ_{max}) of 660 nm, regardless of pH from 3.0 to 7.0.

In the presence of 30 μM β-Lg at pH 7.0, the peak FI of 1.2 μM Nile Red increased to about 165 and was blue-shifted with a maximum emission at around 606 nm. At pH 3.0 or 4.5, the FI of Nile red was also enhanced (to around 49) and λ_{max} was blue-shifted to wavelengths between 625 and 632 nm. Therefore, these results clearly proved the binding of Nile red to β-Lg, whereby the dye entered a less polar environment relative to water. As a minor amount of α-lactalbumin was present in the samples, similar experiments were also performed with very pure β-Lg and identical spectra were obtained (data not shown). Accordingly, β-Lg played a dominant role here and the existence of a minor α-lactalbumin fraction did not affect the conclusions (Brown, 1993). Considering the pH-dependent λ_{max}, it was hypothesized that Nile red could bind to two different sites (i.e. with different polarities) at neutral and acidic pH conditions, respectively. As mentioned in the introduction section (i.e. the existence of two binding sites), it can be inferred that Nile red mainly binds to the inner hydrophobic cavity of β-Lg at pH 7.0 but to the exterior surface at pH 3.0 and 4.5. These differences could be related to the conformational changes of β-Lg, where the E-F loop occludes the entrance to the inner cavity in the latter case (Uhrínová et al., 2000).

To further elucidate the interactions, the fluorescence spectra of Nile red were determined as a function of protein concentration at different pH levels. In Figure 5.2, the FI was gradually enhanced and the λ_{max} was blue-shifted as the protein concentration was increased. Moreover, the fluorescence stability of Nile red (i.e. 0 min versus 60 min) increased at higher protein concentrations. At pH 7.0, the λ_{max} leveled off at 606 nm at 10 μM β-Lg, whereas at pH 3.0 and 4.5 the λ_{max} continuously decreased until 40 μM, and then leveled off at 625–632 nm. Note that the molar ratio is much higher than the common 1:1 or 1:2 stoichiometry, and yet it has not reached saturation. The time effect on the stability of FI is thought to be due to the fact that the

Nile red in a polar solvent has a strong tendency to self-aggregate into larger aggregates, leading to the loss of fluorescence (Ray et al., 2019). At higher protein concentrations, the probability of the dye molecule finding a protein molecule will improve and thus binding will increase. Therefore, Nile Red is more likely to bind to the protein than to aggregate with itself.

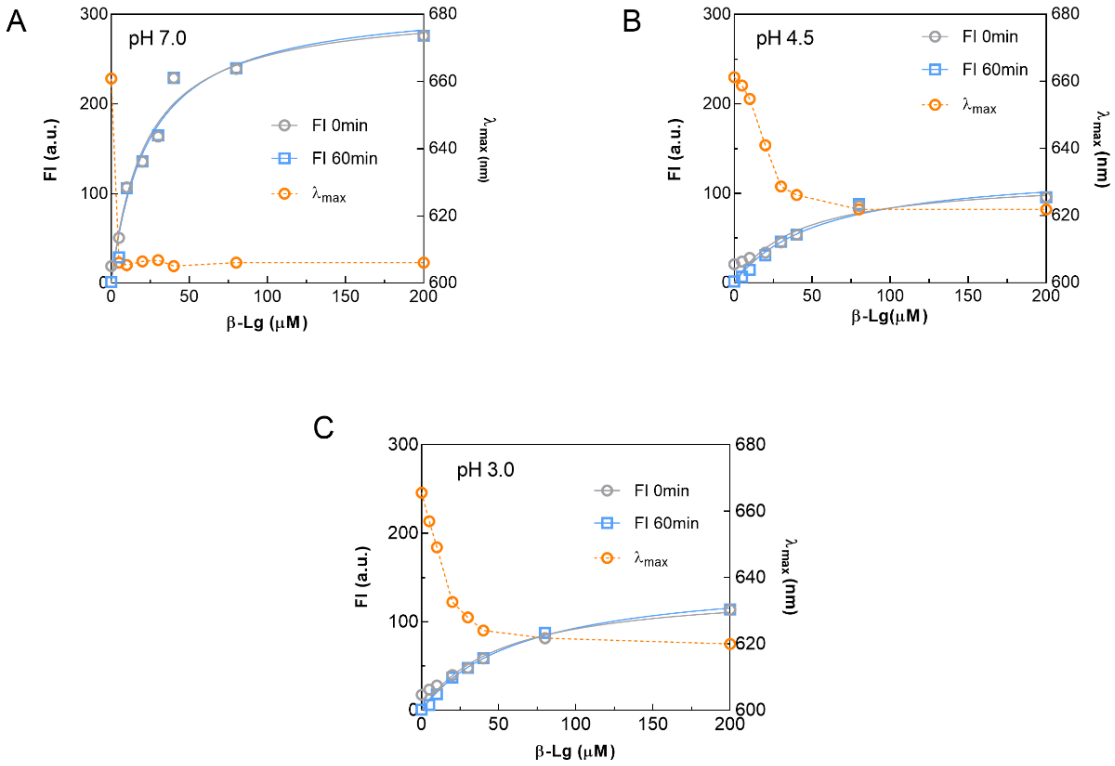

Figure 5.2: Fluorescence intensity (FI) and maximum emission wavelength (λ_{max}) of 1.2 μM Nile red as a function of β-Lg concentration at pH 7.0 (A), 4.5 (B), or 3.0 (C).

Moreover, the dissociation constants (K_d) at different pH conditions were determined by fitting the obtained results with a non-linear Langmuir-type equation (Eq 5-1). In Table 5.1, the lowest K_d was found at pH 7.0, followed by comparable values at pH 4.5 and 3.0. Generally, the lower the K_d, the more favorable the protein-ligand binding. The largely varied K_d combined with the polarity difference (e.g. shifted λ_{max} and reduced fluorescence quantum yield) could support the previous hypothesis of the existence of two different binding sites and a higher binding affinity at pH 7.0. The 3D spectra below provide further evidence for this point.

Table 5.1: The dissociation constant (K_d) of protein-dye complexes at various pH levels

pH	β-Lg-Nile red		β-Lg-retinol		β-Lg-curcumin	
	K_d (μM)	R^2	K_d (μM)	R^2	K_d (μM)	R^2
3.0	61.6±5.2a	0.995	18.3±1.6b	0.998	52.9±2.9b	0.998
4.5	54.6±11.4a	0.973	30.4±3.1a	0.997	68.0±2.8a	0.999
7.0	23.8±4.5b	0.970	2.9±0.3c	0.989	58.8±8.8ab	0.986

Note: different letters indicate a significant difference ($p<0.05$)

During pH titration of pre-formed protein-dye complexes from pH 7.0 to 3.0, the fluorescence spectra of the protein-dye interaction were recorded in real-time. The results are summarized in Figure 5.3A and B. The FI decreased sharply between pH 7.0-6.0 and remained constant between pH 5.5–4.0, and then slightly increased when the pH was further lowered to 3.0. Meanwhile, the λ_{max} red-shifted during acidification. The solution color changed from pink to purple upon visual observation. The reduced FI can be due to that more Nile red molecules were in a more polar environment (i.e. with lower fluorescence quantum yield), as indicated by the 3D spectra (Figure 5.3C and D). Moreover, due to the larger K_d under acidic conditions (Table 5.1), the decreased FI could be attributed to the dissociation between Nile red and the hydrophobic cavity of β-Lg.

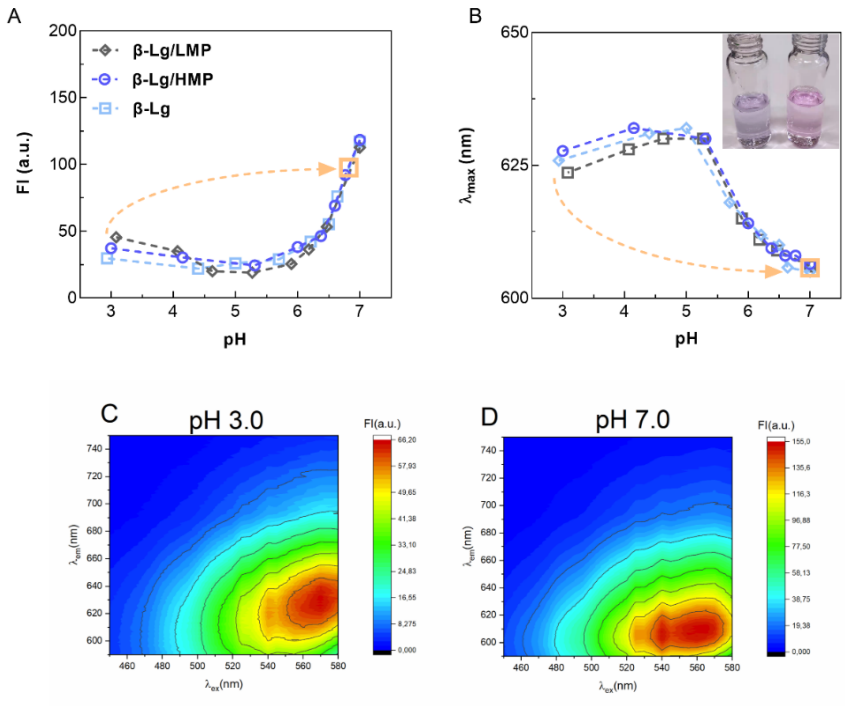

Figure 5.3: Fluorescence intensity (FI, A) and maximum emission wavelength (λ_{max}, B) of 1.2 μM Nile red in the presence of β-Lg (0.4 mg/mL) or β-Lg-pectin (LMP or HMP) mixtures (0.4 mg/mL+0.4 mg/mL) during acidification from pH 7.0 to 3.0. The inserted photograph shows the reversible color change of samples from pH 3.0 (left) to 7.0 (right).The yellow arrow indicates the pH adjustment from 3.0 to 7.0; 3D-spectra of Nile red (1.2μM) in the presence of β-Lg (40μM) at pH 3.0 (C) and pH 7.0 (D)

In fact, the so-called "Tanford transition" also occurs in pH 6.0-7.0, where the E-F loop structure tends to close the gate to the inner cavity as the pH is lowered. Unexpectedly, the encapsulated dye was also released or excluded from the cavity (e.g. about 80% loss of FI at pH 5.5, in Figure 5.3A), possibly due to the unfavorable steric interactions arising from the dye molecule and the EF loop (Ragona et al., 2000). Below pH 5.0, the λ_{max} fluctuated in 625-630 nm, which indicated that the Nile red was bound to a more polar site, probably corresponding to the exterior surface of β-Lg. These results reflect those of Zsila et al., (2005), who also found that the bound piperine in the cavity of β-Lg was gradually released upon lowering pH from 7.0 to 4.5. This finding is also in line with an NMR spectroscopy study demonstrating the reduced peak area of palmitic acid in β-Lg/palmitic acid complexes upon lowering the pH from 7.0 to 2.0, and

quantitative analysis revealed that 78% of the bound palmitic acid had been released from the inner cavity (Ragona et al., 2000). According to the authors, a possible explanation is that a salt bridge between the side chain of Lys83 (strand E) and Glu74 (strand D) is disrupted upon acidification, thus softening the structure of the molecule near the entrance. The loss of a salt bridge, together with the electrostatic repulsion of positive charges, could trigger the release of the ligand. The reason for the slightly increased FI at pH 3.0 is not clear. Whereas this effect might be ascribed to the slight protonation of Nile red, a similar phenomenon was also observed for retinol (as discussed later).

Figure 5.3A and B also clearly show that the FI and λ_{max} of Nile red were unaffected by the presence of pectin (either LMP or HMP) at pH 7.0. Upon acidification, the FI curves basically overlapped with that in the absence of pectin (at pH 4.5-7.0). Prior studies using light scattering and QCM-D (in Chapter 2) have proved that the formation of whey protein-low methoxy pectin intramolecular complexes is initiated around pH 6.5 (Girard et al., 2002; Li et al., 2021). Upon lowering the pH, the electrostatic attraction becomes more favorable, and soluble complexes are formed. Below pH 4.5, insoluble aggregates or coacervates can be obtained. Nevertheless, it seems that the complexation with pectin chains was not able to prevent the dye molecules from being released from the cavity during acidification. Additionally, soluble complexes pre-formed at pH 5.0 were also mixed with 1.2 μM Nile red (data not shown), where the FI and λ_{max} were comparable to that obtained by acidification from pH 7.0 to 5.0. These results imply that the encapsulation performance of β-Lg is not affected by the addition of anionic LMP or HMP at pH 4.5–7.0, which enables the formation of soluble complexes around the IEP of the protein and prevents its aggregation/precipitation. At pH 3.0-4.5, insoluble complexes (especially for the highly charged LMP) were formed. As a further consequence, the accuracy of the FI measurements may be affected, and the data should be treated with care. The slightly higher FI values could be due to the interference from background fluorescence (e.g. caused by light scattering of turbid solutions) that could not be fully corrected, as discussed further in Section 5.3.3. Note that β-Lg molecules at pH 4.5 tend to form oligomers due to reduced electrostatic repulsion around IEP and the protein solution became slightly turbid at a concentration of 200 μM. However, the good fitting results

in Table 5.1 (R^2>0.97) can basically exclude the presence of measurement pitfalls. Additionally, the soluble content of β-Lg was not reduced at this pH since the denatured protein fraction (i.e. insoluble at pH 4.6) had been removed during the purification process.

Finally, the pH was adjusted back to 7.0. The FI increased to 60-80% of the original FI at pH 7.0 and the λ_{max} returned to around 606 nm, suggesting the reversibility of the dye-binding (both in the presence and absence of pectin). Meanwhile, it was observed that the purple color at acidic pH conditions reversibly became pink at pH 7.0 (image not shown).

These results suggest that Nile red can be used as a sensitive fluorescent probe to investigate the effect of changing environmental conditions on the conformational changes or ligand-binding properties of a protein. In order to further validate these findings, two additional food-related hydrophobic fluorescent probes (i.e. retinol and curcumin) were analyzed according to similar protocols.

5.3.2 Binding of retinol with β-Lg

It has been well recognized that retinol binds primarily into the cavity of β-Lg under neutral pH conditions (Cho et al., 1994; Considine et al., 2020). Accordingly, the binding properties of retinol are expected to be similar to those of Nile red. As shown in Figure 5.4A, in the absence of β-Lg, the FI was less than 1, irrespective of pH variations. The spectra peaks can hardly be observed possibly because of the much higher log K_{ow} (5.68) of retinol than Nile red (2.76) and curcumin (3.29).

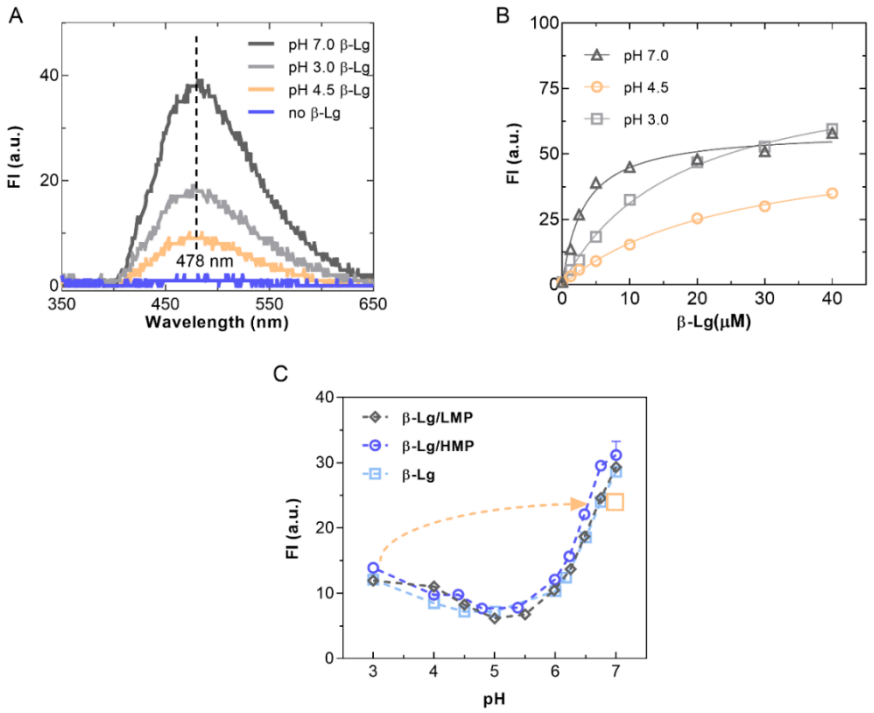

Figure 5.4: Fluorescence intensity (FI) of 1.6 μM retinol in the presence or absence of 5 μM β-Lg (A) and as a function of protein concentration (B) at various pH values. FI and λ_{max} of 1.6 μM retinol in the presence of β-Lg (0.1 mg/mL) or β-Lg-pectin (LMP or HMP) mixtures (0.1mg/mL+0.1mg/mL) during acidification from pH 7.0 to 3.0 (C). The yellow arrow indicates the pH adjustment from 3.0 to 7.0.

With the presence of β-Lg, the FI was largely enhanced to 9.2 at pH 4.5, 18.2 at pH 3.0, and 38.9 at pH 7.0. To be noted, the FI of β-Lg-retinol reached the stable values within seconds after mixture and remained basically constant within 1 h. Meanwhile, the λ_{max} was observed at 478 nm regardless of pH, which may be due to the fact that retinol is less sensitive to probe polarity differences compared with that of Nile red. At pH 7.0, the inner cavity could be the primary binding site, and the highest FI was observed. In contrast, the inner cavity was not available at pH 3.0 and 4.5, and hence the retinol could mainly bind to the outer surface of β-Lg. Besides, the FI at pH 3.0 was significantly stronger than that at pH 4.5 at all tested protein concentrations (Figure 5.4B). Moving now to dissociation constants in Table 5.1, the lowest K_d was observed at pH 7.0 (i.e., around 3.2 μM), much smaller than that at pH 3.0 (17.2 μM) and 4.5 (27.3 μM), suggesting that the open conformation of β-Lg (i.e., accessible inner cavity) is more favorable for binding retinol. The K_d at pH 7.0 determined in this study is

comparable to some previous values (i.e., between 0.02 and 10 μM), despite the fact that these values vary considerably depending on experimental parameters, such as temperature, selection of fitting models, and the correction of inner filter effect (Keppler et al., 2014). Likewise, a fluorescence quenching method observed the pH-dependent K_d of β-Lg-retinol complexes (Dufour et al., 1994). However, Fugate & Song, (1980) claimed that retinol binding to β-Lg was pH-independent in pH 2.0-7.5.

Regarding the β-Lg/retinol interactions at pH 3.0 and 4.5, this increased FI at pH 3.0 may result from retinol interacting with positively charged patches of the β-Lg through dipole affinity to its conjugated double bonds, also known as the pi-cation interaction (Benjamin et al., 2012). Additionally, considering the larger oligomeric structures formed at pH 4.5, it is also possible that the reduced surface area caused by protein self-aggregation impeded the retinol-binding.

The FI of retinol upon lowering the pH from 7.0 to 3.0 is shown in Figure 5.4C. The FI decreased steeply from pH 7.0 to 5.5, which could suggest the release of retinol from the inner cavity. Subsequently, the FI slightly increased at pH below 5.0. Moreover, no significant differences can be observed between the FI curves upon acidification, independent of the addition of anionic pectin. These results are consistent with those obtained when Nile red is used. Finally, when the pH was returned from 3.0 to 7.0, the FI of retinol increased to around 22, indicating reversible binding between β-Lg and retinol.

5.3.3 Binding of curcumin with β-Lg

The binding site of curcumin on β-Lg has long been controversial. Some previous studies reported that curcumin was mainly bound into the cavity of β-Lg at pH 7.0 based on a higher association constant at pH 7.0 than at pH 6.0, which was obtained through a fluorescence quenching method (Li et al., 2013; Sneharani et al., 2010). However, Hosseini et al., (2015) suggested the main binding site for curcumin existing on the outer surface of β-Lg, which was also supported by another molecular docking study (Zhang et al., 2022).

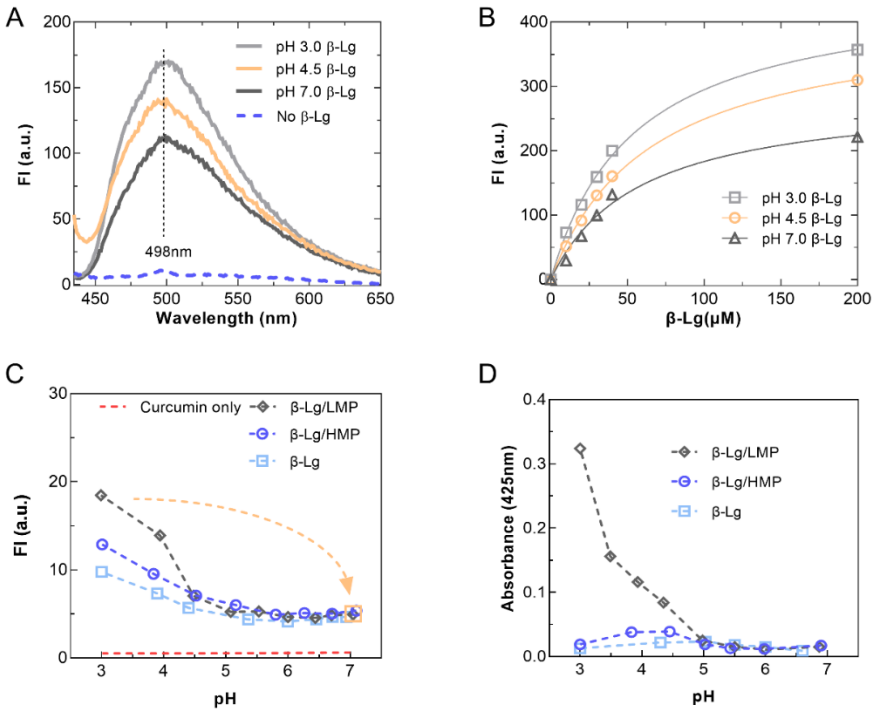

Figure 5.5: Fluorescence intensity (FI) of 1.2 μM curcumin in the presence or absence of 30 μM β-Lg (A) and as a function of protein concentration (B) at various pH values. FI of 1.6 μM curcumin in the presence of β-Lg (0.4 mg/mL) or β-Lg-pectin (LMP or HMP) mixtures (0.4 mg/mL+0.4 mg/mL) during acidification from pH 7.0 to 3.0 (C); Absorbance value at 425 nm of β-Lg and β-Lg/pectin solutions without curcumin as a function of pH (D).

The present results show that the β-Lg/curcumin interactions are less affected by pH variations, and even became more favorable upon lowering the pH from 7.0 to 3.0. The FI of curcumin reached a stable value upon mixing with β-Lg and remained almost constant within an hour (data not shown). As depicted in Figure 5.5A, the fluorescence of curcumin was very weak without β-Lg: it was approximately 10 at a λ_{max} of 498 nm, regardless of the pH values. For clarification, the detector voltage in these measurements was enhanced to 800 V as the intrinsic FI of curcumin (even in the presence of β-Lg) was much lower than that of the other two probes.

Upon mixing with 30 μM β-Lg, the FI was enhanced to around 110 at pH 7.0 or 6.0, 139 at pH 4.5, and 169 at pH 3.0. The fluorescent spectrum at pH 6.0 was not shown since it was very close to that at pH 7.0. Meanwhile, the λ_{max} at 498 nm was not affected by the pH changes. Curcumin may be less sensitive to polarity than Nile red, which is

also the case for retinol. Another possible explanation is that curcumin primarily binds to the exterior of β-Lg, which is unaffected by pH because of the high structural stability of the protein.

FI as a function of protein concentration in Figure 5.5B can be readily linked to the binding affinity as a function of pH: more curcumin binding would produce stronger fluorescence. As shown in Table 5.1, no significant differences in K_d were observed between pH 4.5 and 7.0 ($p<0.05$). Despite the fact that the average K_d was slightly lower at pH 3.0, the influence of pH was subtle or insignificant when compared to the cases of Nile red and retinol.

Thus, instead of binding to the interior cavity, it seems that curcumin mainly binds to the exterior surface of β-Lg that is highly stable under pH changes. This hypothesis is also supported by some previous studies. Riihimäki et al., (2008) compared the interactions between various phenolic compounds (e.g. myricetin and daidzein) and β-Lg and observed insignificant pH effects (i.e. pH 7.0 versus 2.0). Similarly, Liang & Subirade (2012) reported the acid stability of β-Lg/resveratrol complexes upon acidification from pH 7.0 to 2.0. Both studies proposed that the phenolic compounds could bind to the outer surface of β-Lg rather than to the inner cavity. Accordingly, curcumin could exhibit a similar binding pattern.

The pH titration method was used to assess the pH stability of pre-formed β-Lg-curcumin complexes at neutral pH. Since a high detector voltage (e.g. 800V) also produces a much higher background signal, e.g. due to light scattering in high turbidity samples, only the results at a voltage of 600V were shown. Note that the detector voltage does not influence the conclusions. As shown in Fig. 5C, the FI of curcumin was less than 0.6 at pH 3.0–7.0 without protein. In the presence of β-Lg, the FI slightly fluctuated (i.e. within 10%) upon lowering the pH from 7.0 to 5.5. In contrast to Nile red and retinol (i.e. 80% FI loss), the results indicate that the curcumin binding is relatively unaffected by the accessibility of the inner cavity. Additionally, no significant red or blue shifts in blue or red were observed during the pH reduction. The higher FI and lower K_d at pH 3.0 could suggest increased curcumin binding, which may be due to increased pi-cation interactions, as discussed in the last section. Some previous studies also claimed that curcumin interacting with proteins (e.g. β-casein) through

electrostatic interactions at pH 2.0-3.0 (Zembyla et al., 2018; Zhao et al., 2021), but it is less likely considering the high pKa of curcumin (i.e. between 7.7 and 9.0).

At pH 4.5-7.0, the FI curves of β-Lg-HMP and β-Lg-LMP essentially overlapped with that of only β-Lg, suggesting that the HMP and LMP complexation had no effect on the binding sites of curcumin. The FI was, however, much larger in the presence of pectin (especially LMP) below pH 4.5. In fact, a large number of insoluble complexes (particularly for LMP) were formed at pH 4.5-3.0, resulting in a largely increased solution turbidity and background fluorescence. The higher turbidity for LMP was attributed to its higher charge density which could bind more protein molecules at saturation (Girard et al., 2002; Jones et al., 2010). Accordingly, the larger FI was due to the fact that the strong light scattering effect could not be effectively corrected by the simple subtraction (see section 5.2.3), rather than to enhanced curcumin binding (Panigrahi & Mishra, 2019). Generally, the light scattering effect is less pronounced at higher excitation wavelengths and lower total biopolymer concentrations, as demonstrated in the experiments with Nile red and retinol.

Nevertheless, the addition of pectin is primarily intended to enhance the colloidal stability of the protein around its IEP (i.e. around 5.2). Above pH 4.5, the interference with FI due to light scattering was basically absent, as confirmed by the absorbance values at 425 nm (Figure 5.5D) of the β-Lg/pectin mixtures. In this scenario, the results can prove that the electrostatic complexation with pectin did not adversely influence the binding of curcumin. Lastly, a pH adjustment from 3.0 to 7.0 restored the FI to its original value (i.e. around 5) before acidification.

5.4 Conclusions

In the pH 3.0-7.0 region, the most favorable pH for β-Lg binding with Nile red or retinol was observed at pH 7.0 because of the open conformation (i.e. accessible inner cavity) of β-Lg. At pH 3.0-4.5, the interactions between the two probes and β-Lg were less favorable and the dyes could be only bound to the outer surface of β-Lg, possibly because the EF-loop occludes the entrance to the inner cavity. For the pre-formed β-Lg-Nile red or β-Lg-retinol complexes at pH 7.0, the acidification caused the release of ligands from the inner cavity of β-Lg (e.g. burst release from pH 7.0 to 5.5), which could be due to some steric interactions at acidic pH conditions. Despite the fact that

the anionic pectin forms molecular complexes with β-Lg below pH 6.5, it seems that the release of the hydrophobic probes cannot be prevented.

In terms of curcumin, its binding affinity with β-Lg was less affected by pH variations, although fluorescence intensity was slightly higher at pH 3.0 than in other pH conditions. The current results suggest that curcumin is mainly bound to the outer surface of β-Lg. Likewise, acidification from pH 7.0 to 3.0 increased the FI of pre-formed protein-curcumin complexes, potentially due to more curcumin binding. Moreover, adding anionic pectin (LMP or HMP) barely affected the curcumin binding at pH 4.5-7.0. Below pH 4.5, the formation of insoluble β-Lg/pectin complexes (i.e. turbid solutions) caused pitfalls in fluorescence measurements. Furthermore, these protein-ligand interactions were found to be reversible. This research may provide valuable insights into the design of fat-free and food-grade delivery systems by whey protein-polysaccharide soluble complexes, e.g. enrichment of bioactive compounds into clear beverages.

Chapter 6 General Conclusions and Future Perspectives

6.1 General conclusions

Protein-polysaccharide complexation may not only combine the attributes of the biopolymers constituting them but also present distinct structural and functional properties not possessed by their parent biopolymers. This provides great opportunities for the development of novel food formulations. One attractive application is to design delivery vehicles (e.g. emulsions, soluble complexes) for hydrophobic ingredients. Ideally, a delivery system should be able to encapsulate (or bind) and protect the bioactive ingredients from degradation in harsh environments, and subsequently release them on demand. In this dissertation, we aimed to better understand and manipulate protein-polysaccharide interactions at the oil-water interfaces and in the bulk under changing environmental conditions (e.g. food processing, gastrointestinal digestion), since they may determine the fate of the encapsulated bioactive ingredients. The non-covalent, electrostatic interactions between WPI (enriched in β-Lg) and pectin (both LMP and HMP with varying charge densities) are the focus of this work. This biopolymer combination is chosen as characteristic models for globular proteins and anionic polysaccharides, whereby the used methodology and obtained conclusions may be easily extended to other similar biopolymers. This section is divided into three parts,

In PART I, a real-time QCM-D approach was developed to investigate the effect of pH on the sequential adsorption of WPI and LMP at an O/W mimicking interface. The obtained findings were validated at the MCT O/W interface with a modified drop shape tensiometer allowing subphase exchange. Regarding the WPI layer, a maximum interfacial viscoelasticity was observed when the pH was close to the isoelectric point of WPI, corresponding to the minimum degree of hydration. Moreover, those changes were found to be reversible. The interfacial complexation between the pre-adsorbed WPI and LMP occurred over a wide pH range, i.e. both below and above WPI's IEP, which can be mainly ascribed to the charge heterogeneity of the protein charges. Overall, the LMP deposition became more favorable upon lowering the pH from 6.5 to 3.0. Above pH 6.5, both WPI and LMP are highly negatively charged, and hence no interfacial complexation occurred. Additionally, the adsorption of LMP resulted in increased interfacial dilatational elasticity, but its magnitude was largely dependent on the pH conditions. Below pH 5.0, WPI and LMP have opposite charges. The interfacial

complexation became stronger and was accompanied by more structural rearrangements within the adsorbed layer. As a result of the electrostatic attraction, the anionic pectin adsorbs on top of the positively charged protein layer, thus neutralizing positive charges and facilitating intra-/inter protein interactions, resembling the role of a cross-linker. Additionally, the WPI/LMP bilayer-coated droplets exhibited excellent stability against coalescence in long-term storage or centrifugation-induced compression when compared with the individual WPI layer. Moreover, it was found that the interfacial complexation between WPI and anionic pectin at the oil-water interface was reversible, giving rise to pH-responsive assembly/disassembly, which was mainly driven by electrostatic interactions.

In PART II, the developed methodologies in the previous two chapters were applied to examine the in vitro gastric digestion stability of the WPI/pectin (both LMP and HMP) bilayer at the O/W interface, aiming to design gastric-stable emulsions. The WPI/HMP bilayer adopted a more extended conformation into the aqueous phase, whereas the WPI/LMP bilayer formed a compact composite layer. Interfacial proteolysis led to the break-down of the interfacial protein network, as evidenced by the increased interfacial tension and decreased interfacial dilatational elasticity. In the presence of pectin, the proteolysis was largely delayed (especially for LMP) and its magnitude was reduced. Moreover, extensive coalescence and oiling-off occurred for the WPI-stabilized emulsion. In contrast, the presence of an anionic pectin layer can prevent or at least largely delay gastric destabilization, thus limiting a migration (or leakage) of the encapsulated lipophilic compounds. In this regard, the LMP exhibited a better performance than HMP, which was primarily due to its higher charge density (that repels the adsorption of pepsin), as well as its formation of a denser composite layer with the pre-adsorbed WPI layer.

In PART III, the effect of changing pH levels and complexation with pectin (LMP and HMP) on the hydrophobic binding sites of β-Lg was examined. Three solvatochromic fluorescent probes (i.e. Nile red, retinol and curcumin) were selected as representative models of hydrophobic compounds that were bound to the inner cavity or/and the outer surface of β-Lg. For a hydrophobic compound (e.g. Nile red, retinol) bound to the inner cavity of β-Lg at neutral pH, acidification caused the release of ligands from the inner cavity of β-Lg (e.g. burst release from pH 7.0 to 5.5, corresponding to ca.80%

loss of FI). Despite the added anionic pectin forming intermolecular complexes with β-Lg below pH 6.5, the release of hydrophobic probes was not inhibited. In contrast, with respect to curcumin, its binding affinity with β-Lg was relatively less affected by pH variations. The results suggested that curcumin was mainly bound to the outer surface of β-Lg. Acidification from pH 7.0 to 3.0 even increased the FI of pre-formed protein-curcumin complexes, potentially due to more curcumin binding. Moreover, adding anionic pectin (either LMP or HMP) barely affected the curcumin binding within the pH 4.5-7.0 range. Below pH 4.5, the formation of insoluble β-Lg/pectin complexes (i.e. turbid solutions) caused pitfalls in fluorescence measurements. However, still, the electrostatic complexation had no adverse effect on the binding affinity of curcumin to β-Lg.

In terms of the used methodologies, it can be clearly seen that in combination with the subphase exchange setup, dynamic surface tension, interfacial rheology and some in-situ, real-time surface techniques (e.g. QCM-D, ellipsometry) are valuable tools to investigate the complex interfacial phenomena in food emulsions. These interfacial studies will benefit the formulation design of food emulsions with tailored functionalities. Furthermore, they may provide fundamental insights into the (de)stabilization mechanisms of food emulsions under changing environmental conditions. For instance, they may enable the fast in vitro screening of food emulsifiers with desired gastrointestinal fate using only a small number of materials.

Controlling intestinal lipolysis of lipid droplets has attracted great interest in the last decade since it may control calorie intake and help weight management. However, it is essentially impossible to tune the intestinal lipolysis kinetics by the WPI-pectin bilayer systems from the interfacial level since the adsorbed pectin detached immediately in the small intestine (around pH 7) and the partially hydrolyzed WPI will be then exposed to trypsin. Moreover, these droplets should have a larger total surface area than the highly coalescing protein-coated droplets, which may even accelerate the rate of lipolysis. Also, the detached pectin in the continuous phase may also affect the overall digestion. Moreover, these peptides at the interfaces may be easily displaced by biosurfactants (e.g. bile salts). The pH-responsive behaviors of pectin should be also applicable to other anionic polysaccharides containing mainly carboxyl groups, e.g. sodium alginate, or carboxymethyl cellulose.

Nevertheless, based on the results of static in vitro gastric digestion, the protein/anionic polysaccharide bilayer emulsions/microcapsules may be promising delivery systems for functional ingredients (e.g. hydrophobic compounds, lactic acid bacteria) to the small intestine. The deposition of anionic polysaccharides on the protein layer forms a thicker interfacial membrane and increases protein-protein interactions. This can be accompanied by a decreased permeability of the biopolymeric membrane at the interfaces as well.

Its ligand-binding properties enable β-Lg to be an interesting nanoscale delivery system for hydrophobic compounds. In terms of the hydrophobic compounds binding into the inner cavity of β-Lg molecules at neutral pH, however, most of them are leaked or released from the protein assemblies into the aqueous phase upon acidification. Some researchers in this field proposed to use β-Lg as a molecular nanocarrier since the protein is resistant to pepsin proteolysis. However, this is not an effective way to protect the gastric unstable ingredients. Besides, although β-Lg is widely used as a characteristic model for these studies, the application of this protein may be limited due to its allergenic properties.

6.2 Future perspectives

With respect to protein-polysaccharide mixtures, it seems interesting to put some effort into the polysaccharide chemistry. In terms of pectin, besides the esterification degree, the role of the molecular weight, and of the distribution of the methyl esters (either random or blocky) still needs to be evaluated. Besides, the performance of sulfated polysaccharides, carboxyl polysaccharides and cationic chitosan in different applications remains unclear.

In Part II, the static in vitro gastric digestion model used in this dissertation simplifies the dynamic changes (e.g., pH variations, and peristalsis) in the human stomach. Hence, it is advisable in future studies to employ dynamic in vitro digestion models or in vivo studies to further evaluate this type of system. Furthermore, the bioaccessibility or bioavailability of the encapsulated hydrophobic ingredients needs to be examined.

These interfacial design strategies based on food proteins and polysaccharides may be applied to multiple emulsions (e.g. W/O/W, O/W/O) as well. For instance, a compact

protein-polysaccharide composite layer may prevent or delay the leakage of the inner phase into the external phase.

Although the protein-polysaccharide bilayer emulsions exhibit better performance in several aspects than using individual proteins, their preparation requires a two-step adsorption procedure. From an industrial perspective, this increases the production cost and could only be applicable to products with high added values. Moreover, the preparation of a bilayer emulsion is difficult to fulfill when the volume percent of the disperse phase is high since severe flocculation could occur. Instead, a facile way is to prepare previously formed complexes before emulsification, which can be used as interfacial stabilizers as well. Even though some interfacial rheological studies showed that the pre-formed complexes might hinder the formation of a cohesive protein network at the interfaces, some studies also speculated that the adsorbed (pre-formed) complexes at the interfaces would slowly evolve into a bilayer structure with time from a thermodynamic perspective. This speculation still needs to be tested both at the interfaces and in bulk emulsions. Moreover, it seems interesting to investigate the influence of thermal treatment (e.g. above the denaturation temperature of the protein) on the interfacial properties of the previously adsorbed electrostatic complexes (after emulsification), as well as their performance in emulsion stability, since the heating could accelerate protein-protein interactions (e.g. through disulfide bonds), and meanwhile embed the polysaccharide chains into the interfacial layers.

Additionally, this dissertation is only limited to the non-covalent electrostatic interactions between protein and anionic polysaccharide. The protein-polysaccharide covalent conjugates (e.g. Maillard conjugates) have been demonstrated to be robust interfacial stabilizers. However, the number of studies focusing on their interfacial properties and relevant applications is still limited.

To better understand the behavior of emulsions in food processing or after ingestion (in vitro studies), an in-situ, multilength scale approach is always advisable, i.e. from the interfacial level, over a single droplet level, to the bulk emulsion level. Combined with interfacial studies, some state-of-the-art techniques (e.g. droplet microfluidics with customized geometry) could provide inspiring opportunities for food scientists.

Regarding the results in PART III, it is possible that the results of the fluorescent probe study could be applicable to many bioactive compounds binding to β-Lg. However, the binding site and affinity of various hydrophobic compounds (e.g. bioactive compounds) to β-Lg (in the presence or absence of pectin) as a function of pH needs to be further investigated by NMR spectroscopy and more quantitative studies. Moreover, the role of salt and thermal treatment (either before or after binding) on the ligand-binding properties, as well as the stability of the binding phenomena (or encapsulation performance) on a longer time scale (e.g. weeks or months) should be evaluated.

Driven by food sustainability concerns, there is a growing interest to replace animal proteins with plant-based proteins. As opposed to extensively studied milk proteins, the surface activity and ligand-binding properties of those plant proteins remain mostly unclear. It can be foreseen that an increasing number of studies focusing on plant-based proteins will emerge.

References

Acquistapace, S., Patel, L., Patin, A., Forbes-Blom, E., Cuenoud, B., & Wooster, T. J. (2019). Effects of interesterified lipid design on the short/medium chain fatty acid hydrolysis rate and extent (in vitro). *Food and Function*, *10*(7), 4166–4176. https://doi.org/10.1039/c9fo00671k

Amara, S., Bourlieu, C., Humbert, L., Rainteau, D., & Carrière, F. (2019). Variations in gastrointestinal lipases, pH and bile acid levels with food intake, age and diseases: possible impact on oral lipid-based drug delivery systems. *Advanced Drug Delivery Reviews*, *142*, 3–15. https://doi.org/10.1016/j.addr.2019.03.005

Andreeva, N. S., & James, M. N. G. (1991). Why does pepsin have a negative charge at very low pH? an analysis of conserved charged residues in aspartic proteinases. *Advances in Experimental Medicine and Biology*, *306*, 39–45. https://doi.org/10.1007/978-1-4684-6012-4_4

Antonov, Y. A., Lashko, N. P., Glotova, Y. K., Malovikova, A., & Markovich, O. (1996). Effect of the structural features of pectins and alginates on their thermodynamic compatibility with gelatin in aqueous media. *Food Hydrocolloids*, *10*(1), 1–9. https://doi.org/10.1016/s0268-005x(96)80047-6

Araiza-Calahorra, A., & Sarkar, A. (2019). Designing biopolymer-coated pickering emulsions to modulate: in vitro gastric digestion: a static model study. *Food and Function*, *10*(9), 5498–5509. https://doi.org/10.1039/c9fo01080g

Armand, M. (2007). Lipases and lipolysis in the human digestive tract: where do we stand? *Current Opinion in Clinical Nutrition and Metabolic Care*, *10*(2), 156–164. https://doi.org/10.1097/mco.0b013e3280177687

Bain, C. D., Biebuyck, H. A., & Whitesides, G. M. (1989). Comparison of self-assembled monolayers on gold: coadsorption of thiols and disulfides1. *Langmuir*, *5*(3), 723–727. https://doi.org/10.1021/la00087a027

Beicht, J., Zeeb, B., Gibis, M., Fischer, L., & Weiss, J. (2013). Influence of layer thickness and composition of cross-linked multilayered oil-in-water emulsions

on the release behavior of lutein. *Food and Function*, *4*(10), 1457–1467. https://doi.org/10.1039/c3fo60220f

Benjamin, O., Lassé, M., Silcock, P., & Everett, D. W. (2012). Effect of pectin adsorption on the hydrophobic binding sites of β-lactoglobulin in solution and in emulsion systems. *International Dairy Journal*, *26*(1), 36–40. https://doi.org/10.1016/j.idairyj.2011.12.007

Benjamin, O., Silcock, P., Leus, M., & Everett, D. W. (2012). Multilayer emulsions as delivery systems for controlled release of volatile compounds using pH and salt triggers. *Food Hydrocolloids*, *27*(1), 109–118. https://doi.org/10.1016/j.foodhyd.2011.08.008

Bergfreund, J., Bertsch, P., & Fischer, P. (2021). Adsorption of proteins to fluid interfaces: role of the hydrophobic subphase. *Journal of Colloid and Interface Science*, *584*, 411–417. https://doi.org/10.1016/j.jcis.2020.09.118

Bergfreund, J., Bertsch, P., Kuster, S., & Fischer, P. (2018). Effect of oil hydrophobicity on the adsorption and rheology of β-lactoglobulin at oil-water interfaces. *Langmuir*, *34*(16), 4929–4936. https://doi.org/10.1021/acs.langmuir.8b00458

Bergfreund, J., Diener, M., Geue, T., Nussbaum, N., Kummer, N., Bertsch, P., Nyström, G., & Fischer, P. (2021). Globular protein assembly and network formation at fluid interfaces: effect of oil. *Soft Matter*, *17*(6), 1692–1700. https://doi.org/10.1039/d0sm01870h

Berton-Carabin, C. C., Sagis, L., & Schroën, K. (2018). Formation, structure, and functionality of interfacial layers in food emulsions. *Annual Review of Food Science and Technology*, *9*(January), 551–587. https://doi.org/10.1146/annurev-food-030117-012405

Berton-Carabin, C. C., Schröder, A., Rovalino-Cordova, A., Schroën, K., & Sagis, L. (2016). Protein and lipid oxidation affect the viscoelasticity of whey protein layers at the oil–water interface. *European Journal of Lipid Science and Technology*, *118*(11), 1630–1643. https://doi.org/10.1002/ejlt.201600066

Bertsch, P., Thoma, A., Bergfreund, J., Geue, T., & Fischer, P. (2019). Transient

measurement and structure analysis of protein-polysaccharide multilayers at fluid interfaces. *Soft Matter*, *15*(31), 6362–6368. https://doi.org/10.1039/c9sm01112a

Biswas, S., Melton, L. D., Nelson, A. R. J., Le Brun, A. P., Heinrich, F., McGillivray, D. J., & Xu, A. Y. (2022). The assembly mechanism and mesoscale architecture of protein-polysaccharide complexes formed at the solid-liquid interface. *Langmuir*, *38*(41), 12551–12561. https://doi.org/10.1021/acs.langmuir.2c02003

Bohin, M. C., Vincken, J.-P., van der Hijden, H. T. W. M., & Gruppen, H. (2012). Efficacy of food proteins as carriers for flavonoids. *Journal of Agricultural and Food Chemistry*, *60*(16), 4136–4143. https://doi.org/10.1021/jf205292r

Boland, M., & Singh, H. (2019). Milk proteins: from expression to food. In *Milk Proteins: From Expression to Food*.

Brodkorb, A., Egger, L., Alminger, M., Alvito, P., Assunção, R., Ballance, S., Bohn, T., Bourlieu-Lacanal, C., Boutrou, R., Carrière, F., Clemente, A., Corredig, M., Dupont, D., Dufour, C., Edwards, C., Golding, M., Karakaya, S., Kirkhus, B., Le Feunteun, S., … Recio, I. (2019). INFOGEST static in vitro simulation of gastrointestinal food digestion. *Nature Protocols*, *14*(4), 991–1014. https://doi.org/10.1038/s41596-018-0119-1

Brown, M. B. (1993). *The use of long wavelength fluorescence in the study of ligand-protein interactions*. Loughborough University.

Burgess, D. J., & Sahin, N. O. (1997). Interfacial rheological and tension properties of protein films. *Journal of Colloid and Interface Science*, *189*(1), 74–82. https://doi.org/10.1006/jcis.1997.4803

Burova, T. V., Grinberg, N. V., Dubovik, A. S., Plashchina, I. G., Usov, A. I., & Grinberg, V. Y. (2022). Energetics and mechanism of β-lactoglobulin binding to dextran sulfate. *Food Hydrocolloids*, *122*, 107027. https://doi.org/10.1016/j.foodhyd.2021.107027

Cai, B. (2020). *Engineering Interfacial Structure of Proteins to Resist Surfactant-Induced Competitive Displacement*. University of Wisconsin-Madison.

Cao, L., Lu, W., Mata, A., Nishinari, K., & Fang, Y. (2020). Egg-box model-based gelation of alginate and pectin: a review. *Carbohydrate Polymers*, *242*, 116389. https://doi.org/10.1016/j.carbpol.2020.116389

Cardoso, M. J., Caridade, S. G., Costa, R. R., & Mano, J. F. (2016). Enzymatic degradation of polysaccharide-based layer-by-layer structures. *Biomacromolecules*, *17*(4), 1347–1357. https://doi.org/10.1021/acs.biomac.5b01742

Cheng, H., Fang, Z., Liu, T., Gao, Y., & Liang, L. (2018). A study on β-lactoglobulin-triligand-pectin complex particle: formation, characterization and protection. *Food Hydrocolloids*, *84*, 93–103. https://doi.org/10.1016/j.foodhyd.2018.05.055

Cho, Y., Batt, C. A., & Sawyer, L. (1994). Probing the retinol-binding site of bovine beta-lactoglobulin. *Journal of Biological Chemistry*, *269*(15), 11102–11107. https://doi.org/10.1016/s0021-9258(19)78097-1

Cho, Y. H., & McClements, D. J. (2009). Theoretical stability maps for guiding preparation of emulsions stabilized by protein-polysaccharide interfacial complexes. *Langmuir*, *25*(12), 6649–6657. https://doi.org/10.1021/la8006684

Considine, T., Flanagan, J., Loveday, S. M., & Ellis, A. (2020). Interaction between milk proteins and micronutrients. *Milk Proteins: From Expression to Food*, 537–571. https://doi.org/10.1016/b978-0-12-815251-5.00014-1

Corstens, M. N., Osorio Caltenco, L. A., de Vries, R., Schroën, K., & Berton-Carabin, C. C. (2017). Interfacial behaviour of biopolymer multilayers: influence of in vitro digestive conditions. *Colloids and Surfaces B: Biointerfaces*, *153*, 199–207. https://doi.org/10.1016/j.colsurfb.2017.02.019

Cui, S. W. (2005). Food carbohydrates: chemistry, physical properties, and applications. In *Food Carbohydrates: Chemistry, Physical Properties, and Applications*.

Dan, A., Gochev, G., Krägel, J., Aksenenko, E. V., Fainerman, V. B., & Miller, R. (2013). Interfacial rheology of mixed layers of food proteins and surfactants. *Current Opinion in Colloid and Interface Science*, *18*(4), 302–310.

https://doi.org/10.1016/j.cocis.2013.04.002

de Oliveira, F. C., Coimbra, J. S. dos R., de Oliveira, E. B., Zuñiga, A. D. G., & Rojas, E. E. G. (2016). Food protein-polysaccharide conjugates obtained via the maillard reaction: a review. *Critical Reviews in Food Science and Nutrition*, *56*(7), 1108–1125. https://doi.org/10.1080/10408398.2012.755669

De Vries, J. A., Rombouts, F. M., Voragen, A. G. J., & Pilnik, W. (1982). Enzymic degradation of apple pectins. *Carbohydrate Polymers*, *2*(1), 25–33. https://doi.org/10.1016/0144-8617(82)90043-1

Deeth, H. C., & Bansal, N. (2018). Whey proteins: from milk to medicine. In *Whey Proteins: From Milk to Medicine*. https://doi.org/10.1016/c2016-0-02581-0

Demetriades, K., & Julian McClements, D. (2000). Influence of sodium dodecyl sulfate on the physicochemical properties of whey protein-stabilized emulsions. *Colloids and Surfaces A: Physicochemical and Engineering Aspects*, *161*(3), 391–400. https://doi.org/10.1016/s0927-7757(99)00210-1

Dickinson, E. (2008). Interfacial structure and stability of food emulsions as affected by protein-polysaccharide interactions. *Soft Matter*, *4*(5), 932–942. https://doi.org/10.1039/b718319d

Dickinson, E. (2011). Mixed biopolymers at interfaces: competitive adsorption and multilayer structures. *Food Hydrocolloids*, *25*(8), 1966–1983. https://doi.org/10.1016/j.foodhyd.2010.12.001

Dickinson, E. (2015). Microgels - an alternative colloidal ingredient for stabilization of food emulsions. *Trends in Food Science and Technology*, *43*(2), 178–188. https://doi.org/10.1016/j.tifs.2015.02.006

Dickinson, E., & Matsumura, Y. (1991). Time-dependent polymerization of β-lactoglobulin through disulphide bonds at the oil-water interface in emulsions. *International Journal of Biological Macromolecules*, *13*(1), 26–30. https://doi.org/10.1016/0141-8130(91)90006-g

Dixon, M. C. (2008). Quartz crystal microbalance with dissipation monitoring: enabling real-time characterization of biological materials and their interactions.

Journal of Biomolecular Techniques, *19*(3), 151–158.

Ducel, V., Richard, J., Popineau, Y., & Boury, F. (2005). Rheological interfacial properties of plant protein - arabic gum coacervates at the oil-water interface. *Biomacromolecules*, *6*(2), 790–796. https://doi.org/10.1021/bm0494601

Dufour, E., Genot, C., & Haertlé, T. (1994). β-lactoglobulin binding properties during its folding changes studied by fluorescence spectroscopy. *Biochimica et Biophysica Acta (BBA)/Protein Structure and Molecular*, *1205*(1), 105–112. https://doi.org/10.1016/0167-4838(94)90098-1

Engelhardt, K., Lexis, M., Gochev, G., Konnerth, C., Miller, R., Willenbacher, N., Peukert, W., & Braunschweig, B. (2013). pH effects on the molecular structure of β-lactoglobulin modified air-water interfaces and its impact on foam rheology. *Langmuir*, *29*(37), 11646–11655. https://doi.org/10.1021/la402729g

Fischer, P. (2013). Rheology of interfacial protein-polysaccharide composites. *European Physical Journal: Special Topics*, *222*(1), 73–81. https://doi.org/10.1140/epjst/e2013-01827-x

Flanagan, J., & Singh, H. (2006). Conjugation of sodium caseinate and gum arabic catalyzed by transglutaminase. *Journal of Agricultural and Food Chemistry*, *54*(19), 7305–7310. https://doi.org/10.1021/jf061220k

Flower, D. R. (1996). The lipocalin protein family: structure and function. *Biochemical Journal*, *318*(1), 1–14. https://doi.org/10.1042/bj3180001

Fugate, R. D., & Song, P. S. (1980). Spectroscopic characterization of β-lactoglobulin-retinol complex. *Biochimica et Biophysica Acta (BBA) - Protein Structure*, *625*(1), 28–42. https://doi.org/10.1016/0005-2795(80)90105-1

Ganzevles, R. A., Kosters, H., van Vliet, T., Cohen Stuart, M. A., & de Jongh, H. H. J. (2007). Polysaccharide charge density regulating protein adsorption to air/water interfaces by protein/polysaccharide complex formation. *Journal of Physical Chemistry B*, *111*(45), 12969–12976. https://doi.org/10.1021/jp075441k

Ganzevles, R. A., Zinoviadou, K., van Vliet, T., Cohen Stuart, M. A., & de Jongh, H. H.

J. (2006). Modulating surface rheology by electrostatic protein/polysaccharide interactions. *Langmuir*, *22*(24), 10089–10096. https://doi.org/10.1021/la061537e

Gao, J. Y., & Dubin, P. L. (1999). Binding of proteins to copolymers of varying hydrophobicity. *Biopolymers*, *49*(2), 185–193. https://doi.org/10.1002/(sici)1097-0282(199902)49:2<185::aid-bip6>3.0.co;2-6

Garti, N., & McClements, D. J. (2012). Encapsulation technologies and delivery systems for food ingredients and nutraceuticals. In *Encapsulation Technologies and Delivery Systems for Food Ingredients and Nutraceuticals*. https://doi.org/10.1533/9780857095909

Girard, M., Sanchez, C., Laneuville, S. I., Turgeon, S. L., & Gauthier, S. F. (2004). Associative phase separation of β-lactoglobulin/pectin solutions: a kinetic study by small angle static light scattering. *Colloids and Surfaces B: Biointerfaces*, *35*(1), 15–22. https://doi.org/10.1016/j.colsurfb.2004.02.002

Girard, M., Turgeon, S. L., & Gauthier, S. F. (2002). Interbiopolymer complexing between β-lactoglobulin and low- and high-methylated pectin measured by potentiometric titration and ultrafiltration. *Food Hydrocolloids*, *16*(6), 585–591. https://doi.org/10.1016/s0268-005x(02)00020-6

Golding, M., Wooster, T. J., Day, L., Xu, M., Lundin, L., Keogh, J., & Cliftonx, P. (2011). Impact of gastric structuring on the lipolysis of emulsified lipids. *Soft Matter*, *7*(7), 3513–3523. https://doi.org/10.1039/c0sm01227k

Graham, D. E., & Phillips, M. C. (1980). Proteins at liquid interfaces. v. shear properties. *Journal of Colloid and Interface Science*, *76*(1), 240–250. https://doi.org/10.1016/0021-9797(80)90290-8

Guzey, D., & McClements, D. J. (2006). Formation, stability and properties of multilayer emulsions for application in the food industry. *Advances in Colloid and Interface Science*, *128–130*, 227–248. https://doi.org/10.1016/j.cis.2006.11.021

Harnsilawat, T., Pongsawatmanit, R., & McClements, D. J. (2006). Characterization

of β-lactoglobulin-sodium alginate interactions in aqueous solutions: a calorimetry, light scattering, electrophoretic mobility and solubility study. *Food Hydrocolloids*, *20*(5), 577–585. https://doi.org/10.1016/j.foodhyd.2005.05.005

Hinderink, E. B. A., Sagis, L., Schroën, K., & Berton-Carabin, C. C. (2021). Sequential adsorption and interfacial displacement in emulsions stabilized with plant-dairy protein blends. *Journal of Colloid and Interface Science*, *583*, 704–713. https://doi.org/10.1016/j.jcis.2020.09.066

Ho, K. K. H. Y., Schroën, K., San Martín-González, M. F., & Berton-Carabin, C. C. (2018). Synergistic and antagonistic effects of plant and dairy protein blends on the physicochemical stability of lycopene-loaded emulsions. *Food Hydrocolloids*, *81*, 180–190. https://doi.org/10.1016/j.foodhyd.2018.02.033

Höök, F., Kasemo, B., Nylander, T., Fant, C., Sott, K., & Elwing, H. (2001). Variations in coupled water, viscoelastic properties, and film thickness of a mefp-1 protein film during adsorption and cross-linking: a quartz crystal microbalance with dissipation monitoring, ellipsometry, and surface plasmon resonance study. *Analytical Chemistry*, *73*(24), 5796–5804. https://doi.org/10.1021/ac0106501

Hosseini, S. M. H., Emam-Djomeh, Z., Sabatino, P., & Van der Meeren, P. (2015). Nanocomplexes arising from protein-polysaccharide electrostatic interaction as a promising carrier for nutraceutical compounds. *Food Hydrocolloids*, *50*, 16–26. https://doi.org/10.1016/j.foodhyd.2015.04.006

Johannsmann, D., Reviakine, I., Rojas, E., & Gallego, M. (2008). Effect of sample heterogeneity on the interpretation of QCM-D data: comparison of combined quartz crystal microbalance/atomic force microscopy measurements with finite element method modeling. *Analytical Chemistry*, *80*(23), 8891–8899. https://doi.org/10.1021/ac8013115

Jones, O. G., Lesmes, U., Dubin, P., & McClements, D. J. (2010). Effect of polysaccharide charge on formation and properties of biopolymer nanoparticles created by heat treatment of β-lactoglobulin-pectin complexes. *Food Hydrocolloids*, *24*(4), 374–383.

https://doi.org/10.1016/j.foodhyd.2009.11.003

Jung, J.-M., Savin, G., Pouzot, M., Schmitt, C., & Mezzenga, R. (2008). Structure of heat-induced β-lactoglobulin aggregates and their complexes with sodium-dodecyl sulfate. *Biomacromolecules*, *9*(9), 2477–2486. https://doi.org/10.1021/bm800502j

Keogh, J. B., Wooster, T. J., Golding, M., Day, L., Otto, B., & Clifton, P. M. (2011). Slowly and rapidly digested fat emulsions are equally satiating but their triglycerides are differentially absorbed and metabolized in humans. *Journal of Nutrition*, *141*(5). https://doi.org/10.3945/jn.110.131110

Keppler, J. K., Sönnichsen, F. D., Lorenzen, P. C., & Schwarz, K. (2014). Differences in heat stability and ligand binding among β-lactoglobulin genetic variants a, b and c using 1H NMR and fluorescence quenching. *Biochimica et Biophysica Acta - Proteins and Proteomics*, *1844*(6), 1083–1093. https://doi.org/10.1016/j.bbapap.2014.02.007

Kieserling, H., Alsmeier, I. M., Steffen-Heins, A., Keppler, J. K., Sevenich, R., Rauh, C., Wagemans, A. M., & Drusch, S. (2021). Interfacial film formation and film stability of high hydrostatic pressure-treated β-lactoglobulin. *Food Hydrocolloids*, *119*, 106746. https://doi.org/10.1016/j.foodhyd.2021.106746

Kieserling, H., Pankow, A., Keppler, J. K., Wagemans, A. M., & Drusch, S. (2021). Conformational state and charge determine the interfacial film formation and film stability of β-lactoglobulin. *Food Hydrocolloids*, *114*, 106561. https://doi.org/10.1016/j.foodhyd.2020.106561

Labourdenne, S., Gaudry-Rolland, N., Letellier, S., Lin, M., Cagna, A., Esposito, G., Verger, R., & Rivière, C. (1994). The oil-drop tensiometer: potential applications for studying the kinetics of (phospho)lipase action. *Chemistry and Physics of Lipids*, *71*(2), 163–173. https://doi.org/10.1016/0009-3084(94)90068-x

Lee, H. S., Myers, C., Zaidel, L., Nalam, P. C., Caporizzo, M. A., Daep, C. A., Eckmann, D. M., Masters, J. G., & Composto, R. J. (2017). Competitive adsorption of polyelectrolytes onto and into pellicle-coated hydroxyapatite investigated by QCM-D and force spectroscopy. *ACS Applied Materials and Interfaces*, *9*(15),

13079–13091. https://doi.org/10.1021/acsami.7b02774

Li, H., Wang, D., Liu, C., Zhu, J., Fan, M., Sun, X., Wang, T., Xu, Y., & Cao, Y. (2019). Fabrication of stable zein nanoparticles coated with soluble soybean polysaccharide for encapsulation of quercetin. *Food Hydrocolloids*, *87*, 342–351. https://doi.org/10.1016/j.foodhyd.2018.08.002

Li, H., Wang, T., Hu, Y., Wu, J., & Van der Meeren, P. (2022). Designing delivery systems for functional ingredients by protein/polysaccharide interactions. *Trends in Food Science & Technology*, *119*, 272–287. https://doi.org/10.1016/j.tifs.2021.12.007

Li, H., Wu, J., Doost, A. S., Su, J., & Van der Meeren, P. (2021). Electrostatic interaction between whey proteins and low methoxy pectin studied by quartz crystal microbalance with dissipation monitoring. *Food Hydrocolloids*, *113*, 106489. https://doi.org/10.1016/j.foodhyd.2020.106489

Li, M., Blecker, C., & Karboune, S. (2021). Molecular and air-water interfacial properties of potato protein upon modification via laccase-catalyzed cross-linking and conjugation with sugar beet pectin. *Food Hydrocolloids*, *112*, 106236. https://doi.org/10.1016/j.foodhyd.2020.106236

Li, M., Ma, Y., & Ngadi, M. O. (2013). Binding of curcumin to β-lactoglobulin and its effect on antioxidant characteristics of curcumin. *Food Chemistry*, *141*(2), 1504–1511. https://doi.org/10.1016/j.foodchem.2013.02.099

Li, N., & Zhong, Q. (2021). Conjugation of α-, β-, and κ-caseins with propylene glycol alginate using a transacylation reaction as novel emulsifiers. *Biomacromolecules*, *22*(10), 4395–4407. https://doi.org/10.1021/acs.biomac.1c00971

Liang, L., A. Tajmir-Riahi, H., & Subirade, M. (2007). Interaction of β-lactoglobulin with resveratrol and its biological implications. *Biomacromolecules*, *9*(1), 50–56. https://doi.org/10.1021/bm700728k

Liang, L., & Subirade, M. (2012). Study of the acid and thermal stability of β-lactoglobulin–ligand complexes using fluorescence quenching. *Food Chemistry*, *132*(4), 2023–2029. https://doi.org/10.1016/j.foodchem.2011.12.043

Liu, S. X., & Kim, J. T. (2009). Application of kevin—voigt model in quantifying whey protein adsorption on polyethersulfone using qcm-d. *Journal of Laboratory Automation*, *14*(4), 213–220. https://doi.org/10.1016/j.jala.2009.01.003

Livney, Y. D. (2010). Milk proteins as vehicles for bioactives. *Current Opinion in Colloid & Interface Science*, *15*(1–2), 73–83. https://doi.org/10.1016/j.cocis.2009.11.002

Livney, Y. D. (2012). Biopolymeric amphiphiles and their assemblies as functional food ingredients and nutraceutical delivery systems. In *Encapsulation Technologies and Delivery Systems for Food Ingredients and Nutraceuticals* (pp. 252–286). https://doi.org/10.1016/b978-0-85709-124-6.50010-x

Luo, Y., Wang, Q., & Zhang, Y. (2020). Biopolymer-based nanotechnology approaches to deliver bioactive compounds for food applications: a perspective on the past, present, and future. *Journal of Agricultural and Food Chemistry*, *68*(46), 12993–13000. https://doi.org/10.1021/acs.jafc.0c00277

MacCarini, M., Himmelhaus, M., Stoycheva, S., & Grunze, M. (2005). Characterisation and stability of hydrophobic surfaces in water. *Applied Surface Science*, *252*(5), 1941–1946. https://doi.org/10.1016/j.apsusc.2005.03.157

MacIerzanka, A., Sancho, A. I., Mills, E. N. C., Rigby, N. M., & MacKie, A. R. (2009). Emulsification alters simulated gastrointestinal proteolysis of β-casein and β-lactoglobulin. *Soft Matter*, *5*(3), 538–550. https://doi.org/10.1039/b811233a

Malagelada, J. R., Go, V. L. W., & Summerskill, W. H. J. (1979). Different gastric, pancreatic, and biliary responses to solid-liquid or homogenized meals. *Digestive Diseases and Sciences*, *24*(2), 101–110. https://doi.org/10.1007/bf01324736

Maldonado-Valderrama, J. (2019). Probing in vitro digestion at oil–water interfaces. *Current Opinion in Colloid and Interface Science*, *39*, 51–60. https://doi.org/10.1016/j.cocis.2019.01.004

Maldonado-Valderrama, J., & Rodríguez Patino, J. M. (2010). Interfacial rheology of protein-surfactant mixtures. In *Current Opinion in Colloid and Interface Science* (Vol. 15, Issue 4, pp. 271–282).

https://doi.org/10.1016/j.cocis.2009.12.004

Mao, L., Pan, Q., Yuan, F., & Gao, Y. (2019). Formation of soy protein isolate-carrageenan complex coacervates for improved viability of bifidobacterium longum during pasteurization and in vitro digestion. *Food Chemistry*, *276*, 307–314. https://doi.org/10.1016/j.foodchem.2018.10.026

Matsuyama, S., Kazuhiro, M., Nakauma, M., Funami, T., Nambu, Y., Matsumiya, K., & Matsumura, Y. (2021). Stabilization of whey protein isolate-based emulsions via complexation with xanthan gum under acidic conditions. *Food Hydrocolloids*, *111*, 106365. https://doi.org/10.1016/j.foodhyd.2020.106365

McClements, D. J. (2004). Protein-stabilized emulsions. *Current Opinion in Colloid and Interface Science*, *9*(5), 305–313.

McClements, D. J. (2012). Advances in fabrication of emulsions with enhanced functionality using structural design principles. *Current Opinion in Colloid and Interface Science*, *17*(5), 235–245. https://doi.org/10.1016/j.cocis.2012.06.002

McClements, D. J. (2015). Food emulsions: principles, practices, and techniques, third edition. In *Food Emulsions: Principles, Practices, and Techniques, Third Edition*. https://doi.org/10.1201/b18868

McClements, D. J., Decker, E. A., & Weiss, J. (2007). Emulsion-based delivery systems for lipophilic bioactive components. *Journal of Food Science*, *72*(8), R109–R124. https://doi.org/10.1111/j.1750-3841.2007.00507.x

McMahon, D. J., & McManus, W. R. (1998). Rethinking casein micelle structure using electron microscopy. *Journal of Dairy Science*, *81*(11), 2985–2993. https://doi.org/10.3168/jds.s0022-0302(98)75862-x

Mekhloufi, G., Sanchez, C., Renard, D., Guillemin, S., & Hardy, J. (2005). pH-induced structural transitions during complexation and coacervation of β-lactoglobulin and acacia gum. *Langmuir*, *21*(1), 386–394. https://doi.org/10.1021/la0486786

Mezzenga, R. (2018). Protein-templated oil gels and powders. In *Edible Oleogels* (pp. 307–329). https://doi.org/10.1016/b978-0-12-814270-7.00013-7

Mezzenga, R., & Fischer, P. (2013). The self-assembly, aggregation and phase transitions of food protein systems in one, two and three dimensions. *Reports on Progress in Physics*, *76*(4), 046601. https://doi.org/10.1088/0034-4885/76/4/046601

Miquelim, J. N., Lannes, S. C. S., & Mezzenga, R. (2010). PH influence on the stability of foams with protein-polysaccharide complexes at their interfaces. *Food Hydrocolloids*, *24*(4), 398–405. https://doi.org/10.1016/j.foodhyd.2009.11.006

Møller, A. H., Wijaya, W., Jahangiri, A., Madsen, B., Joernsgaard, B., Vaerbak, S., Hammershøj, M., Van der Meeren, P., & Dalsgaard, T. K. (2020). Norbixin binding to whey protein isolate - alginate electrostatic complexes increases its solubility and stability. *Food Hydrocolloids*, *101*, 105559.

Moreno, E. M., Levy, D., M. Moreno, E., & Levy, D. (2000). Role of the comonomer glymo in ormosils as reflected by nile red spectroscopy. *Chemistry of Materials*, *12*(8), 2334–2340. https://doi.org/10.1021/cm001048e

Murray, B. S. (2002). Interfacial rheology of food emulsifiers and proteins. *Current Opinion in Colloid and Interface Science*, *7*(5–6), 426–431. https://doi.org/10.1016/s1359-0294(02)00077-8

Murray, B. S. (2011). Rheological properties of protein films. *Current Opinion in Colloid and Interface Science*, *16*(1), 27–35. https://doi.org/10.1016/j.cocis.2010.06.005

Murray, B. S., Ettelaie, R., Sarkar, A., Mackie, A. R., & Dickinson, E. (2021). The perfect hydrocolloid stabilizer: imagination versus reality. *Food Hydrocolloids*, *117*, 106696. https://doi.org/10.1016/j.foodhyd.2021.106696

Nakauma, M., Funami, T., Noda, S., Ishihara, S., Al-Assaf, S., Nishinari, K., & Phillips, G. O. (2008). Comparison of sugar beet pectin, soybean soluble polysaccharide, and gum arabic as food emulsifiers. 1. effect of concentration, ph, and salts on the emulsifying properties. *Food Hydrocolloids*, *22*(7), 1254–1267. https://doi.org/10.1016/j.foodhyd.2007.09.004

Narchi, I., Vial, C., & Djelveh, G. (2009). Effect of protein-polysaccharide mixtures on

the continuous manufacturing of foamed food products. *Food Hydrocolloids*, *23*(1), 188–201. https://doi.org/10.1016/j.foodhyd.2007.12.010

Nguyen, H. T., Marquis, M., Anton, M., & Marze, S. (2019). Studying the real-time interplay between triglyceride digestion and lipophilic micronutrient bioaccessibility using droplet microfluidics. 1 lab on a chip method. *Food Chemistry*, *275*, 523–529. https://doi.org/10.1016/j.foodchem.2018.09.096

Nicolai, T., & Murray, B. (2017). Particle stabilized water in water emulsions. *Food Hydrocolloids*, *68*, 157–163. https://doi.org/10.1016/j.foodhyd.2016.08.036

O'Neal, J. T., Dai, E. Y., Zhang, Y., Clark, K. B., Wilcox, K. G., George, I. M., Ramasamy, N. E., Enriquez, D., Batys, P., Sammalkorpi, M., & Lutkenhaus, J. L. (2018). QCM-D investigation of swelling behavior of layer-by-layer thin films upon exposure to monovalent ions. *Langmuir*, *34*(3), 999–1009. https://doi.org/10.1021/acs.langmuir.7b02836

Olsen, J. M. H., Reine, S., Vahtras, O., Kjellgren, E., Reinholdt, P., Hjorth Dundas, K. O., Li, X., Cukras, J., Ringholm, M., Hedegård, E. D., Di Remigio, R., List, N. H., Faber, R., Cabral Tenorio, B. N., Bast, R., Pedersen, T. B., Rinkevicius, Z., Sauer, S. P. A., Mikkelsen, K. V, … Norman, P. (2020). Dalton project: a python platform for molecular- and electronic-structure simulations of complex systems. *The Journal of Chemical Physics*, *152*(21), 214115. https://doi.org/10.1063/1.5144298

Ouberai, M. M., Xu, K., & Welland, M. E. (2014). Effect of the interplay between protein and surface on the properties of adsorbed protein layers. *Biomaterials*, *35*(24), 6157–6163. https://doi.org/10.1016/j.biomaterials.2014.04.012

Pafumi, Y., Lairon, D., De La Porte, P. L., Juhel, C., Storch, J., Hamosh, M., & Armand, M. (2002). Mechanisms of inhibition of triacylglycerol hydrolysis by human gastric lipase. *Journal of Biological Chemistry*, *277*(31). https://doi.org/10.1074/jbc.m202839200

Pan, K., & Zhong, Q. (2016). Organic nanoparticles in foods: fabrication, characterization, and utilization. *Annual Review of Food Science and Technology*, *7*, 245–266. https://doi.org/10.1146/annurev-food-041715-

033215

Panigrahi, S. K., & Mishra, A. K. (2019). Inner filter effect in fluorescence spectroscopy: as a problem and as a solution. *Journal of Photochemistry and Photobiology C: Photochemistry Reviews*, *41*, 100318. https://doi.org/10.1016/j.jphotochemrev.2019.100318

Patra, D., & Barakat, C. (2011). Synchronous fluorescence spectroscopic study of solvatochromic curcumin dye. *Spectrochimica Acta - Part A: Molecular and Biomolecular Spectroscopy*, *79*(5), 1034–1041. https://doi.org/10.1016/j.saa.2011.04.016

Peng, D., Yang, J., Li, J., Tang, C., & Li, B. (2017). Foams stabilized by β-lactoglobulin amyloid fibrils: effect of ph. *Journal of Agricultural and Food Chemistry*, *65*(48), 10658–10665. https://doi.org/10.1021/acs.jafc.7b03669

Pilichiewicz, A. N., Little, T. J., Brennan, I. M., Meyer, J. H., Wishart, J. M., Otto, B., Horowitz, M., & Feinle-Bisset, C. (2006). Effects of load, and duration, of duodenal lipid on antropyloroduodenal motility, plasma cck and pyy, and energy intake in healthy men. *American Journal of Physiology - Regulatory Integrative and Comparative Physiology*, *290*(3), 668–677. https://doi.org/10.1152/ajpregu.00606.2005

Pinďáková, L., Kašpárková, V., & Bordes, R. (2019). Role of protein-cellulose nanocrystal interactions in the stabilization of emulsion. *Journal of Colloid and Interface Science*, *557*, 196–206. https://doi.org/10.1016/j.jcis.2019.09.002

Polverini, E., Cugini, G., Annoni, F., Abbruzzetti, S., Viappiani, C., & Gensch, T. (2006). Molten globule formation in apomyoglobin monitored by the fluorescent probe nile red. *Biochemistry*, *45*(16), 5111–5121. https://doi.org/10.1021/bi051905y

Ragona, L., Zetta, L., Fogolari, F., Molinari, H., Pérez, D. M., Puyol, P., Kruif, K. De, Löhr, F., & Rüterjans, H. (2000). Bovine β-lactoglobulin: interaction studies with palmitic acid. *Protein Science*, *9*(7), 1347–1356. https://doi.org/https://doi.org/10.1110/ps.9.7.1347

Ray, A., Das, S., & Chattopadhyay, N. (2019). Aggregation of nile red in water:

prevention through encapsulation in β-cyclodextrin. *ACS Omega*, *4*(1), 15–24. https://doi.org/10.1021/acsomega.8b02503

Reis, P., Miller, R., Leser, M., Watzke, H., Fainerman, V. B., & Holmberg, K. (2008). Adsorption of polar lipids at the water-oil interface. *Langmuir*, *24*(11), 5781–5786. https://doi.org/10.1021/la704043g

Reviakine, I., Johannsmann, D., & Richter, R. P. (2011). Hearing what you cannot see and visualizing what you hear: interpreting quartz crystal microbalance data from solvated interfaces. *Analytical Chemistry*, *83*(23), 8838–8848. https://doi.org/10.1021/ac201778h

Riihimäki, L. H., Vainio, M. J., Heikura, J. M. S., Valkonen, K. H., Virtanen, V. T., & Vuorela, P. M. (2008). Binding of phenolic compounds and their derivatives to bovine and reindeer β-lactoglobulin. *Journal of Agricultural and Food Chemistry*, *56*(17), 7721–7729. https://doi.org/10.1021/jf801120a

Rodriguez Patino, J. M., & Pilosof, A. M. R. (2011). Protein-polysaccharide interactions at fluid interfaces. *Food Hydrocolloids*, *25*(8), 1925–1937. https://doi.org/10.1016/j.foodhyd.2011.02.023

Romoscanu, A. I., & Mezzenga, R. (2005). Cross linking and rheological characterization of adsorbed protein layers at the oil-water interface. *Langmuir*, *21*(21), 9689–9697. https://doi.org/10.1021/la051241t

Ron, N., Zimet, P., Bargarum, J., & Livney, Y. D. (2010). Beta-lactoglobulin–polysaccharide complexes as nanovehicles for hydrophobic nutraceuticals in non-fat foods and clear beverages. *International Dairy Journal*, *20*(10), 686–693. https://doi.org/10.1016/j.idairyj.2010.04.001

Roth, S., Murray, B. S., & Dickinson, E. (2000). Interfacial shear rheology of aged and heat-treated β-lactoglobulin films: displacement by nonionic surfactant. *Journal of Agricultural and Food Chemistry*, *48*(5), 1491–1497. https://doi.org/10.1021/jf990976z

Rousi, Z., Malhiac, C., Fatouros, D. G., & Paraskevopoulou, A. (2019). Complex coacervates formation between gelatin and gum arabic with different arabinogalactan protein fraction content and their characterization. *Food*

Hydrocolloids, *96*, 577–588. https://doi.org/10.1016/j.foodhyd.2019.06.009

Sabet, S., Rashidinejad, A., Qazi, H. J., & McGillivray, D. J. (2021). An efficient small intestine-targeted curcumin delivery system based on the positive-negative-negative colloidal interactions. *Food Hydrocolloids*, *111*, 106375. https://doi.org/10.1016/j.foodhyd.2020.106375

Sackett, D. L., & Wolff, J. (1987). Nile red as a polarity-sensitive fluorescent probe of hydrophobic protein surfaces. *Analytical Biochemistry*, *167*(2), 228–234. https://doi.org/10.1016/0003-2697(87)90157-6

Sagis, L. M. C. (2011). Dynamic properties of interfaces in soft matter: experiments and theory. *Reviews of Modern Physics*, *83*(4), 1367–1403. https://doi.org/10.1103/revmodphys.83.1367

Sagis, L. M. C., & Fischer, P. (2014). Nonlinear rheology of complex fluid-fluid interfaces. *Current Opinion in Colloid and Interface Science*, *19*(6), 520–529. https://doi.org/10.1016/j.cocis.2014.09.003

Sagis, L. M. C., & Scholten, E. (2014). Complex interfaces in food: structure and mechanical properties. *Trends in Food Science and Technology*, *37*(1), 59–71. https://doi.org/10.1016/j.tifs.2014.02.009

Salelles, L., Floury, J., & Le Feunteun, S. (2021). Pepsin activity as a function of pH and digestion time on caseins and egg white proteins under static: in vitro conditions. *Food and Function*, *12*(24), 12468–12478. https://doi.org/10.1039/d1fo02453a

Sams, L., Paume, J., Giallo, J., & Carrière, F. (2016). Relevant pH and lipase for in vitro models of gastric digestion. *Food and Function*, *7*(1), 30–45. https://doi.org/10.1039/c5fo00930h

Sassene, P. J., Fanø, M., Mu, H., Rades, T., Aquistapace, S., Schmitt, B., Cruz-Hernandez, C., Wooster, T. J., & Müllertz, A. (2016). Comparison of lipases for in vitro models of gastric digestion: lipolysis using two infant formulas as model substrates. *Food and Function*, *7*(9), 3989–3998. https://doi.org/10.1039/c6fo00158k

Sawyer, L., & Kontopidis, G. (2000). The core lipocalin, bovine β-lactoglobulin. *Biochimica et Biophysica Acta - Protein Structure and Molecular Enzymology*, *1482*(1–2), 136–148. https://doi.org/10.1016/s0167-4838(00)00160-6

Scheuble, N., Geue, T., Windhab, E. J., & Fischer, P. (2014). Tailored interfacial rheology for gastric stable adsorption layers. *Biomacromolecules*, *15*(8), 3139–3145. https://doi.org/10.1021/bm500767c

Scheuble, N., Lussi, M., Geue, T., Carrière, F., & Fischer, P. (2016). Blocking gastric lipase adsorption and displacement processes with viscoelastic biopolymer adsorption layers. *Biomacromolecules*, *17*(10), 3328–3337. https://doi.org/10.1021/acs.biomac.6b01081

Schmidt, U. S., Koch, L., Rentschler, C., Kurz, T., Endreß, H. U., & Schuchmann, H. P. (2015). Effect of molecular weight reduction, acetylation and esterification on the emulsification properties of citrus pectin. *Food Biophysics*, *10*(2), 217–227. https://doi.org/10.1007/s11483-014-9380-1

Schmidt, U. S., Schütz, L., & Schuchmann, H. P. (2017). Interfacial and emulsifying properties of citrus pectin: interaction of pH, ionic strength and degree of esterification. *Food Hydrocolloids*, *62*, 288–298. https://doi.org/10.1016/j.foodhyd.2016.08.016

Schröder, A., Berton-Carabin, C., Venema, P., & Cornacchia, L. (2017). Interfacial properties of whey protein and whey protein hydrolysates and their influence on o/w emulsion stability. *Food Hydrocolloids*, *73*, 129–140. https://doi.org/10.1016/j.foodhyd.2017.06.001

Setiowati, A. D., Saeedi, S., Wijaya, W., & Van der Meeren, P. (2017). Improved heat stability of whey protein isolate stabilized emulsions via dry heat treatment of wpi and low methoxyl pectin: effect of pectin concentration, pH, and ionic strength. *Food Hydrocolloids*, *63*, 716–726. https://doi.org/10.1016/j.foodhyd.2016.10.025

Setiowati, A. D., Vermeir, L., De Neve, L., Sedaghat Doost, A., Sinnaeve, D., & Van der Meeren, P. (2019). Quantification of the electrostatic and covalent interaction between whey proteins and low methoxyl pectin using pfg-nmr

diffusometry. *Magnetic Resonance in Chemistry*, *57*(9), 719–729. https://doi.org/10.1002/mrc.4812

Shafaei, Z., Ghalandari, B., Vaseghi, A., Divsalar, A., Haertlé, T., Saboury, A. A., & Sawyer, L. (2017). β-lactoglobulin: an efficient nanocarrier for advanced delivery systems. *Nanomedicine: Nanotechnology, Biology, and Medicine*, *13*(5), 1685–1692. https://doi.org/10.1016/j.nano.2017.03.007

Shpigelman, A., Shoham, Y., Israeli-Lev, G., & Livney, Y. D. (2014). β-lactoglobulin-naringenin complexes: nano-vehicles for the delivery of a hydrophobic nutraceutical. *Food Hydrocolloids*, *40*, 214–224. https://doi.org/10.1016/j.foodhyd.2014.02.023

Skoda, M. W. A. (2019). Recent developments in the application of x-ray and neutron reflectivity to soft-matter systems. *Current Opinion in Colloid and Interface Science*, *42*, 41–54. https://doi.org/10.1016/j.cocis.2019.03.003

Sneharani, A. H., Karakkat, J. V., Singh, S. A., & Rao, A. G. A. (2010). Interaction of curcumin with ß-lactoglobulin;stability, spectroscopic analysis, and molecular modeling of the complex. *Journal of Agricultural and Food Chemistry*, *58*(20), 11130–11139. https://doi.org/10.1021/jf102826q

Steingoetter, A., Radovic, T., Buetikofer, S., Curcic, J., Menne, D., Fried, M., Schwizer, W., & Wooster, T. J. (2015). Imaging gastric structuring of lipid emulsions and its effect on gastrointestinal function: a randomized trial in healthy subjects. *American Journal of Clinical Nutrition*, *101*(4), 714–724. https://doi.org/10.3945/ajcn.114.100263

Stender, E. G. P., Birch, J., Kjeldsen, C., Nielsen, L. D., Duus, J. O., Kragelund, B. B., & Svensson, B. (2019). Alginate trisaccharide binding sites on the surface of β-lactoglobulin identified by nmr spectroscopy: implications for molecular network formation. *ACS Omega*, *4*(4), 6165–6174. https://doi.org/10.1021/acsomega.8b03532

Stephen, A. M., Phillips, G. O., & Williams, P. A. (2016). Food polysaccharides and their applications: second edition. In *Food Polysaccharides and Their Applications: Second Edition*.

Sturm, M. T., Horn, H., & Schuhen, K. (2021). The potential of fluorescent dyes—comparative study of nile red and three derivatives for the detection of microplastics. *Analytical and Bioanalytical Chemistry*, *413*(4), 1059–1071. https://doi.org/10.1007/s00216-020-03066-w

Tcholakova, S., D. Denkov, N., B. Ivanov, I., & Campbell, B. (2002). Coalescence in β-lactoglobulin-stabilized emulsions: effects of protein adsorption and drop size. *Langmuir*, *18*(23), 8960–8971. https://doi.org/10.1021/la0258188

Tcholakova, S., Denkov, N. D., Sidzhakova, D., Ivanov, I. B., & Campbell, B. (2005). Effects of electrolyte concentration and pH on the coalescence stability of β-lactoglobulin emulsions: experiment and interpretation. *Langmuir*, *21*(11), 4842–4855. https://doi.org/10.1021/la046891w

Teo, A., Dimartino, S., Lee, S. J., Goh, K. K. T., Wen, J., Oey, I., Ko, S., & Kwak, H. S. (2016). Interfacial structures of whey protein isolate (WPI) and lactoferrin on hydrophobic surfaces in a model system monitored by quartz crystal microbalance with dissipation (QCM-D) and their formation on nanoemulsions. *Food Hydrocolloids*, *56*, 150–160. https://doi.org/10.1016/j.foodhyd.2015.12.002

Teo, W., Caprariello, A. V., Morgan, M. L., Luchicchi, A., Schenk, G. J., Joseph, J. T., Geurts, J. J. G., & Stys, P. K. (2021). Nile red fluorescence spectroscopy reports early physicochemical changes in myelin with high sensitivity. *Proceedings of the National Academy of Sciences of the United States of America*, *118*(8), e2016897118. https://doi.org/10.1073/pnas.2016897118

Tian, L., Zhang, S., Yi, J., Zhu, Z., Li, M., Decker, E. A., & McClements, D. J. (2021). Formation of antioxidant multilayered coatings for the prevention of lipid and protein oxidation in oil-in-water emulsions: lycium barbarum polysaccharides and whey proteins. *Journal of Agricultural and Food Chemistry*, *69*(51), 15691–15698. https://doi.org/10.1021/acs.jafc.1c06585

Tuinier, R., Rolin, C., & de Kruif, C. G. (2002). Electrosorption of pectin onto casein micelles. *Biomacromolecules*, *3*(3), 632–638. https://doi.org/10.1021/bm025530x

Uhrínová, S., H. Smith, M., B. Jameson, G., Uhrín, D., Sawyer, L., & N. Barlow, P. (2000). Structural changes accompanying pH-induced dissociation of the β-lactoglobulin dimer,. *Biochemistry*, *39*(13), 3565–3574. https://doi.org/10.1021/bi992629o

Voinova, M. V, Rodahl, M., Jonson, M., & Kasemo, B. (1999). Viscoelastic acoustic response of layered polymer films at fluid-solid interfaces: continuum mechanics approach. *Physica Scripta*, *59*(5), 391–396. https://doi.org/10.1238/physica.regular.059a00391

Wagoner, T., Vardhanabhuti, B., & Foegeding, E. A. (2016). Designing whey protein-polysaccharide particles for colloidal stability. *Annual Review of Food Science and Technology*, *7*, 93–116. https://doi.org/10.1146/annurev-food-041715-033315

Wijaya, W., Patel, A. R., Setiowati, A. D., & Van der Meeren, P. (2017). Functional colloids from proteins and polysaccharides for food applications. *Trends in Food Science and Technology*, *68*, 56–69. https://doi.org/10.1016/j.tifs.2017.08.003

Wijaya, W., Van der Meeren, P., & Patel, A. R. (2017). Cold-set gelation of whey protein isolate and low-methoxyl pectin at low pH. *Food Hydrocolloids*, *65*, 35–45. https://doi.org/10.1016/j.foodhyd.2016.10.037

Wijaya, W., Van der Meeren, P., Wijaya, C. H., & Patel, A. R. (2017). High internal phase emulsions stabilized solely by whey protein isolate-low methoxyl pectin complexes: effect of pH and polymer concentration. *Food and Function*, *8*(2), 584–594. https://doi.org/10.1039/c6fo01027j

Wilson, A., Ekanem, E. E., Mattia, D., Edler, K. J., & Scott, J. L. (2021). Keratin-chitosan microcapsules via membrane emulsification and interfacial complexation. *ACS Sustainable Chemistry and Engineering*, *9*(49), 16617–16626. https://doi.org/10.1021/acssuschemeng.1c05304

Wooster, T. J., & Augustin, M. A. (2006). β-lactoglobulin-dextran maillard conjugates: their effect on interfacial thickness and emulsion stability. *Journal of Colloid and Interface Science*, *303*(2), 564–572. https://doi.org/10.1016/j.jcis.2006.07.081

Xu, A. Y., Melton, L. D., Ryan, T. M., Mata, J. P., Rekas, A., Williams, M. A. K., & McGillivray, D. J. (2018). Effects of polysaccharide charge pattern on the microstructures of β-lactoglobulin-pectin complex coacervates, studied by saxs and sans. *Food Hydrocolloids*, *77*, 952–963. https://doi.org/10.1016/j.foodhyd.2017.11.045

Xu, D., Yuan, F., Gao, Y., Panya, A., McClements, D. J., & Decker, E. A. (2014). Influence of whey protein-beet pectin conjugate on the properties and digestibility of β-carotene emulsion during in vitro digestion. *Food Chemistry*, *156*, 374–379. https://doi.org/10.1016/j.foodchem.2014.02.019

Zembyla, M., Murray, B. S., Sarkar, A., S. Murray, B., & Sarkar, A. (2018). Water-in-oil pickering emulsions stabilized by water-insoluble polyphenol crystals. *Langmuir*, *34*(34), 10001–10011. https://doi.org/10.1021/acs.langmuir.8b01438

Zhao, R., Qin, X., & Zhong, J. (2021). Interaction between curcumin and β-casein: multi-spectroscopic and molecular dynamics simulation methods. *Molecules*, *26*(16). https://doi.org/10.3390/molecules26165092

Zhu, J., Li, H., Xu, Y., & Wang, D. (2019). Construction of fucoxanthin vector based on binding of whey protein isolate and its subsequent complex coacervation with lysozyme. *Journal of Agricultural and Food Chemistry*, *67*(10), 2980–2990. https://doi.org/10.1021/acs.jafc.8b06679

Zsila, F., Hazai, E., & Sawyer, L. (2005). Binding of the pepper alkaloid piperine to bovine β-lactoglobulin: circular dichroism spectroscopy and molecular modeling study. *Journal of Agricultural and Food Chemistry*, *53*(26), 10179–10185. https://doi.org/10.1021/jf051944g

Annexes

(For Chapter 2)

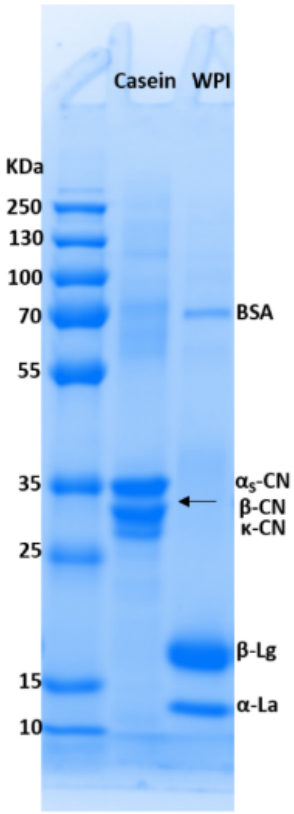

Figure A1: SDS-PAGE of a molecular weight marker in lane 1, and the WPI sample used in lane 3; to enable comparison, lane 2 shows the protein composition of dairy casein micelles. All measurements were performed under reducing conditions.

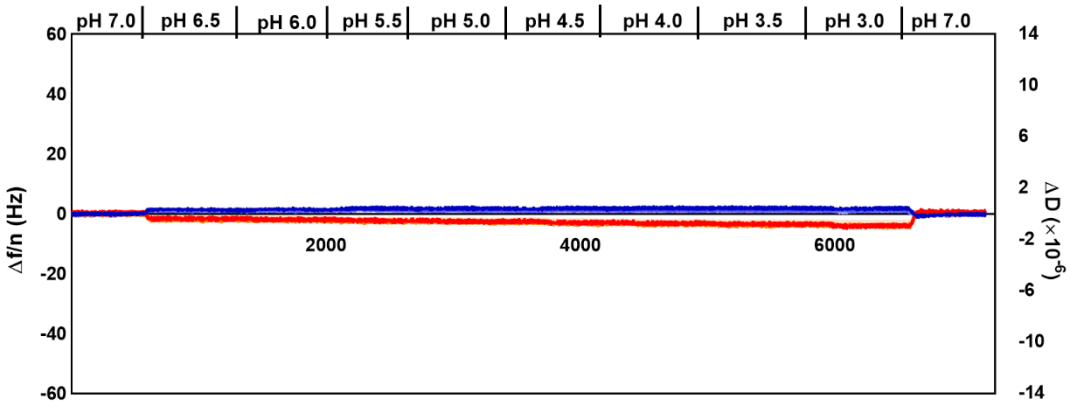

Figure A2: Effect of buffer pH on the normalised frequency (blue) and dissipation (red) shifts as a function of time (s) for the 3rd, 5th, 7th, and 9th overtones. The baseline was established by the pH 7.0 buffer on a hydrophobically modified gold surface (without WPI or LMP).

Table A1: Normalised frequency (in Hz) and dissipation shifts (in 10^{-6}) upon contacting a hydrophobically modified gold sensor with a sequence of buffers of different pH (data from Figure A2, 5th overtone).

pH	Δf/n	ΔD
7.0 (baseline)	0.107±0.096	0.005±0.071
6.5	0.969±0.110	-0.451±0.055
6.0	1.245±0.164	-0.500±0.047
5.5	1.440±0.091	-0.590±0.047
5.0	1.289±0.103	-0.621±0.044
4.5	1.384±0.091	-0.776±0.054
4.0	1.308±0.162	-0.773±0.046
3.5	1.357±0.128	-0.865±0.050
3.0	1.248±0.150	-0.917±0.064

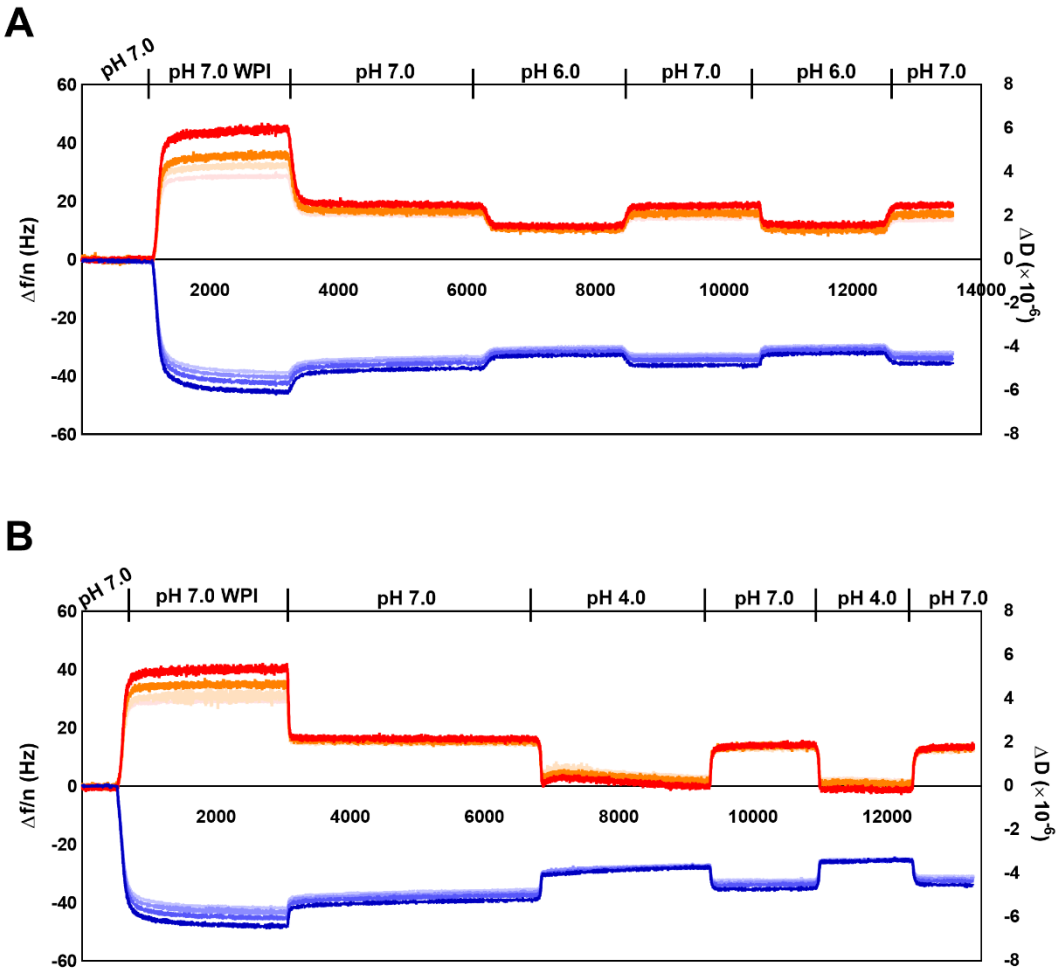

Figure A3: Normalized frequency (blue) and dissipation (red) shifts as a function of time (s) for the 3rd, 5th, 7th, and 9th overtones of a pre-adsorbed WPI layer upon repeated rinsing with a combination of a pH 6.0 buffer and the pH 7.0 buffer (A) or a pH 4.0 buffer and the pH 7.0 buffer (B).

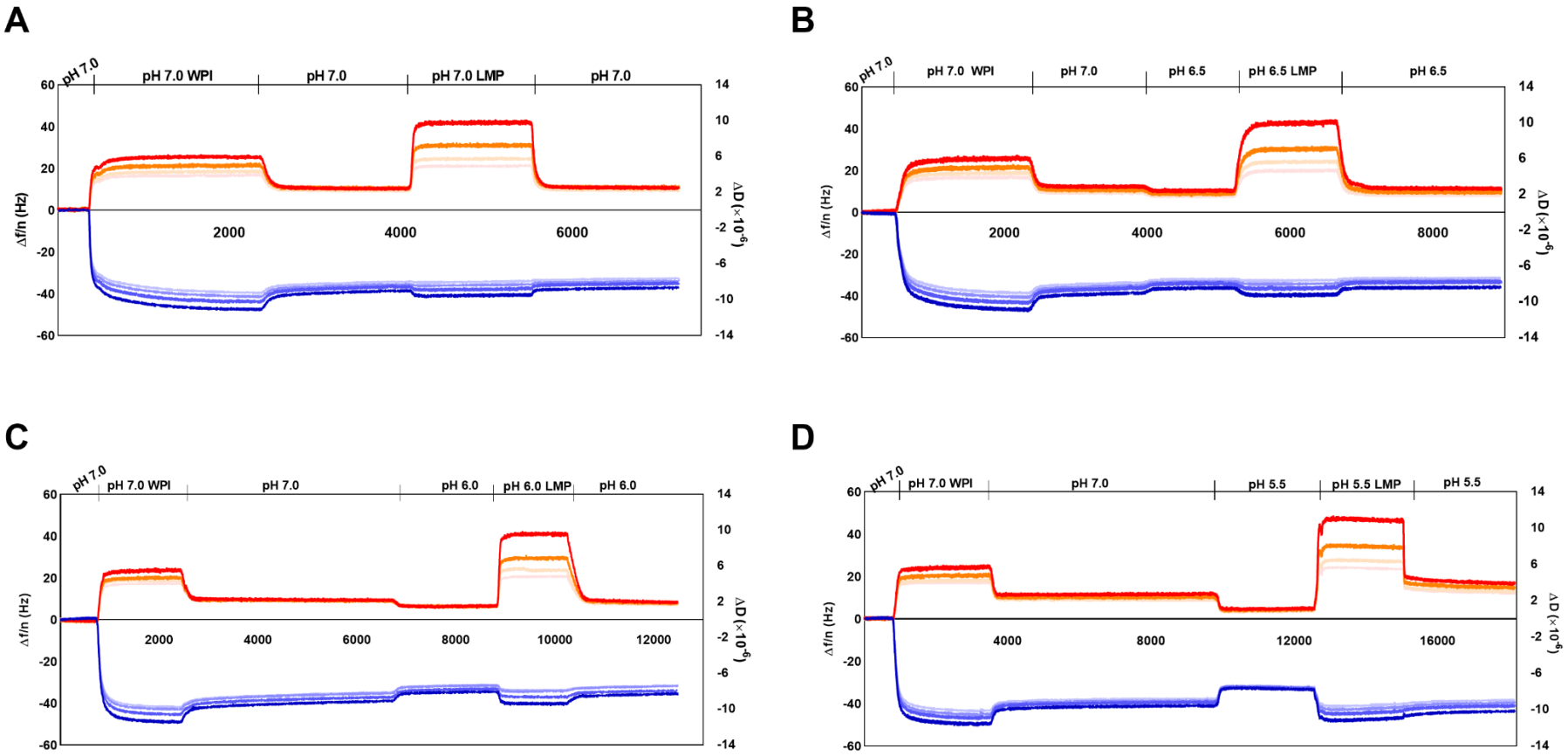
A
pH 7.0
pH 7.0 WPI
pH 7.0
pH 7.0 LMP
pH 7.0
Δf/n (Hz)
ΔD (×10⁻⁶)
2000
4000
6000
B
pH 7.0
pH 7.0 WPI
pH 7.0
pH 6.5
pH 6.5 LMP
pH 6.5
Δf/n (Hz)
ΔD (×10⁻⁶)
2000
4000
6000
8000
C
pH 7.0
pH 7.0 WPI
pH 7.0
pH 6.0
pH 6.0 LMP
pH 6.0
Δf/n (Hz)
ΔD (×10⁻⁶)
2000
4000
6000
8000
10000
12000
D
pH 7.0
pH 7.0 WPI
pH 7.0
pH 5.5
pH 5.5 LMP
pH 5.5
Δf/n (Hz)
ΔD (×10⁻⁶)
4000
8000
12000
16000

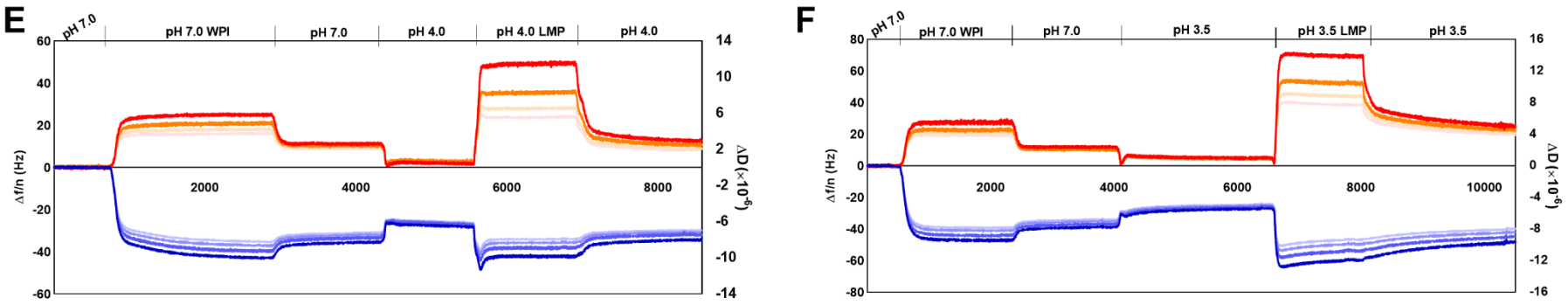

Figure A4: Normalized frequency (blue) and dissipation (red) shifts as a function of time (s) for the 3rd, 5th, 7th, and 9th overtones (with fading colors for increasing overtones) upon sequential adsorption of WPI (1.0 %, w/w) at pH 7.0 and LMP (0.4%, w/w) at pH 7.0 (A), 6.5 (B), 6.0 (C), and 5.5 (D) onto a hydrophobically modified surface.

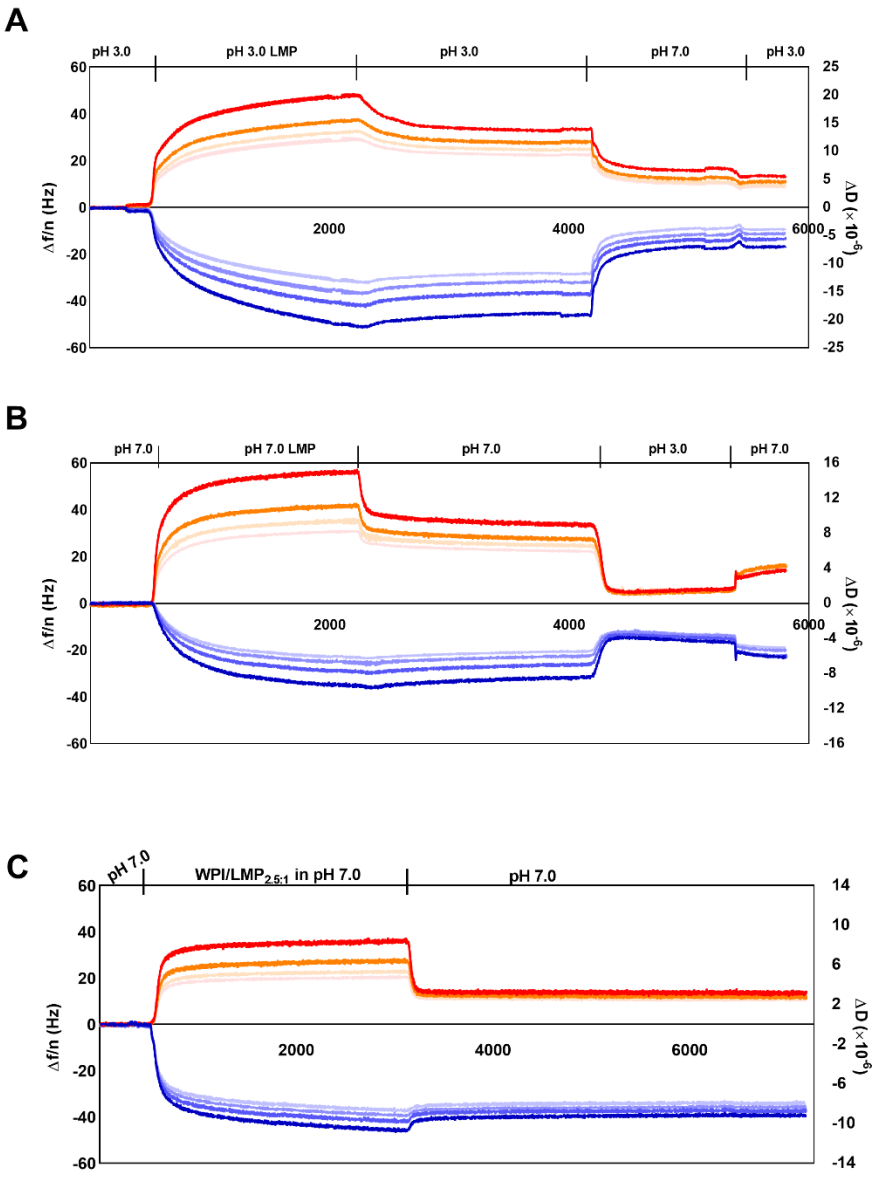

Figure A5: Normalized frequency (blue) and dissipation (red) shifts as a function of time (s) for the 3rd, 5th, 7th, and 9th overtones (with fading colors for increasing overtones) upon adsorption of LMP (0.4%) onto the hydrophobic surface at pH 7.0 (A); Adsorption of LMP (0.4%) onto the hydrophobic surface at pH 3.0 (B); Adsorption of the mixture of WPI and LMP (0.5%: 0.2%, w/w) onto the hydrophobic surface at pH 7.0 (C).

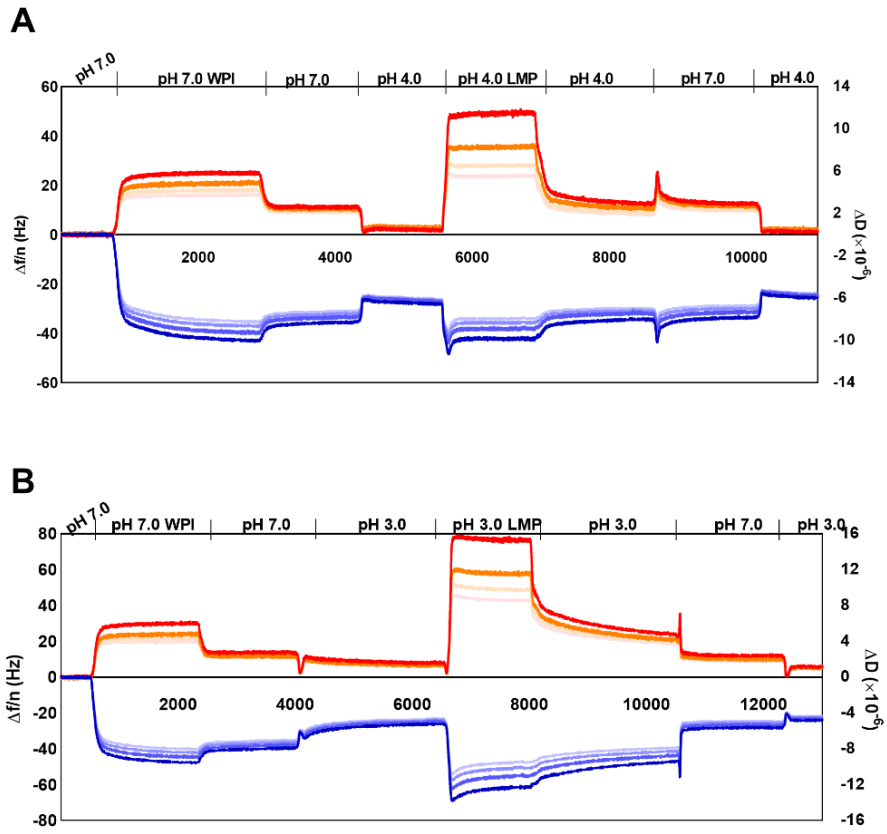

Figure A6: Normalized frequency (blue) and dissipation (red) shifts as a function of time (s) for the 3rd, 5th, 7th, and 9th overtones upon sequential adsorption of WPI (1.0 %, w/w) and LMP (0.4%, w/w) onto the hydrophobically modified surface at pH 4.0 (A) and 3.0 (B). After removing the excess LMP, the mixed layer was rinsed sequentially by a pH 7.0 buffer and a pH 4.0 or pH 3.0 buffer.

Curriculum vitae

HAO LI

Nationality: Chinese
Gender: Male
Date of birth: 16th March 1993
Email: hao.li@ugent.be; lihaoghent@gmail.com

EDUCATION

Ghent University **Sep 2019-present**
Ghent, Belgium
PhD in Bioscience Engineering: Food Sciences and Nutrition

Ocean University of China **Sep 2016-June2019**
Qingdao, China
Master's degree in food engineering

Huazhong Agricultural University **Sep 2012-June2016**
Wuhan, China
Bachelor's degree in food safety and quality

GRANTS AND AWARDS

CSC scholarship for PhD research	Chinese scholarship council, 2019-2023
Mobility funding by CWO and doctoral school	Ghent University, 2021, 2022
National scholarship	Ministry of Education of China, 2018
Outstanding student	Ocean University of China, 2019

PUBLICATIONS

- Li, H., & Van der Meeren, P. (2023). Designing gastric stable adsorption layers by whey protein-pectin complexation at the oil-water interface. *Journal of Agricultural and Food Chemistry, 71, 18, 7109-7118*
- Li, H., & Van der Meeren, P. (2022). Sequential adsorption of whey proteins and low methoxy pectin at the oil-water interface: An interfacial rheology study. *Food Hydrocolloids, 128, 107570*
- Li, H., Wang, T., Su, J., & Van der Meeren, P. (2022). Influence of pH and low/high-methoxy pectin complexation on the hydrophobic binding sites of β-lactoglobulin studied by a fluorescent probe method. *Food Hydrocolloids, 108020*
- Li, H., Wang, T., Hu, Y., Wu, J., & Van der Meeren, P. (2022). Designing delivery systems for functional ingredients by protein/polysaccharide interactions. *Trends in Food Science & Technology, Volume 199, 272-287*

- Li, H., Wang, T., Su, C., Wu, J., & Van der Meeren, P. (2022). Effect of ionic strength on the sequential adsorption of whey proteins and low methoxy pectin on a hydrophobic surface: A QCM-D study. *Food Hydrocolloids, 122, 107074*.
- Li, H., Wu, J., Doost, A. S., Su, J., & Van der Meeren, P. (2021). Electrostatic interaction between whey proteins and low methoxy pectin studied by quartz crystal microbalance with dissipation monitoring. *Food Hydrocolloids, 113, 106489*
- Li, H., Wang, D., Liu, C., Zhu, J., Fan, M., Sun, X., ... & Cao, Y. (2019). Fabrication of stable zein nanoparticles coated with soluble soybean polysaccharide for encapsulation of quercetin. *Food Hydrocolloids, 87, 342-351*.
- Li, H., Xu, Y., Sun, X., Wang, S., Wang, J., Zhu, J., ... & Zhao, L. (2018). Stability, bioactivity, and bioaccessibility of fucoxanthin in zein-caseinate composite nanoparticles fabricated at neutral pH by antisolvent precipitation. *Food Hydrocolloids, 84, 379-388*.
- Wang, T., Li, H., Denon, Q., To, C. M., & Van der Meeren, P. (2023). Investigating the effect of diluents and fat globules on the size measurement of casein micelles by dynamic light scattering. *International Dairy Journal, 142, 105640*.
- Wu, J., Li, H., A'yun, Q., Doost, A. S., De Meulenaer, B., & Van der Meeren, P. (2021). Conjugation of milk proteins and reducing sugars and its potential application in the improvement of the heat stability of (recombined) evaporated milk. *Trends in Food Science & Technology, 108, 287-296*.
- Zhi, Z., Yan, L., Li, H., Dewettinck, K., Van der Meeren, P., Liu, R., & Van Bockstaele, F. (2022). A combined approach for modifying pea protein isolate to greatly improve its solubility and emulsifying stability. *Food Chemistry, 380, 131832*.

PRESENTATIONS IN CONFERENCES

18th Zsigmondy Colloquium	Berlin, Germany, 2023
36th European Colloid & Interface Society Conference	Crete, Greece, 2022
18th Food Colloids Conference	Lund, Sweden, 2022
4th Food Structure & Functionality Symposium	Online, 2021
12th NIZO Dairy Conference	Online, 2021

TRAINING & SEMINAR

GLiM: Spectral imaging and Raman Spectroscopy	Ghent, Belgium, 2023
ECIS conference training courses	Crete, Greece, 2022
Advanced Academic English	Ghent, Belgium, 2022
ECIS conference training courses	Athene, Greece, 2020
QCM-D training, Biolin	Online, 2020
Rheology training, TA instruments	Antwerp, Belgium, 2019
Benchtop NMR for food applications	Ghent, Belgium, 2019

JOURNAL REVIEWING EXPERIENCES (INVITED REVIEWER SINCE 2021)

Food Hydrocolloids
Food Chemistry
Food Research International
Biotechnology Reports
Trends in Food science & Technology
Food Hydrocolloids for Health
Current Research in Food Science

MASTER THESIS SUPERVISION

Shujun Wang, 2022-2023
Thesis topic: Emulsifying and emulsion stabilization properties of pea globulins/pectin mixtures